

Synthesis, characterization and radiation response of HfO₂ based high-k dielectric materials

A thesis submitted for the degree of
Doctor of Philosophy in Physics

by

N. MANIKANTHABABU



School of Physics
University of Hyderabad
Hyderabad – 500046, Telangana
India

December 2015

Gordon Moore: Dr. Hawking—what will ultimately limit the performance of silicon microprocessors?

Dr. Stephen Hawking: This is not my field; however, I suspect it will be the silicon material and the speed of light in it.

(Discussion as part of visit by Prof. Hawking to Intel in 2004)

Questions many ways don't change but becomes more daunting in the light of destiny in which we live.

*Dedicated to my
Parents and Mentors*



DECLARATION

I, **Mr. N. Manikanthababu** hereby declare that the matter embodied in this thesis entitled “**Synthesis, characterization and radiation response of HfO₂ based high-k dielectric materials**” is the result of investigations carried out by me in the School of Physics, University of Hyderabad, India, under the supervision of **Dr. S V S Nageswara Rao** and **Prof. A P Pathak**. This work has not been submitted for any other degree either in part or in full to this or to any other University or Institution.

A report on plagiarism statistics from the University librarian is enclosed.

Place: Hyderabad

(N. MANIKANTHABABU)

Date:



CERTIFICATE

This is to certify that the work embodied in this thesis entitled “**Synthesis, characterization and radiation response of HfO₂ based high-k dielectric materials**” has been carried out by **Mr. N. Manikanthababu**, under our supervision and this has not been submitted for any degree at this or any other University or Institution.

A report on plagiarism statistics from the University librarian is enclosed.

(S V S Nageswara Rao)

(Anand P Pathak)

Place: Hyderabad

Date:

Dean

School of Physics

Acknowledgements

It's a great honour and pleasure to acknowledge the contributions of all, without whom this doctoral thesis would not have been concerted.

First and foremost, I express my profound gratitude to my supervisor, Dr. S V S Nageswara Rao, Associate Professor, School of Physics, University of Hyderabad (UoH), for his invaluable guidance to accomplish this thesis work. I have been introduced to this enthralling field of research with his immense guidance as I feel it is a gratifying experience. His best teaching skills with logical consistency and composure levels in numerous aspects have an enormous impact on my life at various stages. I feel proud to be trained under one of the best teachers in my life as he comes down to our stage to explain some of the basic and preliminary insights of the subject. He played various roles in my life over the years as a guide, philosopher and a friend and even took the responsibilities at times required as my father. He is not only a person with great intellect and integrity but also shared with me his knowledge, thoughtful vision and humor over the years. I owe him a lot for all of his consistent, instructive suggestions and help. I also thank his family members Sailaja madam, Sri Nidhi and his parents for their support (wishes and dishes).

I express my adorable, sincere and heartfelt thanks to my co-supervisor, Prof. Anand P Pathak, School of Physics, University of Hyderabad (UoH). He is a person with an astounding caliber and an impeccable intellectual agility who engenders interest with "Work is Worship" notion. His contributions to scientific world in ion beam channeling show his renowned stature and nobility. It's a great privilege for me to work with such an eminent scientist. Cheerful smile, strict time scales and superior understanding capacities are the conspicuous and distinct features of him and eventually showed a path for the younger generations. I wish him in good health and prosperity in future. I also thank his family members for their support.

It is a great privilege to have Prof. M Ghanashyam Krishna, Prof. C S Sunandana and Dr. Surajit Dhara as my Doctoral Committee members. They have always helped me in improving my level of understanding of essential concepts for interpreting our results. Prof. M Ghanashyam Krishna's expertise in the fabrication of thin-films and related devices has helped me in a great manner during the course of this work. He has as an incredible ability to find out the gaffes during the presentations and interaction sessions, which helped me a lot in this thesis work. I would like to thank Prof. C S Sunandana, who has given his novel thoughts and

suggestions to understand the new dimensions of physics. I sincerely thank Dr. Surajit Dhara for all his encouragement and wonderful suggestions during the presentations.

I express my sincere thanks to Prof. R Singh, Dean, School of Physics and former Deans Prof. S Chaturvedi, Prof. S P Tewari and Prof. C Bansal for providing indispensable facilities in the School. The significant support over the years by Mr. T. Abraham has been greatly acknowledged.

I am very much grateful to Dr. D K Avasthi for his valuable suggestions and inputs during beam time experiments at IUAC, New Delhi. I intently thank Dr. D Kanjilal, Director, IUAC for his suggestions during discussions. I thank Dr. D Kabiraj and Mr. Abhilash for allowing us to utilize the facilities in target lab. I thank Dr. K Asokan for his useful suggestions during in-situ electrical measurements. I thank Dr. Saif A Khan for his extensive help during the beam time experiments. I am also thankful to the members of Pelletron group and other supporting labs in IUAC for necessary support during experiments. I also thank Dr. GBVS Lakshmi garu and her family for their interaction during our stay at IUAC. I thank Dr. K G M Nair and Dr. B Sundaravel for their suggestions and help during our experiments at IGCAR, Kalpakkam.

I express my sincere thanks to Prof. L C Feldman, Vice-President, Rutgers University, USA for providing ALD grown samples and for excellent discussions over e-mails. Also, I thank Prof. T Osipowicz, Director of CIBA, NUS, Singapore for allowing us to use HRBS and RBS facilities. I thank Dr. T K Chan and Dr. Saumithra Vajandar for their help in performing HRBS measurements and Prof. Mark Breese, Director of SSSL, NUS, Singapore for allowing us to use the synchrotron facilities. I extend my sincere thanks to Prof. Y Ping for his useful discussions and for his help in performing SSSL based XRR measurements.

I thank Dr. Shammi Verma, Dr. Ashish Kumar, Mr. Ramcharan Meena, Ms. Manjubala, Mr. K Phaneendra for their help in performing in-situ electrical measurements. I also thank Dr. Udai Bhanu Singh, Mr. Sunil Ojha and others for their help at IUAC. I also like to thank Mr. Ch Ravikumar, Mr. S L D Varma and Arun for their support in performing the electrical measurements. I take this opportunity to acknowledge CFN, UoH for extending the access to its sophisticated experimental facilities.

My special word of thanks and appreciation to all my lab seniors, Dr. N Srinivasa Rao, Dr. G Devaraju, Dr. V Saikiran and Dr. V S Vendamani for consistent and endless encouragement and support. A special thanks to Saikiran for valuable research discussions as well as for his

personal interest and friendly support. It is great pleasure to have Dhanunjaya, Arun and Vinod as lab-mates for creating a friendly and enjoyable atmosphere. I wish them all the success in their future endeavours.

I also thank technical staff Mr. Laxmi Narayana, Mr. Thirumalaiah, Ms. Sandhya, Ms. Sunitha, Ms. Reshma and Mr. Durga Prasad for their help. I thank all non-teaching staff of our school for their support over these years.

I thank all my friends from my childhood. It is difficult to mention all the names here but a special mention of cheers for the help and support received from good friends Trinadh, Vasu, Lakshmi, Chaithanya, Subbu, Ganesh, Govindaraju, Suman, Srinivas, Deepthi, Sandhya is essential. My stay on this campus has been pleasant due to association of many other students and friends from various labs. On this occasion, I thank each and every one for their interaction and help. A special thanks to I. V. Sankar for his splendid discussions and our friendship has been lively since 2007. I thank B. Ravikumar for all his unforgettable help whenever I needed. I thank all the '09, '10 batch-mates, Dr. Rajesh Khanna, Narasimhappa, Dr. S. Pavan Kumar Naik, Uma Shankar, Raju Botta, Pasha, Ramesh and others for having wonderful time on the campus. I thank Binoy, Suadat, Dr. Mandar Kirkire, Krishna Kumar and others for their help and support.

I thank UGC-India for providing the financial support in the form of UGC-JRF and SRF. I thank UoH for BBL fellowship and IUC-DAE-CSR Kalpakkam for a project fellowship in a research project sanctioned to Prof. A P Pathak. I thank UPE-II for their partial international travel support which made my first ever visit to USA to present my work (an oral and a poster) in 23rd CAARI 2014 international conference in San Antonio, Texas, USA.

I convey my sincere thanks to all my teachers right after my childhood till date for their consistent encouragement who have taught me the basic concepts and given me the opportunity to learn and lead a successful life and career.

This is the time to express my gratitude to all my relatives right from my grandparents for their consistent support and encouragement.

Last but the MOST, I can't express my gratitude in words to my parents Sri. N Chittiah and Smt. Jessie Rajeswari. My father is a role model and an idol for me who gave every space of freedom to learn. This improved my level of confidence to grow into a better person. All the

prayers of my mother are the monograms of my triumphs over the years. I thank them for their indubitable support throughout my career from the deepest insights of my heart. It is because of them that my name on earth has emerged and mere expression of thanks does not suffice for their unconditional love.

Above all, I am indebted to the God almighty for this invaluable opportunity for me in life and giving me the strength to strive forward with a composed character.

I thank all of them who have involved either directly or indirectly for the successful completion of this thesis.

Synthesis, characterization and radiation response of HfO₂ based high-k dielectric materials

Abstract

Hafnium Oxide (HfO₂) based high dielectric constant materials are critical for the *state-of-the-art* integrated circuit technology. The traditional gate dielectric material SiO₂ has been replaced with HfO₂ in the evolution of 45 nm generation Metal Oxide Semiconductor (MOS) devices to reduce high leakage currents. Performance, durability and reliability of HfO₂ based MOS devices in the terrestrial/space applications in radiation ambience is an interesting study. Current thesis aims to elucidate the effects of gamma and swift heavy ion (SHI) irradiations to test the radiation hardness and reliability of these devices by investigating the radiation induced effects on the structural and electrical properties. HfO₂ samples prepared by Atomic Layer Deposition (ALD), Radio Frequency (RF) magnetron sputtering and e-beam (EB) evaporation methods have been studied in this work. The structural and electrical properties of these samples have been characterized by well-established techniques. This study indicates that the nature and concentration of defects and their evolution during irradiation is sensitive to the method of deposition. Further, the SHI induced diffusion of Hf across HfO₂/SiO₂ interface and the consequent effects on the electrical properties have been studied in detail. In-situ electrical measurements performed during SHI irradiation form the basis for reliable analysis of these devices. Primarily, we have observed radiation induced annealing of defects at lower fluences followed by deterioration of devices at higher fluences. Hence, this study provides useful information for improving the device quality as well as to understand the radiation response of HfO₂/Si and HfO₂/SiO₂ interfaces which are at the heart of the current integrated circuit technology.

Glossary

AC	Alternative Current
AD	As Deposited
ALD	Atomic Layer Deposition
AN	Annealed
APCVD	Atmospheric Pressure Chemical Vapor Deposition
BRIT	Board of Radiation and Isotope Technology
C-V	Capacitance-Voltage
CCM	Channel-Cut Monochromatic
CFN	Center for Nano Technology
CVD	Chemical Vapor Deposition
DC	Direct Current
EB	e-beam evaporation
EHPs	Electron Hole Pairs
FESEM	Field Emission Scanning Electron Microscopy
GIXRD	Glazing Incidence X-Ray Diffraction
GUI	Graphical User Interface
HRBS	High-resolution Rutherford Backscattering Spectrometry
I-V	Current-Voltage
IC's	Integrated Circuit's
IUAC	Inter University Accelerator Centre
JCPDS	Joint Committee on Powder Diffraction Standards
LPCVD	Low Pressure Chemical Vapor Deposition
LVDT	Linear Variable Differential Transformer
MBE	Molecular Beam epitaxy
MCA	Multi- Channel Analyzer
MCP-FPD	Micro-Channel Plate Focal Plane Detector Stack
MCSNICS	Multi Cathode Source of Negative Ions by Cesium Sputtering
MFCMU	Multi Frequency Capacitance Measurement Unit
ML	Mono Layer
MOS	Metal Oxide Semiconductor
MOSFET	Metal Oxide Semiconductor Field Effective Transistor
NEC	National Electrostatics Corporation
NUS	National University of Singapore
PECVD	Plasma Enhanced Chemical Vapor Deposition
PVD	Physical Vapor Deposition
RBS	Rutherford Backscattering Spectrometry
RCA	Radio Corporation of America
RF	Radio Frequency
RTA	Rapid Temperature Annealing
SCCU	Single Channel Control Unit
SF ₆	Sulphur Hexa-Fluoride
SHI	Swift Heavy Ion
SIMNRA	Simulation of Ions in Matter and Nuclear Reaction Analysis
SSLS	Singapore Synchrotron Light Source
T&R	Transmittance and Reflectance
UHV	Ultra-High Vacuum

UV-Vis	Ultra Violet Visible
XDD	X-Ray Demonstration and Development
XRD	X-Ray Diffraction
XRR	X-Ray Reflectometry

Table of contents

Declaration	i
Certificate	ii
Acknowledgements	iii
Abstract	vii
Glossary	viii
Chapter 1 Introduction	1
1.1 Introduction	2
1.2 Motivation	3
1.3 Objectives	4
1.4 MOS capacitor	4
1.4.1 I-V characteristics of a MOS capacitor	7
1.4.2 C-V characteristics of a MOS capacitor	8
1.4.3 Role of defects/impurities in MOS capacitor	9
1.5 Organization of the thesis	11
1.6 References	16
Chapter 2 Experimental Methods	19
2.1 Synthesis	20
2.2 Irradiation techniques and facilities	20
2.2.1 Gamma irradiation Facility	20
2.2.2 SHI irradiation facility	22
A The Pelletron Accelerator	22
B Beam line and chambers	24
C Irradiation details	24
2.3 Ion beam characterization techniques	25
2.3.1 Rutherford Backscattering Spectrometry	25
A Kinematics of RBS	27
B Scattering cross-section	27
C RBS Channeling	28
2.3.2 High-resolution Rutherford Backscattering Spectrometry	28
2.4 Other characterization techniques	30

2.4.1	X-ray Diffraction	30
2.4.2	Field Emission Scanning Electron Microscopy	32
2.4.3	Profilometer	33
2.4.4	Ultraviolet–Visible (UV-Vis) spectrophotometer	34
2.4.5	Electrical characterization	35
2.4.6	Rapid thermal annealing (RTA)	36
2.5	Experimental details	38
2.5.1	Sample specifications	38
2.5.2	Material treatment and characterization techniques	38
2.6	References	40
Chapter 3	Synthesis and characterization of HfO₂ thin films	41
3.1	Introduction	42
3.1.1	Thermal evaporation technique for depositing metal contacts	43
3.1.2	e-beam evaporation method	43
3.1.3	Sputtering techniques	44
	A DC sputtering	44
	B RF sputtering technique	45
3.2	Experimental details	45
3.3	Growth kinetics – Nature of the traps associated during film growth	50
3.4	Results and discussion	50
3.4.1	HfO ₂ thin films deposited by RF magnetron sputtering	50
	A Structural and optical characterization of HfO ₂ thin films	51
	B Samples of interest (Structural, optical and electrical characterization of HfO ₂ thin films)	56
3.4.2	HfO ₂ thin films deposited by e-beam evaporation	61
	A As-deposited samples prepared by e-beam evaporation	61
	B Effects of thermal annealing	64
3.4.3	HfO ₂ ultra-thin films deposited by Atomic Layer Deposition (ALD)	65

3.5	Conclusions	65
3.6	References	67
Chapter 4	Gamma irradiation studies of HfO₂ based MOSCAPs	69
4.1	Introduction	70
4.2	Experimental details	70
4.2.1	e-beam evaporation	71
4.2.2	RF magnetron sputtering	71
4.3	Results and Discussion	73
4.3.1	HfO ₂ thin films deposited by e-beam evaporation	73
	A Effects of thermal annealing	73
	B Effects of Gamma irradiation	74
4.3.2	HfO ₂ /Si samples deposited by RF magnetron sputtering	77
4.4	Conclusions	81
4.5	References	82
Chapter 5	SHI irradiation effects on the structural and electrical properties of HfO₂ based MOS devices	83
5.1.	Introduction	84
5.2	Experimental	85
5.3	Results and Discussion	86
5.3.1	Ultra-thin HfO ₂ films deposited by ALD	86
	A Effects of 80 MeV Ni ion irradiation	86
	B Effects of 120 MeV Au ion irradiation	91
5.3.2	HfO ₂ thin films deposited by RF magnetron sputtering – Effects of 80 MeV Ni ion irradiation	95
5.4	Conclusions	97
5.5	References	99
Chapter 6	In-situ studies on the electrical properties of HfO₂ based MOSCAPs under SHI irradiation	101
6.1	Introduction	102
6.2	Experimental details	103
6.3	Results and Discussions	104
6.3.1	Effects of 120 MeV Ag ion irradiation on ALD grown H3 series samples	104

6.3.2	Effects of 120 MeV Au ion irradiation on RF series samples	111
6.4	Conclusions	115
6.5	References	116
Chapter 7	Summary and Future scope	117
7.1	Summary of the results	118
7.2	Future scope	120

Introduction

This chapter provides an introduction to HfO_2 based high-k gate dielectric materials. The significance, need and importance of HfO_2 in new generation MOS devices have been described. Specific motivation and the organization of the thesis have been presented along with the principle and operation of a MOS capacitor.

1.1 Introduction

The continuous miniaturization of the Metal Oxide Semiconductor (MOS) devices has an unprecedented role to enhance the comprehensive performance and enabling the higher speed devices at lower costs and in the evolution and development of new dimensional Integrated Circuits (ICs) [1]. However, there are several advantages in conjunction with high packaging density, high speed and low power dissipation [2]. Substantial efforts have been made by the semiconductor industry for attaining these explicitly ever-increasing uncompromised qualities to prompt the stability, durability and reliability of MOS devices [3]. The incessant downscaling at an incredible pace has been impeded by the material fundamental dimensions [4]. Scaling sets limited extendibility on the practical choice of the traditional gate dielectric material SiO_2 even though it has been endowed with robust characteristics in the Si based microelectronics [5-6]. When SiO_2 is scaled down to a few nanometers thickness, it results in a serious drawback of large gate leakage currents [7]. For example, ~ 1 nm thickness of SiO_2 results in an unendurable levels of leakage currents of the order of 100 A/cm^2 [8-9]. These high off-state leakage currents extremely test the device tolerance and jeopardize the performance, durability and reliability [10-11]. The prerequisite of reduced off-state leakage currents in MOS devices demands an innovative era of device evolution with relatively new materials to replace SiO_2 [12]. These practical implications have been resolved by introducing high dielectric constant materials in MOS technology as gate dielectrics to maintain the same level of capacitance as obtained from SiO_2 and low leakage current densities with feasible thicker high-k gate dielectrics [13]. Gd_2O_3 , Er_2O_3 , Ta_2O_5 , TiO_2 , ZrO_2 , HfO_2 , Al_2O_3 etc., are some of the high-k gate materials which have not been found up to the extent quality level of SiO_2 [14-15]. Therefore, optimization and characterization of these materials to be integrated into the current trends of MOS technology have been tested and probed for the insights of these materials [16]. Several critical requirements such as low temperature crystallization and thermal stability have constrained each material from their integration in MOS technology [17-19]. These exposed drawbacks inherited by each material have resulted in an optimized choice of HfO_2 for its successful integration into the recent new generation MOS devices [20]. HfO_2 has several advantages such as high dielectric constant (25), moderate band gap (5.68 eV), high heat of formation (271 kcal/mol) and good thermodynamic stability etc [19]. These expedient qualities made HfO_2 as a significantly useful material in the new generation MOS devices [21]. The trade-off between the high dielectric constant (25) and low band offset

(1.5 eV) has yielded HfO_2 as an emerging material [22-23]. As a result, HfO_2 has already been incorporated in commercial integrated circuit technology because of its stability, durability and reliability [23].

1.2 Motivation

The radiation in space can cause either permanent damage or transient effects on the operation of MOS devices. Moderately low level of radiation occurs in terrestrial environments [24]. Long-term damage effects can be a result of this low level of radiation. The transient effects are also dominant in high-speed devices which need very small amounts of charge for switching [25,26]. Hence, the functionality, reliability and durability of these devices in terrestrial applications have to be understood. The sustenance and reliability of these devices are the challenges for manufacturing the promising radiation hardened MOS devices. Gamma radiation is one of the major cosmic radiations in space and the effects of gamma irradiation are well understood in SiO_2 based MOS devices [27-29]. However, the radiation response of high-k materials is still under investigation and forms an important objective for this thesis work. The possible evolution of gamma irradiation induced effects on the electrical characteristics has been studied as a part of this work.

It is well-known that the Swift Heavy Ion (SHI) irradiation plays a vital role in synthesis, modification and characterization of materials [30]. Interface engineering schemes using SHI irradiation have been extensively studied over the past few years to elucidate the intermixing / diffusion issues [31]. It is well known that ion beam mixing has an imperative role in the formation of silicides in various systems like Fe/Si, Co/Si, Mo/Si, Mn/Si, Ti/Si, Zr/Si etc [32]. To the best of our knowledge, there are no reports on SHI induced mixing of Hf/Si or HfO_2 /Si interfaces even-though some reports exist on ion beam studies of HfO_2 based high-k dielectric materials [33-34]. Moreover, tuning the dielectric constant of these materials using SHI irradiation and defects annealing/creation (based upon the fluence) is also an interesting study [35-36]. These changes in the structural properties and consequent effects on the electrical properties form a basis for newly emerging ternary oxides or nitrides of HfO_2 . Hence, the effects of SHI irradiation on the structural and electrical properties of HfO_2 based MOS devices have been studied as another important aspect of this thesis work.

1.3 Objectives

This thesis aims to report on the synthesis, characterization, radiation response and reliability studies of HfO₂ based MOS devices with following objectives:

- 1) To optimize the synthesis of these films by depositing HfO₂ films in different deposition conditions on different substrates.
- 2) To study the effects of gamma irradiation on the electrical properties of these materials. Further, to study the influence of deposition method on the nature and evolution of defects during irradiation
- 3) To study the swift heavy ion induced diffusion of Hf across HfO₂/SiO₂ and HfO₂/Si interfaces and to study the consequent effects on their electrical properties.

These studies have provided useful information for understanding the effects of gamma and ion irradiation on the structural and electrical properties of HfO₂ based high-k dielectric materials.

Electrical properties of these films have been investigated by fabricating HfO₂ based MOS capacitors. The basic structure and operation of MOS capacitors and I-V & C-V measurements under bias conditions have been discussed briefly. The effects of defects/impurities on these measurements have also been discussed.

1.4 MOS capacitor

Metal Oxide Semiconductor Field Effective Transistor (MOSFET) is the key device in MOS technology. MOS capacitor is at the heart of MOSFETs. MOS capacitor consists of a Si substrate on which a thin gate oxide layer is deposited. The entire discussion of the MOS capacitor has been focused on a p-type Si substrate. A thin metal gate electrode (usually Au) is deposited on the top of the gate oxide layer. On the back side of the silicon substrate, another metal electrode such as Al or Ag paste can be used. The capacitance of any parallel capacitor is given by,

$$C = \frac{k\epsilon_0 A}{d} \quad (1.1)$$

where C is the capacitance, k is the dielectric constant of dielectric material, A is the area of the gate electrode, ϵ_0 is the vacuum permittivity and d is the thickness of the gate dielectric. A schematic view of a MOS capacitor is shown in the Fig. 1.1.

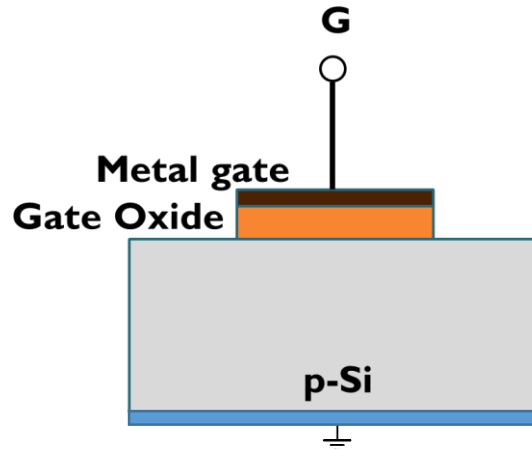


Fig. 1.1: Cross-sectional view of a MOS capacitor

Fig. 1.2 shows the energy band diagram of an ideal MOS structure made on a p-type semiconductor under thermal equilibrium condition. For an ideal MOS structure the essential features are: 1) The metal and semiconductor should have the same work function and 2) No charges should be present in the oxide, semiconductor or at the interface.

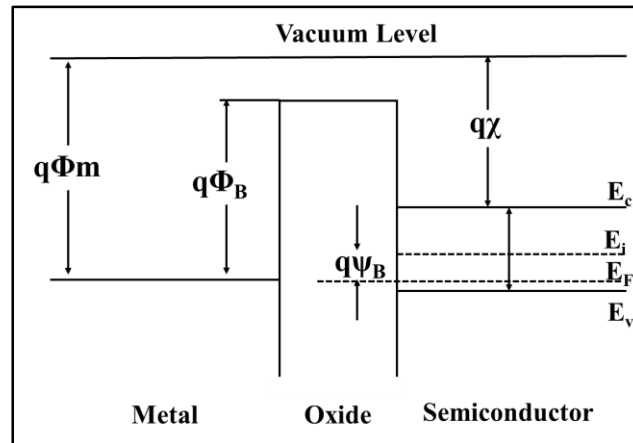


Fig. 1.2: Energy band diagram of an ideal MOS capacitor on a p-type semiconductor

The quantity $q(\phi_m - \phi_{sc})$ is the work function difference between the semiconductor (ϕ_{sc}) and the metal (ϕ_m). $q\chi$ is the electron affinity and qV_p is the energy difference between conduction band edge (E_c) and Fermi level (E_F). The energy difference between metal

Fermi level and oxide conduction band, $q\phi_B$, is the metal to oxide barrier height. The significance of this energy barrier height is that it averts carriers flowing from the metal to semiconductor or vice versa.

In an ideal MOS capacitor, no current flows in the structure, so the Fermi level remains flat in the semiconductor. It is the difference of metal and semiconductor work function given by,

$$V_{FB} = \phi_m - \phi_{sc} \quad (1.2)$$

Basically, three types of regions are created while applying positive and negative bias on the gate material (Fig. 1.3). For a p-type semiconductor, when a negative voltage ($V < 0$) is applied to the metal gate, the valence-band edge E_v bends upward near the surface and

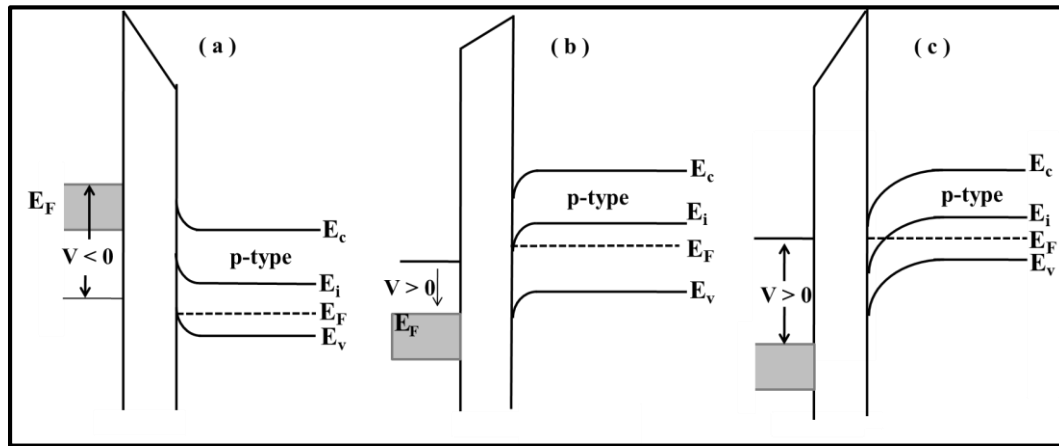


Fig. 1.3: Energy-band diagrams for ideal MIS capacitors under different bias, for the conditions of: (a) accumulation, (b) depletion and (c) inversion

comes close to the Fermi level. Hence, there is an accumulation of majority carriers (holes) near the semiconductor surface. This is called as accumulation region (see Fig. 1.3(a)). When a small positive bias ($V > 0$) is applied, the bands bend downward and the majority carriers are depleted. This is known as the depletion region (see Fig. 1.3(b)). Deep depletion may occur when measuring the capacitance at high-frequencies while sweeping the gate voltage fast in which the device is not in a thermal equilibrium. When the voltage ramp from flatband to threshold is beyond the inversion layer, then partially generated minority carriers cannot form the inversion layer. Therefore, the depletion layer increases beyond its maximum thermal equilibrium value which results in the further decrease of capacitance with voltage. When a larger positive voltage is applied, the bands bend even more

downward so that the intrinsic level E_i at the surface crosses over the Fermi level E_F . In that situation, the number of electrons (minority carriers) at the surface are more than the number of holes; the surface is thus inverted and hence the name, inversion region (see Fig. 1.3(c)).

1.4.1 I-V characteristics of a MOS capacitor

The best method to elucidate the current transport phenomenon is to examine I-V characteristics. The leakage current across the device decides the practical applicability of a gate oxide in the MOS capacitor. Even though the gate oxide is a perfect insulating film it conducts small leakage current especially at high voltages. When the bias voltage surpasses the breakdown voltage of the dielectric film, the film becomes extremely conducting and consequently the leakage current increases. Particularly below this breakdown voltage, the current transportation through the gate oxide can be described by four phenomena: 1) Thermionic Emission (J_{TE}), 2) Frenkel-Poole emission (J_{FP}), 3) Direct tunneling (J_{DT}) and 4) Fowler-Nordheim tunneling (J_{FN}).

In thermionic emission, the leakage current is contributed by the carriers whose energy is equal to or greater than the barrier. The leakage current density J in thermionic equation is given by,

$$J = A^* T^2 \exp \left[- \frac{q \left(\phi_B - \sqrt{\frac{qE}{4\pi\epsilon_i\epsilon_0}} \right)}{kT} \right] \quad (1.3)$$

where A^* is the effective Richardson constant, ϕ_B is the barrier height at the interface, ϵ_i is the high frequency permittivity, T is the temperature and E is the electric field

Frenkel-Poole emission arises due to the defects/impurities produced electron/hole traps. These trapped electrons/holes can escape by thermal emission. So, the current flows due to the electrons jumping from a trap to another trap in the presence of an electric field. It is given by,

$$J = CE \exp \left[- \frac{q \left(\phi_B - \sqrt{\frac{qE}{\pi\epsilon_i\epsilon_0}} \right)}{kT} \right] \quad (1.4)$$

The J/E and $E^{1/2}$ characteristics determine the FP emission and the thermionic emission.

The direct tunneling can be described quantum mechanically. The electrons/holes tunneling through the gate oxide which is like a rectangular barrier. The tunneling probability is controlled by width and height of the barrier. The transmission coefficient, T , through the rectangular potential well is given by,

$$T = \frac{1}{1 + \frac{1}{4F(G-F)} \sinh^2(\kappa a)} \quad (1.5)$$

where F is the initial energy state of the electron, G is the conduction band energy of the gate oxide, k is the wave vector and a is the barrier width.

Fowler-Nordheim tunneling leads to the transmission of electrons through the triangular barrier that is posited on the top of the gate oxide. The rectangular barrier of the gate oxide is distorted into a sharp trapezoidal barrier under high field. The current density is given by,

$$J = AE^2 \exp\left(-\frac{4\sqrt{2m_{ox}}(q\phi_B^*)^{\frac{3}{2}}}{3q\hbar E}\right) \quad (1.6)$$

where ϕ_B^* is the barrier height, E is the electric field and m_{ox} is the effective electron mass. $\ln(J/E^2)$ vs. $1/E$ determines the occurrence of FN tunneling. From the slope of FN plot, the ϕ_B^* can be estimated by the following relation,

$$Slope_{FN} = \frac{4}{3} \frac{\sqrt{2m_{ox}}}{e\hbar} \phi_B^{* \frac{3}{2}} \quad (1.7)$$

1.4.2 C-V characteristics of a MOS capacitor

Depending upon the choice of the frequency level (low or high), the variation in the capacitances can be observed in the accumulation, depletion and inversion regimes. If the applied bias is negative, then capacitance is maximum which implies the accumulation of holes. While the negative voltage is reduced, a depletion region acting as a dielectric layer is formed near the semiconductor surface with a decrease of capacitance. When the applied bias is positive, then a weak or strong inversion depending on electron concentration at the surface can be observed. When the inversion layer contracts, electrons must fill the states

in conduction band at the silicon surface to higher bands. In the same way, when the inversion layer broadens, electrons must fill the states in conduction band at the silicon surface to lower bands than the equilibrium level. This increment of inversion layer occurs only at the low frequencies (see Fig. 1.4).

When a small ac voltage applied on the DC voltage across the MOS capacitor changes rapidly, the electron concentration in the inversion layer cannot change instantaneously. The C-V characteristics will then be a function of the frequency of the ac signal.

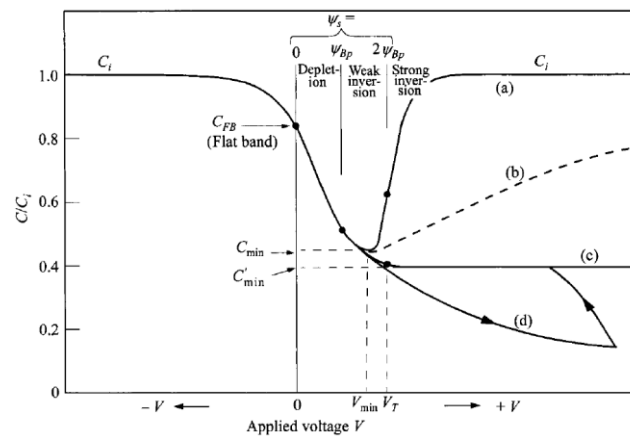


Fig. 1.4: C-V characteristics. Voltage is applied to the metal relative to the substrate (p-semiconductor). (a) Low frequency. (b) Intermediate frequency. (c) High frequency. (d) High frequency with fast sweep (deep depletion). Flat-band voltage of $V = 0$ is assumed.

At low frequency, generation rate of electrons in the depletion region is fast enough and a layer of holes forms at the interface of oxide and semiconductor. Because of the electrons layer, the charge in the depletion region will not change with the applied voltage. The equivalent capacitor is only the oxide capacitor. At high frequency, the generation rate of electrons at the depletion region is not fast enough to form the layer of electrons at the surface, and the thickness of the region reaches a maximum. The charge in the depletion region still changes with the applied voltage, working as a capacitor.

1.4.3 Role of defects/impurities in MOS capacitor

In non-ideal case of the MOS capacitor, the interface of the semiconductor and the gate oxide layer plays a vital role. This interface is enclosed with interface traps and oxide charges which affect the C-V characteristics of the MOS capacitor. In general, there are four types of charges associated with the MOS system. 1) Fixed oxide charges (Q_f), 2)

Mobile oxide charges (Q_m), 3) Interface trapped charges (Q_{it}) and 4) Oxide trapped charges (Q_{ot}) (see Fig. 1.5).

Fixed oxide charges are normally positive charges that are located at/near the interface (see Fig. 1.6). These charges originate from the dangling bonds at the gate oxide/semiconductor interface. These charges are immobile under an applied electric field and can cause the voltage shift in the C-V characteristics.

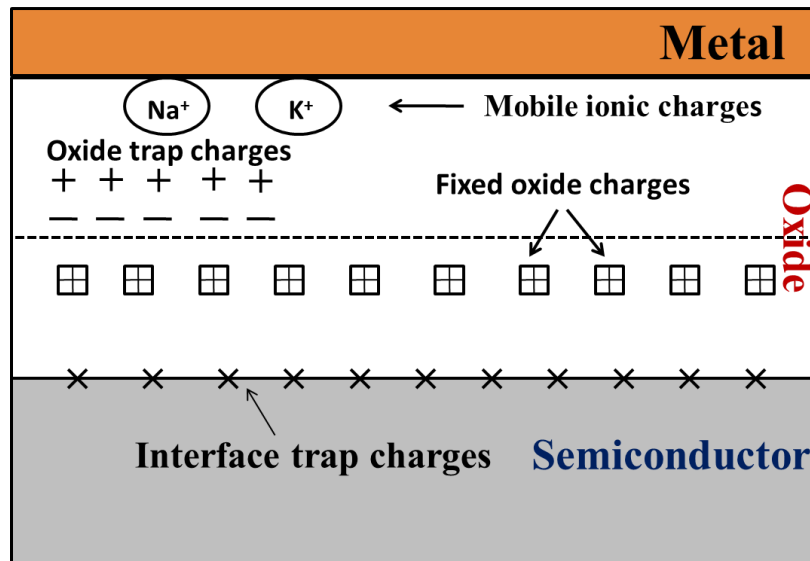


Fig. 1.5: Charges associated with a MOS capacitor

The mobile oxide charges (Q_m) are due to the presence of alkali ions such as Na^+ , K^+ , and Li^+ . In addition to these alkali ions, heavy metal ions may also contribute to this charge. When a voltage is applied to gate, this charge can move through the gate oxide instigating a change in the flat band voltage.

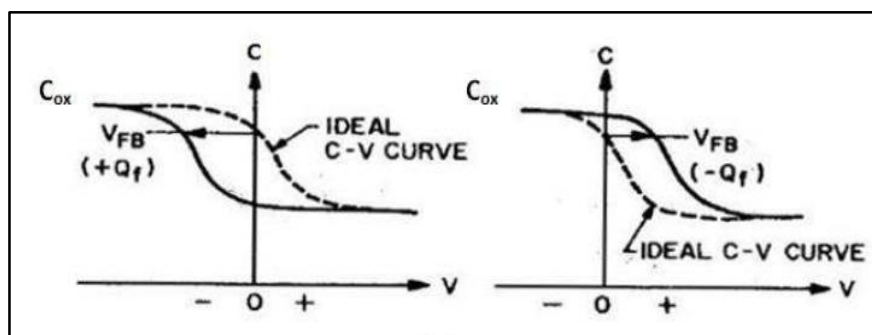


Fig. 1.6: C-V curve voltage shift due to positive and negative fixed oxide charge for a p-type silicon

The interface trapped charges (Q_{it}) can be positive when interface loses an electron and negative when interface gains an electron. Unlike fixed charges or trapped charges, they are in electrical communication with the underlying silicon. However, the interface traps can be charged or discharged, depending upon the surface potential. When the voltage is applied to gate metal, interface trap levels move up/down while the valance level remains stationary. A change of charge in the interface trap arises when it crosses the Fermi level. This change of charge contributes the MOS capacitance and change the ideal C-V characteristics (see Fig. 1.7).

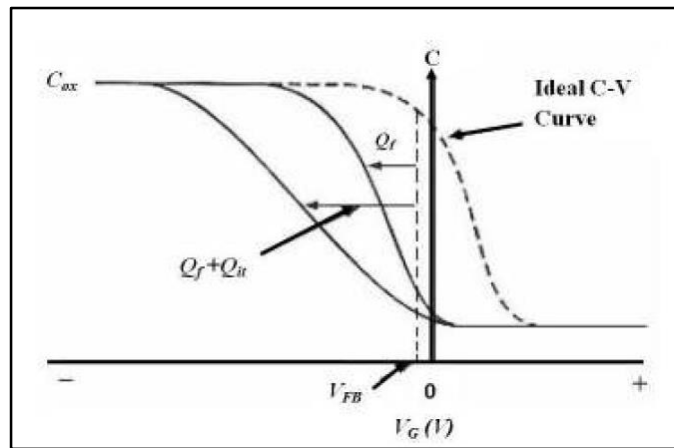


Fig. 1.7: MOS capacitor with a p-type substrate showing effects of interface trapped charge and fixed oxide charge at high frequency

Depending upon the trapped electrons or holes in the bulk of the oxide, the oxide trapped charges are either positive or negative. The trapped charges may be produced from ionizing radiation such as X-ray radiation or hot-electron injection. They are distributed inside the oxide layer. These oxide-trapped charges can be annealed out at low temperatures.

The influence of these various defects on the electrical properties of the HfO_2 based MOS capacitors has been studied in this thesis. The thesis has been organized as follows.

1.5 Organization of the thesis:

Chapter 1: Introduction

The current chapter 1 provides an introduction, motivation and aim of the present thesis work. It comprises of the significance, need and importance of the material under investigation. Pertinent literature survey has been provided to elucidate the clear insights

of the pre-existing literature and to open up the possible areas in which this dissertation is concerted to build up.

Chapter 2: Experimental methods

Chapter 2 describes the characterization techniques and facilities employed to accomplish the investigations of the present thesis work. In brief, HfO_2 thin films were synthesized by RF magnetron sputtering using a newly installed sputtering system in our lab. Some samples were prepared by e-beam evaporation technique at IUAC, New Delhi. ALD grown ultrathin HfO_2 samples were obtained from SEMATECH, USA. These samples were characterized by HRBS, RBS, FESEM, Profilometer and XRR measurements. HRBS and XRR measurements were performed at NUS, Singapore. XPS measurements were performed in IIT Kharagpur. Offline/In-situ electrical measurements such as I-V and C-V characteristics and optical measurements such as UV-Vis measurements were performed at IUAC, New Delhi and UoH, Hyderabad respectively. Gamma and SHI irradiations were performed using GC1200 and 15 MV Pelletron accelerator respectively, at IUAC, New Delhi. The details of the experimental setups, the basics of experimental methods and characterization techniques are described in this chapter.

Chapter 3: Synthesis and Characterization of HfO_2 thin films

Chapter 3 gives the synthesis and characterization of HfO_2 thin films. HfO_2 thin films were deposited on Si by RF sputtering and e-beam evaporation techniques. Good quality HfO_2 thin films were deposited on Si and quartz substrates after the optimization of the synthesis parameters. Au/ HfO_2 /Si MOSCAPs have been fabricated to study the electrical properties. 300 nm thick and 1 mm in diameter Au Metal dots were deposited on the surface of HfO_2 thin films. Ag paste with the help of an Al foil was used for back-side metal contact. On an average, four Au metal dots were deposited on each sample for thorough investigations of I-V and C-V measurements for consistent results. Characterization techniques such as RBS, XRR, FESEM, and Profilometer have also been employed. These results suggest that reliable HfO_2 based MOSCAPs have been synthesized and can be used for further studies.

Chapter 4: Gamma irradiation studies of HfO_2 based MOSCAPs

This chapter presents the gamma irradiation effects on the HfO_2 based MOSCAPs. HfO_2 films deposited on Si by both RF and e-beam evaporation techniques. Structural and

electrical characterizations were performed on both sets of these samples. Gamma irradiation was performed on these samples at different doses starting from 1 kGy to 10 kGy. e-beam evaporated samples show the presence of negatively trapped charges whereas RF sputtered samples show positively trapped charges. However, both the sets of samples have shown similar behavior with gamma irradiation. An increase in the leakage current and capacitance have been observed with the increase in the irradiation doses. Flatband shift and increase in the width of the hysteresis in the C-V characteristics clearly indicate the increase of oxide trapped charge densities and changes in the slopes of these curves show the increase of interface traps. The role of these defects on the electrical properties have been studied. Hence it is important to consider these effects whenever HfO₂ based MOS devices are used in a radiation environment, like space and nuclear electronics.

Chapter 5: SHI irradiation effects on the structural and electrical properties of HfO₂ based MOS devices

This chapter enlightens the SHI irradiation studies on the structural and electrical properties of HfO₂ based MOS devices. ALD grown and RF sputtered samples were irradiated by 80 MeV Ni, 120 MeV Ag and 120 MeV Au ions for these studies.

5.1 Ultra-thin HfO₂ films deposited by ALD:

5.1.1 Effects of 80 MeV Ni ion irradiation:

ALD grown HfO₂ samples with typical sample structure of “HfO₂ (2.5 nm) / SiO₂ (1 nm) / Si (bulk)” have been irradiated by 80 MeV Ni ions at various fluences. HRBS, Channeling and XRR measurements were performed on these samples. These measurements suggest that the interlayer is a mixed Hf_{0.18}Si_{0.32}O_{0.5} (0.6 nm) layer instead of a pure SiO₂ (1 nm) layer as intended. Further, the effects of 80 MeV Ni ion irradiation on this interface have also been studied. A systematic increase in the concentration of Si relative to that of Hf, as a function of fluence is observed in the interlayer. The thickness of this interlayer is also found to increase with increase in fluence. These observations together with XRR analysis confirm that SHI can induce inter-diffusion of Hf and Si across HfSiO/HfO₂ interface. This study yields useful information about ion assisted diffusion across this technologically important “interlayer/HfO₂” interface.

5.1.2 Effects of 120 MeV Au ion irradiation:

80 MeV Ni ion irradiation provided some useful information about SHI induced intermixing. These studies have been further extended to investigate the effects of 120 MeV Au ion irradiation on the structural properties and consequent effects on the electrical properties of a similar set of samples (HfO_2 (3 nm)/ SiO_2 (0.7 nm)/Si (bulk)). HRBS, Channeling, XRR and I-V measurements have been performed on these samples. Results obtained in this study are consistent with those obtained by 80 MeV Ni irradiation. The thickness of the interlayer, a combination of $\text{HfSiO}/\text{SiO}_2$, has been found to increase with increase in the irradiation fluence. Further, I-V measurements confirm these results as the leakage current is found to decrease by one order upon irradiation owing to the increase in the physical thickness of the interlayer and possible defects produced by irradiation. These samples were further processed by RTA at 600 °C in N_2 atmosphere for 60 seconds to study the annealing kinetics. These samples were characterized by XPS and I-V measurements. RTA has resulted in higher leakage currents for all pristine and irradiated samples. These results will be explained in more detail in this chapter.

5.2 RF sputtered films – Effects of 80 MeV Ni ion irradiation

HfO_2 thin films were deposited on Si substrates by using RF magnetron sputtering technique. After optimizing the synthesis of HfO_2 thin films, 10-20 nm films were deposited for structural, optical and electrical characterizations. The pristine samples have been characterized by various techniques to estimate the film thickness, stoichiometry, bandgap, and refractive index. The effects of the defects on HfO_2/Si MOS devices have been studied with 80 MeV Ni ion irradiation. A systematic decrease in the leakage current density is observed with increase in the fluence. SHI induced effects observed on the structural and electrical properties of these films have been discussed in detail.

Chapter 6: In-situ studies on the electrical properties of HfO_2 based MOSCAPs under SHI irradiation

This chapter provides in-situ studies on the electrical properties of HfO_2 based MOSCAPs under SHI ion irradiation. ALD grown HfO_2 (2.7 nm)/ SiO_2 (0.6 nm)/Si samples were studied during 120 MeV Ag ion irradiation. HfO_2 (~15 nm)/Si samples grown by RF magnetron sputtering were also studied during 120 MeV Au ion irradiation at various fluences. On both these sets of samples, in-situ electrical measurements were performed at

IUAC, New Delhi. HRBS, XRR, XPS and TEM measurements were performed to elucidate the structural characterizations. Changes observed in the I-V and C-V characteristics as a function fluence and pertaining physical mechanisms have been discussed in detail.

Chapter 7: Summary and Future scope

This chapter summarizes the prominent features of the present research work and projects the promising future scopes in this field.

The experimental studies presented in this thesis form a basis for further elucidating the radiation response of HfO₂ based MOS devices. These studies are valuable in view of their potential applications in terrestrial space and other radiation environments.

1.6 References

1. R.H Dennard, F.H Gaensslen, H.N Yu, V.L Rideout, E. Bassous and A.R. LeBlanc, *IEEE J. Solid St. Circ.*, **SC-9** (1974) 256.
2. J.R Ligenza and W.G Spitzer, *J. Phys. Chem. Solids*, **14** (1960) 131.
3. J.R Ligenza and W.G Spitzer, *J. Phys. Chem.*, **65** (1961) 2011.
4. G.E Moore, *Progress in digital integrated electronics*. in Electron Devices Meeting, (1975).
5. M. L. Green, E. P. Gusev, R. Degraeve, E. L. Garfunkel, *J. Appl. Phys.*, **90** (2001) 2057.
6. J.N.A. Matthews, *Phys. Today*, **61 (2)** (2008) 25.
7. L. Feldman, E. P. Gusev, and E. Garfunkel, “Fundamental Aspects of Ultrathin Dielectrics on Si-based Devices”, (ed. By) E. Garfunkel, E. P. Gusev, and A. Y. Vul’, Kluwer Publishers, Dordrecht (1998).
8. S.H. Lo, D.A. Buchanan, Y. Taur, W.Wang, *IEEE Electr. Device Lett.* **18** (1997) 209.
9. Paul A. Packan, *Science*, **285** (1999) 2079.
10. R.M. Wallace, G.D. Wilk, *Crit. Rev. Sol. State*, **28** 231 (2003).
11. Takashi Ando, *Materials*, **5** (2012) 478.
12. S. Chattopadhyay, L. D. Driscoll, K. S. K. Kwa, S. H. Olsen and A. G. O’Neill, *Solid-State Electron.*, **48** (2004) 1407.
13. G. D. Wilk, R. M. Wallace and J. M. Anthony, *J. Appl. Phys.*, **89** (2001) 5243.
14. Y.-C. Yeo, *Thin Solid Films*, **34** (2004) 462.
15. J. Robertson, *J. Vac. Sci. Technol. B.*, **18** (2000) 1785.
16. P. D. Kirsh, C. S. Kang, J. Lozano and J. C. Lee, *J. Appl. Phys.*, **91** (2002) 4353.
17. Y.H. Kim and J.C. Lee, *Microelectronics & Reliab.*, **44** (2004) 183.
18. H. Kim, P.C. McIntyre and K.C. Saraswat, *Appl. Phys. Lett.*, **82** (2003) 106.
19. L.V. Goncharova, M. Dalponte, T. Feng, T. Gustafsson, E. Garfunkel, P.S. Lysaght and G. Bersuker, *Phys. Rev. B*, **83** (2011) 115329.
20. Byoung Hun Lee, Laegu Kang, Renee Nieh and Jack C. Lee, *Appl. Phys. Lett.*, **76** (2000) 1926.
21. Tzu-Ray Shan, Bryce D. Devine, Travis W. Kemper, Susan B. Sinnott and Simon R. Phillpot, *Phys. Rev. B*, **81** (2010) 125328.
22. R.K. Nahar, V. Singh, A. Sharma, *J. Mater. Sci. Mater. Elec.*, **18** (2007) 615.

23. B. Aguirre, R.S. Vemuri, D. Zubia, M.H. Engelhard, V. Shutthanandan, K.K. Bharathi and C.V. Ramana, *Appl. Surf. Sci.*, **257** (2011) 2197.
24. C. Claeys and E. Simoen, “Radiation effects in advanced semiconductor materials and devices”, Springer-Verlag, Berlin (2002).
25. Boris I. Kharisov Oxana, V. Kharissova Ubaldo and Ortiz Méndez (ed. by) “Radiation Synthesis of Materials and Compounds”, CRC Press, Boca Raton (2013).
26. Feriz Adrovic (ed. by), “Gamma Radiation”, InTech Publishers000, Croatia (2013).
27. T. Yunogami, T. Mizutani, *J. Appl. Phys.*, **73** (1993) 8184.
28. M. C. Busch, A. Slaoui, P. Siffert, E. Dooryhee, M. Toulemonde, *J. Appl. Phys.*, **71** (1992) 2596.
29. T. P. Ma, Y. Nishioka, E. F. da Silva, “The Physics and Chemistry of SiO₂ and the Si-SiO₂ Interface”, edited by C. R. Helms, B. E. Deal, Plenum press, New York, (1988).
30. D. K. Avasthi and G. K. Mehta, “Swift Heavy Ions for Materials Engineering and Nanostructuring”, Capital Publishing Company, New Delhi (2011).
31. I.C. Kizilyalli, R.Y.S. Huang, P.K. Roy, *IEEE. Ele. Dev. Lett.*, **19** (1998) 423.
32. D.K. Avasthi, *Defence Sci. J.*, **59** (2009) 401.
33. A. Benyagoub, *Nucl. Instr. Meth. Phys. Res., B*, **245** (2006) 225.
34. H. Gruer, *Thin Solid Films*, **509** (2004) 47.
35. R. Singh, S. K. Arora, and D. Kanjilal, *Mater. Sci. Semicond. Process.*, **4** (2001) 425.
36. J. R. Srour, C. J. Marshall, and P. W. Marshall, *IEEE Trans. Nucl. Sci.*, **50** (2003) 653.

Experimental Methods

This chapter provides the complete details of the experimental methods, characterization techniques and facilities that were employed to accomplish the investigations of the current thesis work. Specific experimental parameters that are used in different experiments are given in the relevant chapters.

2.1 Synthesis

HfO₂ thin films synthesized by three different deposition methods have been used for accomplishing the work presented in this thesis. A set of samples were prepared by RF magnetron sputtering system which is a newly installed sputtering system in our lab. Another set of samples were prepared by e-beam evaporation technique at IUAC, New Delhi. ALD grown device quality ultrathin HfO₂ samples were obtained from SEMATECH, USA. More details about synthesis of these films have been conferred in the following chapter.

2.2 Irradiation techniques and facilities

Ion-solid interactions play a significant role in employing ion beams for characterizing and modifying materials [1-4]. In order to study the interaction of radiation with the HfO₂ based MOS devices, two different facilities of irradiation were used viz. gamma and SHI irradiation. These experimental facilities are described below.

2.2.1 Gamma irradiation facility



Fig. 2.1: Gamma Irradiation facility at IUAC [5]

Fig. 2.1 depicts the Gamma chamber GC 1200 manufactured by Board of Radiation and Isotope Technology (BRIT), Mumbai. It is a self-shielded cobalt-60 gamma source contained in a volume of about 1200 cc. Gamma irradiation was performed using a ⁶⁰Co source at IUAC, New Delhi [5]. This experimental set-up mainly consists of the source and

cylindrical cage, a ladder with a sample holder, lead flask and an external cabinet with a mechanical driver system. The samples under investigation for irradiation can be placed inside the chamber located in the vertical drawer. This drawer can be moved up and down with the help of a system of motorized drivers. The dose of irradiation is normally set initially in the auto mode so that the ladder comes out of the chamber automatically on completion of the irradiation dose. It is also possible to move the ladder inside the chamber manually. The maximum effect of irradiation is at the centre of the sample holder. Therefore, the accurate position of the samples can be placed at the centre of the radiation field in the irradiation chamber.

The prevalent isotope ^{60}Co , which is produced by neutron irradiation of stable ^{59}Co decays into a stable ^{60}Ni by emitting two characteristic gamma rays of energies 1.17 and 1.33 MeV. These reactions are shown below in equations 2.1 and 2.2. The schematic is shown in Fig. 2.2.

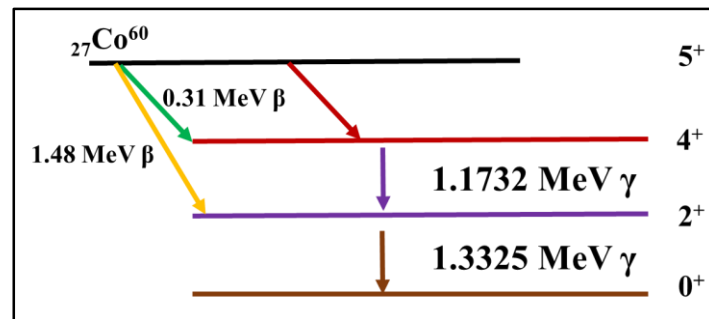
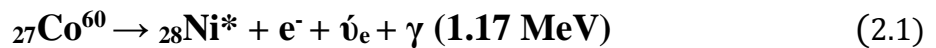


Fig. 2.2: Decay mechanism of ${}_{27}\text{Co}^{60}$ source [5]

Gamma irradiation-induced effects on the electrical properties of the HfO_2 based MOS devices have been studied (see chapter-4). The gamma irradiation has been performed at different doses: 1 kGy, 2 kGy, 4 kGy, 6 kGy, 8 kGy, 10 kGy, 12 kGy and 48 kGy at a constant dose rate of ~ 4.64 kGy/hr. The effects of gamma irradiation on the electrical properties of HfO_2/Si MOS devices have been investigated. More specific experimental details and corresponding results are discussed in chapter 4.

2.2.2 SHI irradiation facility

A. The Pelletron Accelerator

The 15 UD Pelletron accelerator installed at the Inter University Accelerator Center (IUAC), New Delhi [6,7] is a tandem type electrostatic accelerator. Pelletron is a tandem Van de Graaff accelerator manufactured by National Electrostatics Corporation (NEC). A schematic diagram of the Pelletron accelerator is shown in Fig. 2.3.

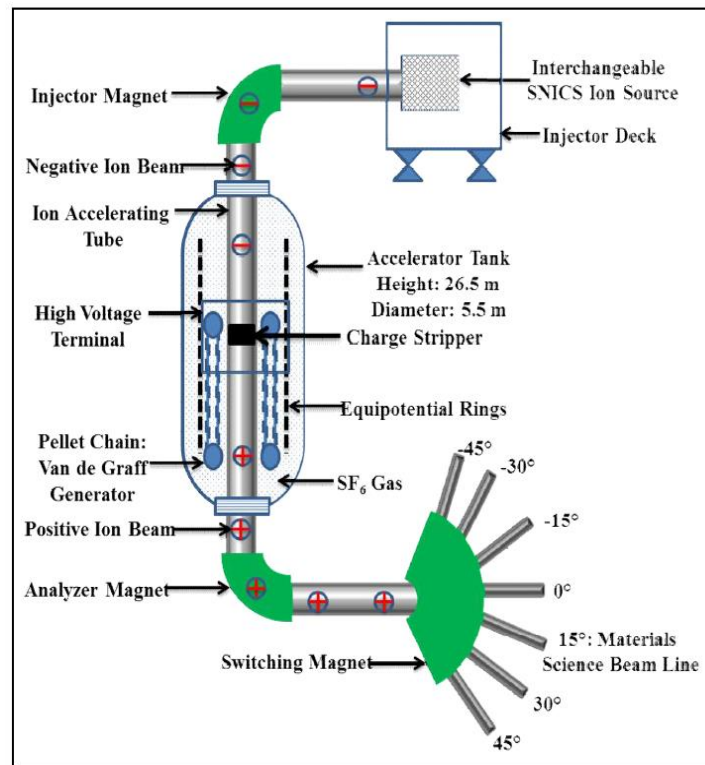


Fig. 2.3: Schematic diagram of Pelletron accelerator [7]

This accelerator has a potential to generate and accelerate all stable nuclei with their energies ranging from 50 to 250 MeV. Pelletron has a vertical geometry which is installed in a tank containing insulating Sulphur hexa-fluoride (SF₆) at high pressure. Negative ions are produced by the ion source situated at the top of the accelerator. In general, there are three types of ion sources that are used in the accelerators, (a) Alphasources (b) MCSNICS and (c) Duoplasmatron. In all of these ion sources, MCSNICS (Multi Cathode Source of Negative Ions by Cesium Sputtering) is the most commonly used ion source and it is used in 15 UD Pelletron accelerator at IUAC. The negative ions, produced by this source, are pre-accelerated to about ~300 keV by the deck potential and these negative ions of different masses are focused and analysed by a 90° dipole magnet commonly known as an injector

magnet. This step is performed before injecting them in the low energy accelerating tubes. The negative ions are bent using the injector magnet by 90° in vertically downward direction in the accelerating column. A very high potential (~15 MV) is attained at the terminal and potential gradient is always maintained throughout the tube. Low energy sections are always above the terminal whereas the high energy sections are down below. This high potential is produced by transferring the charge to the terminal (operation of Van de Graff generator) by a chain of insulated metal pellets. At the center of tank, these energetic ions pass through a gas/foil stripper and get transformed into positive ions. Further, these positive ions are repelled by the high voltage terminal and the ions are accelerated to higher energies. Depending upon the charge state of the ions, they are accelerated to different energies at the bottom of the accelerator because positive ions of various charge states are produced after stripping. The same terminal potential (V_T) is being used two times to accelerate the ions and hence the name “15 UD tandem”. The term “UD” stands for Unit Double. The final energy of the ion Z^{q+} is given by

$$E_i (\text{MeV}) = E_d + (1+q)V_T \simeq (1+q)V_T \quad (2.3)$$

Here E_d is the energy of the ion extracted from the ion source deck and V_T is the high voltage terminal potential (in MV).

The ion beam current is measured by using a device called Faraday cup (FC). The accelerated particles are stopped inside this cup and the collected electric charge is detected as a resultant electric current. Similarly, fluence can be measured using a current integrator. It collects the charge from the target ladder and integrates it (over the time to yield the ion fluence). In order to collect this charge, an electrical connection is provided to the current integrator by placing a metallic clip on the ladder. Fluence / irradiation time can be calculated by

$$t = \frac{fA}{I \times 6.25 \times 10^9} \quad (2.4)$$

where t is the time required (in seconds) for irradiating a material, A is the scan area of the material (in general 1 cm x 1 cm), f is the fluence (ions/cm²) and I is the beam current in particle nano-ampere (pnA). Beam current in pnA can be calculated by dividing the beam current in nano-amperes with its charge state q .

B. Beam line and chambers

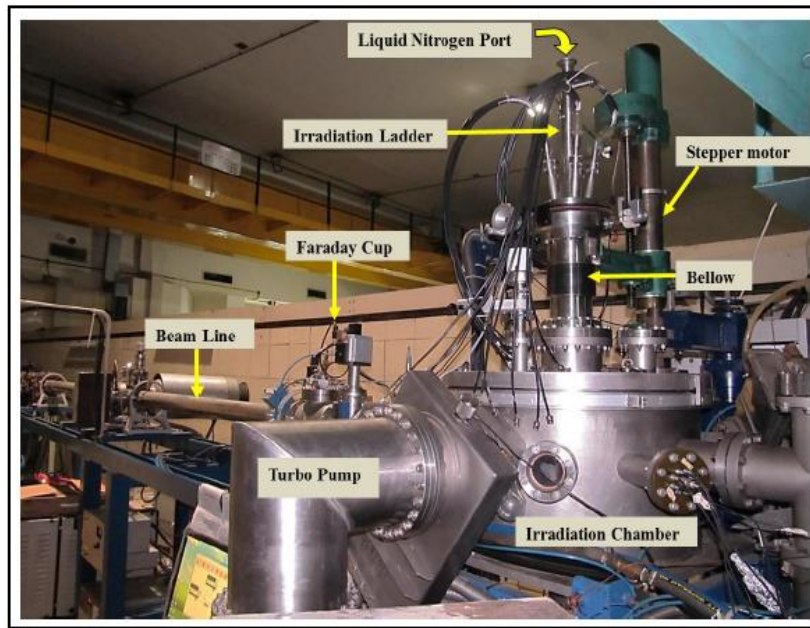


Fig. 2.4: Material science beam line and irradiation chamber at IUAC [7]

The Material-Science (MS) beam line has been utilized for performing this thesis work. This beam line is positioned at 15° to the right of central 0° beam line. Fig. 2.4 depicts this beam line which consists of irradiation chamber, ladder and beam line. The irradiation chamber has been pumped down to 10^{-7} mbar by turbo molecular pump. This chamber has three viewing windows to see inside the chamber and to align the ladder inside the chamber in the beam direction. The ladder with samples mounted on it for irradiation is well connected with a top flange (see Fig. 2.4). Flexible bellows connected to the chamber provides the possibility to move the ladder up and down in vacuum chamber. This motion is controlled by a stepper motor. The CCTV camera connected to one of the view-ports assists in remote monitoring from the control room.

C. Irradiation details

SHI irradiation has been carried out using 80 MeV Ni, 120 MeV Ag, 120 MeV Au ions at various fluences starting from 1×10^{10} to 1×10^{14} ions/cm². The beam was made incident upon 1 cm x 1 cm area of the samples in a scanning mode. Necessary precautions have been taken during irradiation to minimize heating of the samples. Further, low beam currents (0.5 pA to 1 pA) are maintained throughout the experiments and the orientation of the samples has been kept at 5° with the beam axis. The projected ranges of the ions in

the thin films have been calculated so that the damage will be at the end of the range ie. in the bulk substrate.

SHI irradiation-induced effects on the structural and electrical properties of the HfO₂ based high-k dielectric materials have been studied (see chapter 5) using Pelletron accelerator. 80 MeV Ni and 120 MeV Au ion irradiations at various fluences were performed on ALD grown ultrathin films. More specific experimental details have been discussed in detail in the relevant chapter.

2.3 Ion beam characterization techniques

2.3.1 Rutherford Backscattering Spectrometry

Rutherford Backscattering Spectrometry (RBS) has been extensively used as one of the best characterization techniques in material science [1, 8]. Fig. 2.5 depicts a schematic of RBS

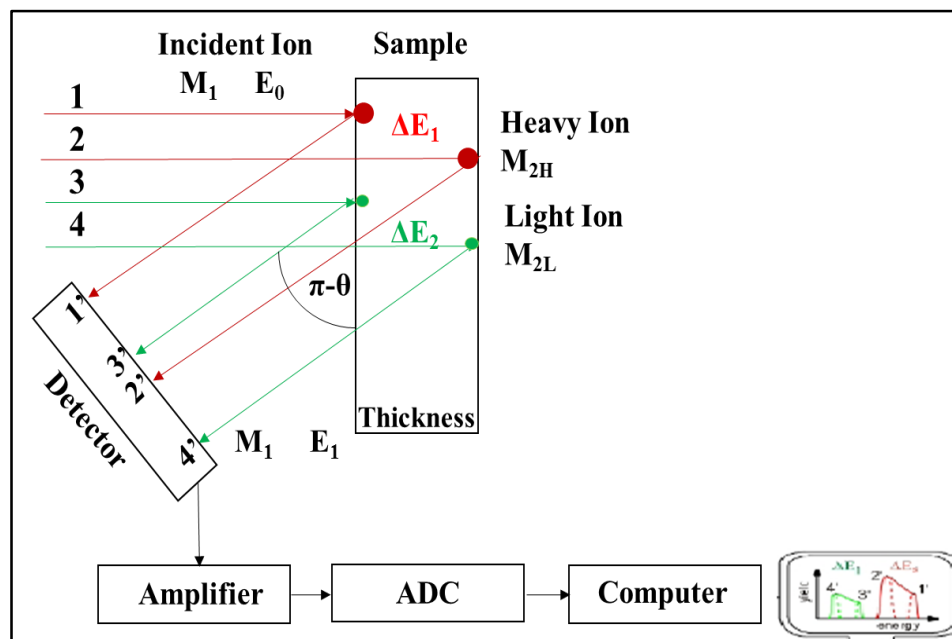


Fig. 2.5: Schematic diagram of RBS setup

experimental set-up and Fig. 2.6 shows a typical RBS set-up at IUAC. RBS employs the quantitative information of the composition of a given material and depth profiles of distinct elements present in that material. Despite of its low sensitivity for lighter elements, RBS has several advantages such as nondestructive nature and a good depth resolution of the order of several nm. In RBS measurements, a target material is bombarded with 0.5 to 2 MeV ions (in general He²⁺) and the energy of the backscattered projectiles is recorded

with an energy sensitive solid state detector. The typical back scattering angles range between 150° - 170° . Generally, protons, He, and Li ions are used as projectiles.

The semiconductor solid state detector produces an analog signal in the form of a voltage pulse. The height of each voltage pulse is proportional to the incident energy of the detected



Fig. 2.6: RBS Facility at IUAC [9]

particles. This voltage pulse is then stored in a Multi-Channel Analyzer (MCA). The magnitude of the voltage pulse splits into equal increments and each increment is featured as a channel. Since, the channel numbers are calibrated in terms of these voltage pulse heights, there is a direct relationship between a channel number and respective energy. However, the magnitude of a particular channel is recorded as count and each channel is registered with a certain number of counts. Hence, the output of the MCA is a series of counts confined in different channels. The analog signal generated by MCA contains quantitative information on a particular parameter of the detected particle. Correspondingly, channel number or energy of the detected particles and the number of counts are displayed in a backscattering energy spectrum.

A. Kinematics of RBS

RBS is governed by simple elastic collisions between the projectile and target nuclei. The momentum transfer between two particles is obtained by employing the conservation laws (Energy and momentum).

The kinematic factor for RBS is given by,

$$K_{RBS} = \frac{E_1}{E_0} = \left[\frac{(M_2^2 - M_1^2 \sin^2 \theta)^{1/2} + M_1 \cos \theta}{M_2 + M_1} \right]^2, \quad (2.5)$$

where M_1 is the mass of projectile ions and M_2 is that of the target ions. E_0 is the initial energy of projectile, E_1 is the energy of scattered projectile and θ is the scattering angle. This kinematic factor provides the required mass perception to identify the constituent elements of target material.

B. Scattering cross-section

When a narrow beam of high energy and heavy ions hits a thin target material, it can recoil the target particles in forward direction. A detector placed at a recoil angle of ϕ , can count the number of recoiled particles in a differential solid angle $d\Omega$ defined by the geometry. The differential scattering cross section $d\sigma/d\Omega$ is given by

$$\frac{d\sigma}{d\omega} = \left(\frac{1}{N_t} \right) \left[\frac{dQ}{d\Omega} \right] \frac{1}{Q}, \quad (2.6)$$

where Q is the total number of incident particles, dQ is the number of detected particles and N_t is the number of target atoms per unit area. Total number of detected particles can be obtained by the following equation

$$A = \sigma \Omega Q N_t, \quad (2.7)$$

The scattering cross-section is defined as

$$\sigma(\theta) = \left(\frac{1}{Q} \int \frac{d\sigma}{d\omega} \right)_{d\Omega}, \quad (2.8)$$

$$\sigma(\theta) = \left(\frac{1}{\Omega} \int \frac{d\sigma}{d\Omega} \right)_{d\Omega}, \quad (2.8)$$

where the differential cross section $d\sigma/d\Omega$ is given by

$$\frac{d\sigma}{d\omega} = \left(\frac{z_1 z_2 e^2 (M_1 + M_2)}{2 E_p M_1} \right)^2 \frac{1}{\cos^2 \phi}, \quad (2.9)$$

C. RBS Channeling

In addition to RBS measurements, channeling measurements have also been performed. When an incoming beam is aligned with a major crystallographic axis/plane of a crystalline target, there is a significant decrease of the backscattered yield, because the incoming ions are steered into the channel/plane, which decreases the probability of direct collisions. From these measurements, the crystalline quality of the lattice (i.e. defects), crystallographic information on radiation damages and elastic strain can be obtained.

RBS measurements were performed at IUAC, New Delhi and NUS, Singapore. Channeling measurements were performed at NUS. HfO₂/Si samples deposited by both RF sputtering and e-beam evaporation techniques were characterized by RBS. These measurements were performed using 2 MeV He²⁺ at IUAC as well as NUS. RBS spectra were analyzed using SIMNRA simulation software [10].

2.3.2 High-resolution Rutherford Backscattering Spectrometry

Conventional RBS provides a quantitative elemental depth profiling of thin films. The typical energy resolution of the detectors used in RBS is of 10 ~ 15 keV which provides a depth resolution of about 5 nm. The thickness of some of the HfO₂ films used in the current thesis are around 2 to 3 nm. Hence, conventional RBS is incapable of providing depth profiles at such small thicknesses. High-resolution Rutherford Backscattering Spectrometry (HRBS) measurements elucidate such depth profiles of even 1 nm films. This is possible because of the good energy resolution of HRBS system which is around ~1 keV. Kobe Steel Ltd. company manufactured HRBS system at CIBA, NUS, Singapore has been used for the current this work [11].

The experimental setup consists of a Main chamber with an attachment of a load lock chamber, Ultra-high Vacuum (UHV) system (pumps, valves and interlocks), Spectrometer magnet and Micro-Channel Plate – Focal Plane Detector stack (MCP-FPD) and 5-axis Goniometer.

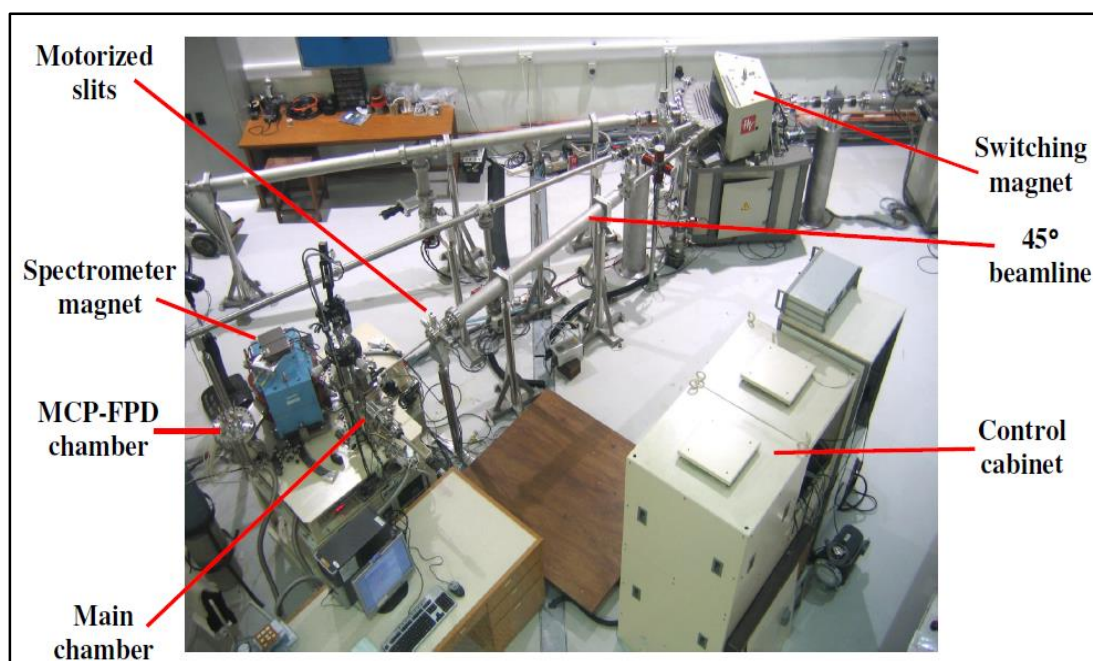


Fig. 2.7: HRBS system at NUS, Singapore

The spectrometer spatially separates the backscattered ions in accordance with their momentum (energy). The role of MCP-FPD is to detect the position of the incidence ions along the focal plane of the spectrometer. Main and the MCP-FPD chambers are always maintained under UHV. A transfer rod is used to exchange the samples which transfers a target holder onto the goniometer attachment in the main chamber from a load-lock chamber through a gate valve. The vacuum interlocks system has been controlled by a program in the control cabinet. So, this facilitates either automatic or manual control of all the valves as well as the goniometer rotation axes. The divergence of the ion beam during the experiments is defined by the motorized slits. Backscattered ions from the sample target enter the detection system, which consists of a spectrometer magnet and a MCP-FPD. The output signal from the FPD is then processed by a system of electronics in the control cabinet to provide information of the position of incidence along the length of the FPD. The output spectrum is sorted by a MCA before the final spectrum is recorded in the computer. The HRBS set-up is shown in Fig. 2.7.

Ultrathin ALD grown $\text{HfO}_2/\text{SiO}_2/\text{Si}$ samples and RF sputtered HfO_2/Si samples have been characterized by HRBS measurements in order to study SHI induced intermixing effects. HRBS and channelling measurements were performed to investigate the film thickness, composition and depth profiles of the samples. These measurements were performed using 500 keV He^+ incident beam. More details have been discussed in the respective chapters.

2.4 Other characterization techniques

2.4.1 X-ray Diffraction

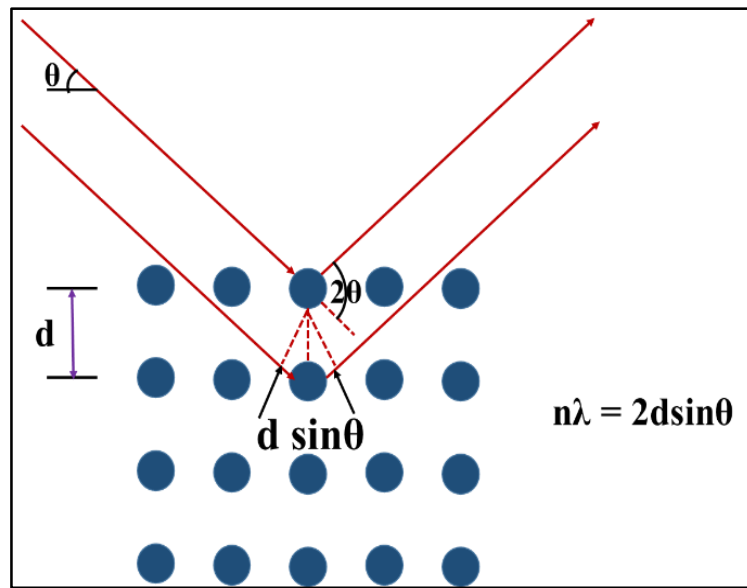


Fig. 2.8: Schematic diagram of XRD pattern

X-ray Diffraction (XRD) is a powerful non-destructive technique for characterizing the crystal structure of materials [12]. Bruker D8 Discover XRD system has been employed in this thesis work. The glancing incidence XRD (GI-XRD), XRD, X-ray reflectivity (XRR) modes can be operated using this system. X-ray diffractometer equipped with $\text{Cu K}\alpha$ ($\lambda=1.5405 \text{ \AA}$) source has been used. The peaks obtained from XRD patterns were indexed by using Joint Committee on Powder Diffraction Standards (JCPDS). XRR measurements were thoroughly performed in this thesis work to investigate the film thickness, surface/interface roughness and density of the samples.

When a monochromatic beam of X-rays is impinged on a crystalline material, a constructive interference can be obtained from the crystal structure of the material under investigation. The schematic of the XRD is shown in Fig. 2.8 and XRD system is shown in Fig. 2.9.

According to Bragg's law, we have

$$2d \sin\theta = n\lambda \quad (2.10)$$

where, d is the inter-planer spacing, θ is the angle between incident beam and lattice planes, λ is the wave length of X-ray and n is an integer (1, 2, ...) [13].

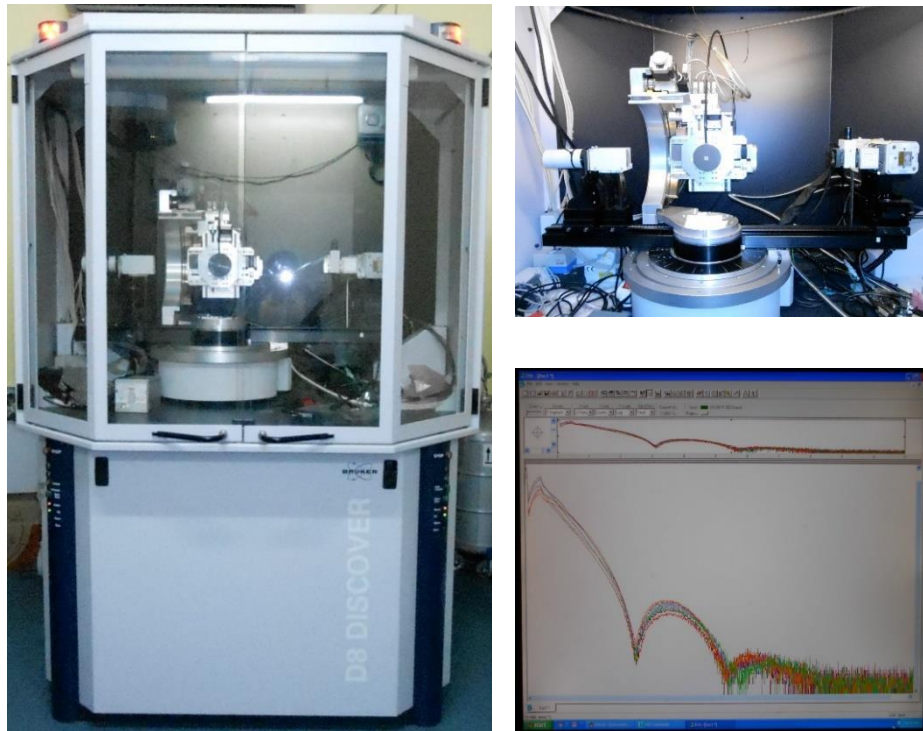


Fig. 2.9: XRD system with goniometer [12]

Some of the samples were further investigated by high resolution X-ray specular reflectometry at grazing incidence angle in the X-ray demonstration and development (XDD) beam line at Singapore Synchrotron Light Source (SSLS), NUS. The diffractometer is the Huber 4-circle system 90000-0216/0, with high-precision 0.0001° step size for omega and two-theta circles. The storage ring, Helios 2, was running at 700 MeV and typically stored electron beam current of 300 mA. X-ray beam was conditioned to select 8.048 keV in photon energy (Cu-K_α radiation equivalent) by a Si (111) channel-cut monochromator (CCM) and toroidal focusing mirror, blocked to be 0.90 mm high in vertical direction and 3.0 mm wide in horizontal direction by a slit system. Such set-up yielded X-ray beam with about 0.01° in vertical divergence. The detector slit was adjusted to be 1.00 mm high to ensure recording all reflected photons. The typical counting time was 5 seconds for every step and step size of 2-theta was 0.02° . Diffuse scattering (background) of off-set scans

were also measured at theta off-set angle of $+0.20^\circ$ in the range of above measurements. The pure reflectivity was obtained by subtracting the diffuse scattering from the raw data. The simulations were performed using M805 and LEPTOS 1.07 release 2004 (Bruker) simulation software.

2.4.2 Field Emission Scanning Electron Microscopy

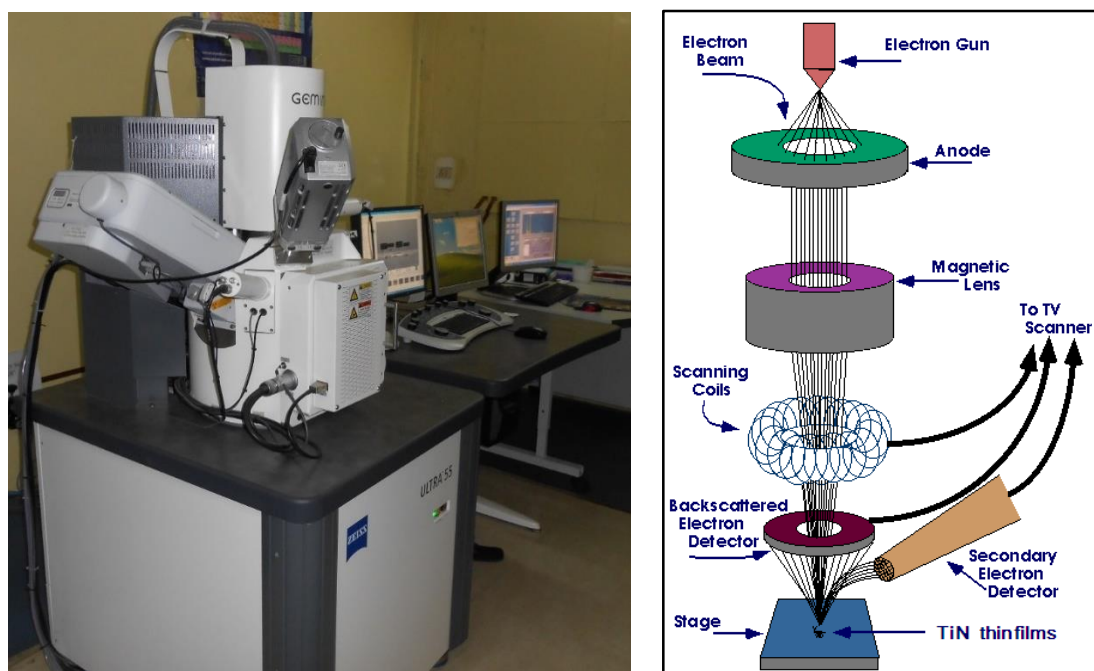


Fig. 2.10: Carl ZEISS, FEG, Ultra 55 FESEM system with its schematic diagram

Field Emission Scanning Electron Microscopy (FESEM) technique has been used to investigate the morphology, elemental composition and the film thickness (cross-sectional FESEM measurements). FESEM system with a schematic representation is shown in Fig. 2.10. FESEM produces an image from a sample's surface by scanning it with high energetic narrow electron beam in a raster scan pattern. This electron beam provides the feasibility of getting micrographs at a larger depths of field and offers a characteristic three dimensional appearance which is very useful for better understanding the surface morphology of the samples. A field emission gun which is specially designed and is made up of tungsten wire moulded in a fashion that the electric field can be focussed at the tip of the wire. The use of field emission gun is the key feature in FESEM which can provide the narrow beams with high electron energy. The high energetic electron beam emanating from this tungsten tip is focused to a spot size of about 1 to 5 nm on the sample surface using

condenser electromagnetic lenses. The necessary scanning mechanism is enabled by a pair of scanning coils. Different types of secondary radiations can be produced when the electrons are interacting with the specimen. This radiation consists of back scattered electrons, secondary electrons and X-rays etc.

Carl ZEISS, FEG, Ultra 55 model has been employed for current thesis work. Surface topology and film thickness (cross-sectional FESEM measurements) of HfO_2 samples deposited by RF and e-beam evaporation methods have been investigated.

2.4.3 Profilometer

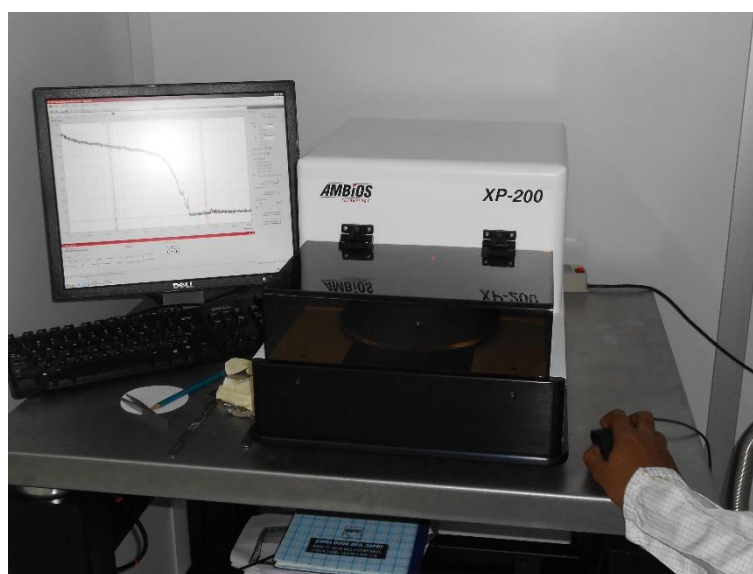


Fig. 2.11: Ambios XP-200 profiler

It is a stylus Ambios Technology profiler [14], Model: XP-200 at CFN, UoH. This stylus profiler offers measurements electromechanically by moving the sample underneath a diamond tipped stylus. A high precision stage moves the sample with a desired scan length, speed and stylus force. The stylus is mechanically coupled to the core of a Linear Variable Differential Transformer (LVDT) and the stylus moves over the sample surface. Surface variations can cause the stylus to be turned vertically. The LVDT changes can be observed in accordance with the stylus movement which produces the electrical signals. The LVDT scales an AC reference signal proportional to the change in the position, which will be converted to a digital format through integrating analog-to- digital converter. In general, the films whose thickness has to be measured is covered with a mask which creates a step on the surface of the sample. Then, the thickness of the sample can be measured precisely

by measuring the vertical motion of the stylus over the step. Ambios XP-200 profiler which is shown in figure 2.11 and the schematic is shown in Fig. 2.12.

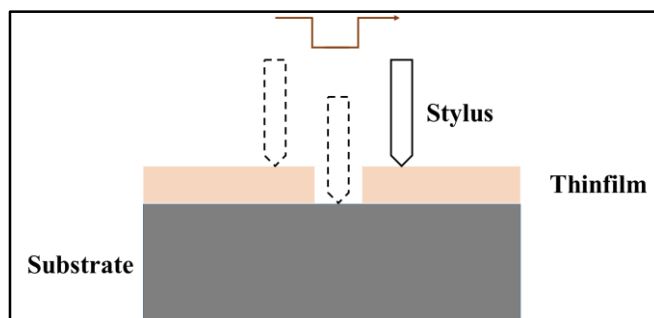


Fig. 2.12: Schematic of stylus profiler

Thickness of e-beam deposited and RF sputtered samples was estimated by Profilometer. More details about these results have been discussed in relevant chapters.

2.4.4 Ultraviolet–Visible (UV-Vis) spectrophotometer



Fig. 2.13: JASCO V-570 double beam spectrophotometer at UoH

UV-Vis spectroscopy is used for to absorption or reflectance spectroscopy in the ultraviolet-visible region [15]. UV–vis absorption spectra were recorded at room temperature in the wavelength range of 200-900 nm. A polished Al mirror is used as a standard sample for reference. Fig.2.13 depicts the UV-Vis spectrophotometer and the schematic is shown in Fig. 2.14. A halogen lamp and a deuterium (D_2) lamp are commonly used for ultraviolet region and visible region respectively. The light from the sources gets reflected from a mirror 1 and then the resultant beam passes through slit-1 and hits a diffraction grating positioned in the same path.

The grating can act as a monochromator to select a preferred wavelength. The selected monochromatic beam passes through the slit-2 and the beam is conceded to pass through the filter. The filter (long pass / short pass) is used for removing the unnecessary higher order reflections. This fine-tuned final light beam hits the second mirror before it gets splitted by the half-wave plate. This transmitted beam is then allowed to pass through a reference sample and the reflected beam passes through the sample. The reflectivity (%R) is expressed as the intensity ratio between the light reflected from the sample (I) and the reference sample (I_0). Absorption, reflection and transmission measurements have been performed on HfO_2 thin films to estimate the energy band gap and refractive index of HfO_2 thin films. These studies have been carried out by using JASCO V-570 UV-Vis double beam spectrophotometer. More details about the estimation of band gap and refractive index of these samples have been discussed in respective chapters.

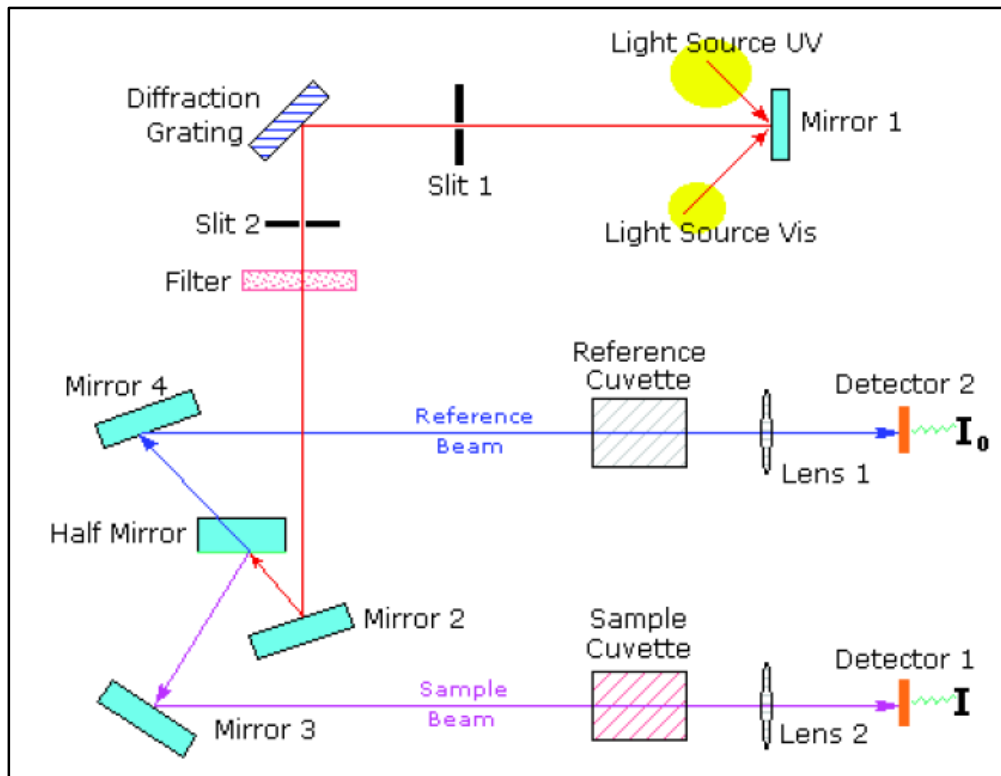


Fig. 2.14: Schematic of UV-Vis spectrophotometer [16]

2.4.5 Electrical characterization

Fig. 2.15 depicts this experimental set-up of Agilent B1500A Semiconductor Device Analyzer with Signatone P1160 probe station. It is a versatile Current-Voltage Analyzer

Series system which supports I-V, C-V, pulse/dynamic I-V and etc. The comprehensive measuring capabilities of this system provide the electrical characterization of the devices with uncompromised reliability and efficiency. Easy EXPERT group+ GUI based characterization software associated with this system makes the characterization tasks at a faster speed. As soon as the device characterization is completed, data will be instantly stored in a specific built-in database (workspace). B1500A system is equipped with standard SMU modules which enables to perform I-V measurements. Further, quasi-Static C-V measurement have also been supported by SMU. Capacitance measurements are supported by MFCMU modules and the switching between I-V and C-V measurements is possible with SCCU without usage of a different external switching matrix.

Electrical measurements (I-V and C-V) were performed to investigate I-V and C-V characteristics of HfO₂ based MOSCAPS using semiconductor device analyzer at Centre for Nanotechnology (CFN), UoH.

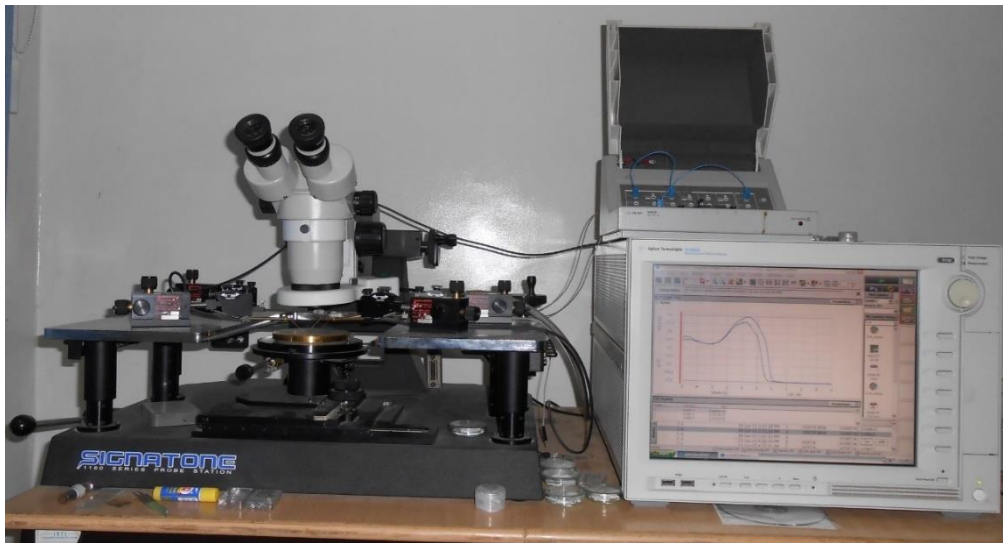


Fig. 2.15: Agilent B1500A Semiconductor device analyzer with Signatone P1160 probe station at CFN, UoH [17]

2.4.6 Rapid thermal annealing

The issues of the thermal budget problems in terms of the peak temperature and exposure time in normal furnace annealing have been resolved by rapid thermal annealing (RTA) processing [18]. The ramp and cooling cycles can be achieved within few minutes and reduce wafer emissivity variation and temperature non-uniformities. In order to attain uniform heat transfer, tungsten-halogen lamps are symmetrically placed above and below.

Fig.2.16 shows the Anneal Sys RTA system available at CFN, UoH. The schematic of RTA processing is shown in Fig. 2.17. In this case, the ramp down rate has been programmed to have slower rates with a holding step at different temperatures in order to minimize slip formation.



Fig. 2.16: AS-One Anneal Sys RTA system at CFN, UoH

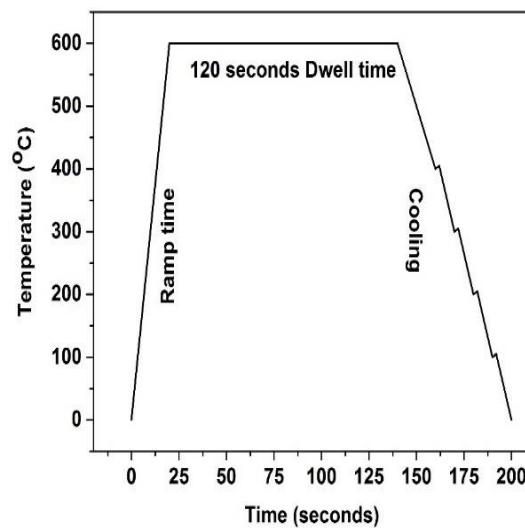


Fig. 2.17: Schematic of typical annealing profile of RTA

HfO₂ based MOSCAPS have been treated by the RTA processing at 600 °C temperature in N₂ atmosphere. Specific details about the effects of RTA processing have been discussed in relevant chapters.

2.5. Experimental details

2.5.1 Sample specifications

A brief summary of sample specifications, material treatment and characterization techniques are given below. Each sample series consists of many samples prepared under identical conditions. More specific details are provided in respective chapters.

Table 2.1: Sample specifications

S.No.	Sample series	Sample structure	Growth technique	Characterization techniques
1.	R	HfO ₂ (~15 nm) / Si	RF sputtering	RBS, XRR, EDS, Profilometer, I-V and C-V
2.	E	HfO ₂ (~15 nm) / Si	e-beam	RBS, XRR, EDS, Profilometer, I-V and C-V
3.	H1	HfO ₂ (3.0 nm) / SiO ₂ (0.7 nm) / Si	ALD	HRBS, XRR and I-V
4.	H2	HfO ₂ (2.5 nm) / SiO ₂ (1 nm) / Si	ALD	HRBS, XRR
5.	H3	HfO ₂ (2.7 nm) / SiO ₂ (0.6 nm) / Si	ALD	HRBS, XRR and in-situ I-V and C-V

2.5.2 Material treatment and characterization techniques

Each sample was cut into a few counter parts and each set of the sample has a pristine sample. Gamma irradiation details and characterization techniques have been mentioned below.

Table 2.2: Gamma irradiation and characterization techniques details

Sample Series	Gamma irradiation	Characterization techniques
R	1-48 kGy at 4.64 kGy/hr	I-V and C-V
E	1-48 kGy at 4.64 kGy/hr	I-V and C-V

R, H1, H2, and H3 series samples were irradiated by SHI irradiation and the details of all the irradiations are mentioned in the following table.

Table 2.3: SHI irradiation and characterization details

Sample Series	Ion Irradiation	Characterization techniques
R	80 MeV Ni ions at 1×10^{11} to 5×10^{13} ions/cm ²	EDS, RBS, XRR, Profilometer and I-V
	120 MeV Au ions at 1×10^{10} to 1×10^{14} ions/cm ²	HRBS, XRR, and in-situ I-V and C-V
H1	120 MeV Au ions at 1×10^{13} to 1×10^{14} ions/cm ²	HRBS, XRR and I-V
H2	80 MeV Ni at 5×10^{12} and 5×10^{13} ions/cm ²	HRBS and XRR
H3	120 MeV Ag ions at 1×10^{13} to 1×10^{14} ions/cm ²	HRBS, XRR and in-situ I- V and C-V

2.6 References:

1. Terry L. Alford, Leonard C. Feldman and James W. Mayer, "Fundamentals of Nanoscale Film Analysis", Prentice-Hall, New Jersey (2007).
2. Wei-Kan Chu, James W. Mayer and Marc-A. Nicolet "Backscattering Spectrometry", Academic Press, Inc. Harcourt Brace Jovanovich Publishers, New York (1978).
3. Bernd Schmidt and Klaus Wetzig, "Ion Beams in Materials Processing and Analysis", Vienna (2013).
4. D. K. Avasthi and G. K. Mehta, "Swift Heavy Ions for Materials Engineering and Nanostructuring", Capital Publishing Company, New Delhi (2011).
5. "Gamma source 1200cc", <http://www.britatom.gov.in/htmldocs/products06c.html>.
6. D Kanjilal, S Chopra, M M Narayanan, I S Iyer, V Jha, R Joshi and S K Datta, *Nucl. Instr. and Meth. A*, **238** (1993) 97.
7. <http://www.iuac.res.in/accel/pell/index.html>.
8. J.W. Mayer and E. Rimini, "Ion beam handbook for material analysis", Eds. Academic press, New York (1977).
9. <http://www.iuac.res.in/accel/paras/>
10. M. Mayer, SIMNRA: Simulation of RBS, ERD and NRA spectra, <http://www.rzg.mpg.de/~mam/>
11. Chan Taw Kuei, Ph.D. thesis, National University of Singapore, Singapore and refs. therein (2009).
12. B. D. Cullity, "Elements of X-ray Diffraction", Addison-Wesley Publishing Company Inc., Reading, Massachusetts (1956).
13. C. Kittel, Introduction to solid state physics, 8th edition, John Wiley & Sons, Inc., Publication, USA (2005).
14. <http://mnmm.physics.mcgill.ca/content/ambios-xp200-profiler>
15. <http://www.jascoinc.com/spectroscopy>
16. O. Stenzel, "The Physics of thin film Optical Spectra: an Introduction", Springer, Germany (1996).
17. <http://www.keysight.com/en/pd-582565-pn-B1500A/semiconductor-device-analyzer?cc=IN&lc=eng>
18. Richard B. Fair, edited "Rapid Thermal Processing: Science and Technology", Academic Press, Harcourt Brace Jovanovich Inc., California (1993).

Synthesis and Characterization of HfO₂ thin films

This chapter provides some experimental results on the synthesis of HfO₂ thin films which were prepared by various deposition techniques such as RF magnetron sputtering, e-beam evaporation and Atomic Layer Deposition. These studies suggested appropriate sample structures for further investigations presented in this thesis.

3.1 Introduction

Integrated Chip (IC) fabrication reconnoitered at a critical rate to produce high-quality thin films to engineer the sophisticated electrical devices which in turn aided the evolution of certain deposition techniques [1]. This rapid evolution of deposition technology has produced a significant growth in improving the quality of thin films [2]. These high-quality thin films in modern technology have different applications. The functionality of the devices evolved from these films are unambiguously expedient owing to their structural, electrical and optical properties [3]. However, it is important to study the role of the surfaces, interfaces and microstructures on the quality of these devices fabricated by various techniques [4]. In the contemporary research fields, intense investigations are essential to comprehend the physical mechanisms during the deposition such as the interaction between charged particles, the surface of the target material, adherence between the substrate and the deposited material and the chemical reactions taking place near the interfaces [5]. In addition to these prominent features, the deposition parameters like working pressure, the density of a target material and the substrate temperature etc. have also been used as controlled parameters to tune the material properties [6]. Most persuasively, MOS devices have been the basis for the *state-of-the-art* integrated circuit technology in the perspective of the emerging trends in IC fabrication [7]. However, thin film technology has shown an imperious role in emerging new generation MOS devices. Developing the basic structure of these devices poses a demand on the current fabrication technology as the thickness of these devices is being scaled down to a few nanometers [8]. Consequently, various deposition methods have been developed to meet these demands. Broadly there are two main streams of the deposition methods, known as Physical and Chemical Vapor Deposition (PVD and CVD) methods. Sputtering, electron beam evaporation, thermal evaporation, Molecular Beam Epitaxy (MBE) and Pulsed Laser Deposition (PLD) fall into the category of PVD method whereas CVD method covers Atomic Layer deposition (ALD), Atmospheric Pressure CVD (APCVD), Plasma Enhanced CVD (PECVD) and Low Pressure CVD (LPCVD) [9].

The present thesis work comprises the study of HfO_2 based MOS devices fabricated by a combination of RF magnetron sputtering, thermal & e-beam evaporation and ALD methods. The details of these methods (except ALD [10]) are described in following sections.

3.1.1 Thermal evaporation technique for depositing metal contacts

Thermal evaporation is one of the simplest PVD deposition techniques. Moreover, it is one of the widely used and convenient technique for depositing thin films and metal contacts. It is a process of heating a source material until it gets evaporated and deposited on the surface of a substrate. This heating of the target material can be achieved by many methods but the simplest is the resistive heating of a source material placed in a crucible made of a refractory metal (tungsten or tantalum) strip or shaped filaments. High currents are used to heat and evaporate the material.

The evaporated atoms will reach the substrate surface and condense on it. Here, the deposition rate is mainly a function of the distance between the source and the substrate and the angle of impingement onto the substrate surface. The growth mechanism of the films depends on the substrate temperature and the purity of the films depends on the pressure during deposition.

In the present study, thermal evaporation method has been employed for depositing Au metal contacts (250 nm to 300 nm) on surface of the HfO_2 samples to form required MOS structures.

3.1.2 e-beam evaporation method

Resistive heating, described in previous section, alone is not sufficient to reach higher melting points of some materials. Hence, e-beam evaporation method is preferred for those materials including HfO_2 . In this method, a highly energetic beam of electrons is produced by a heated filament (tungsten filament) which is directed onto the target surface placed in a crucible by employing necessary magnetic fields. Sufficient thermal energy is produced in this process to evaporate / sublimate the materials of interest. e-beam evaporation system is equipped with an anode (positively biased) and a cathode (either grounded or negatively biased with respect to the anode). Electrons that are emitted from the heated tungsten filament are directed to the charged material by applying a high DC bias voltage (10 - 40 kV). During this process, the crucible is cooled down using a pumping circuit of cooled water so that there are very small chances of impurities in the crucible to contaminate the target material used for evaporation. Some of the HfO_2 samples used in this thesis were grown by e-beam evaporation method at IUAC.

3.1.3 Sputtering techniques

Sputter deposition method yields high-quality thin films with exceptionally good electrical, optical, mechanical and chemical properties. Hence sputtering techniques are considered as versatile techniques for depositing high-quality and well-adhered films of an extensive range of materials with relatively high rates of deposition.

Sputtering is merely a process of erosion of a material from the target surface by the energetic particles, just like atomistic sandblasting. As a result, these sputtered atoms accumulate on the surface of the substrate. The incident species can be atoms, ions, electrons, photons, neutrons or molecules. In most of the cases, sputtering can be made with ion bombardment preferably with inert gas ions such as Ar^+ and Kr^+ . Sputtering depends upon the transfer of physical momentum and kinetic energy of the incident particle to the target surface atoms. The incident particle with sufficient energy impacts the surface atoms of the target material leading to two important processes: 1) bond breaking and 2) dislodging of the target atoms which are then directed towards the substrate surface.

Basically, there are two types of operations in sputtering technique namely: 1) DC sputtering and 2) RF sputtering. Both of these techniques are extensively studied for depositing thin films of various types of materials. In general, depending upon the conductivity of the target material either RF or DC sputtering may be used. The working mechanism of these two distinctive techniques is as follows.

A. DC sputtering

DC sputtering is the simplest type of a plasma device. It consists of an anode and a cathode inside a vacuum chamber. If the target is a conductor, a constant voltage is applied to accelerate the ions and correspondingly a DC power supply is used to create the plasma by providing an adequate voltage across the electrodes under a proper gas pressure (Ar gas). The Ar gas turns in to a plasma by gas discharge. Collisions take place between the energetic electrons that are accelerated by the electric field from the target material and the molecules of the Ar gas to make them positive ions. Secondary electrons are also generated from the cathode after a bombardment of these positive ions with the cathode surface. These secondary electrons are accelerated back and collide with the gas atoms in order to increase the intensity of ionization discharge. More importantly, the ions bombarding the target surface initiate the sputtering phenomena.

DC sputtering has a limitation of so-called low deposition rates. Moreover, since the surface of the target can be charged promptly due to the electrons from the DC power supply, only conductive targets can be sputtered by using this technique. This challenging issue can be resolved by using RF sputtering technique described in next subsection.

B. RF sputtering technique

The issue of the usage of insulating target materials in DC sputtering has been sorted out by replacing the DC power source with an RF source. If the target material is an insulator, the movement of free charges is inhibited naturally. As the ions strike the surface, their charge build up on the surface of the target makes it impossible for further bombardments. So, to relieve these charge buildups, an alternating current is generally used at a frequency in the range of 13.56 MHz. Plasma created by the RF power supply operates at high-level frequencies. High frequency is always used so that the heavy ions cannot follow the fast switching rate and eventually make the electrons to hit the target for neutralizing the charge. However, this RF source operates in a different way than the DC source. Anode and cathode are electrically reversed in each cycle to remove the charge build up on the insulating target material by providing an equal number of ions. This allows insulators or even conductors to be sputtered by RF sputtering. Higher deposition rates, lower voltages and lower gas pressures are the significant features of RF sputtering technique. Sputter cathodes are generally equipped with magnetrons to further enhance the deposition rates by confining the electrons within the region of interest.

RF magnetron sputtering has extensively been used in this thesis to prepare necessary HfO_2 thin films.

3.2 Experimental details

HfO_2 thin films were grown on both, the Si and Quartz for electrical and optical studies respectively. High quality p-type, B-doped (1–10 Ohm-cm) Si (100) substrates have been employed for fabricating HfO_2 based MOS devices. Si substrates were cleaned by using standard Radio Corporation of America (RCA) procedure to remove the native oxide,

organic and inorganic contaminations [11]. A newly installed RF magnetron sputtering system has been used for executing the current thesis work (see Fig. 3.1).



Fig. 3.1: RF magnetron system at UoH



Fig. 3.2: RF sputtering chamber (an inside view)

HfO₂ thin films were grown by RF sputtering technique using a HfO₂ target (99.99% pure) of 2-inch diameter and 3 mm thickness. Fig. 3.2 depicts the inside view of the chamber of RF sputtering system and Fig. 3.3 shows the schematic of this system. The sputtering was performed in high purity (99.999%) Ar ambiance. Prior to the deposition, the chamber was evacuated down to 7×10^{-6} mbar and the deposition pressure was found to saturate at 2×10^{-2} mbar. Fig. 3.4 shows the control panel for programing the process of operation. The synthesis of HfO₂ samples on the quartz and Si substrates was carried out at different

deposition conditions such as RF power, deposition pressure, target to substrate distance and Ar flow (by varying one parameter at a time). After optimizing all these conditions, good quality ~15 nm HfO₂ thin films were deposited on Si and quartz substrates for further investigations.

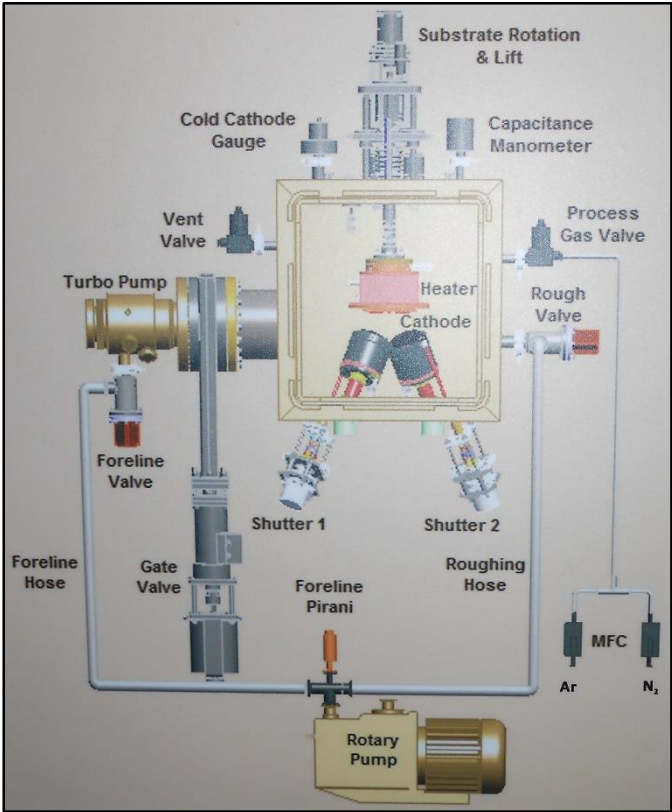


Fig. 3.3: Schematic of the RF magnetron sputtering system

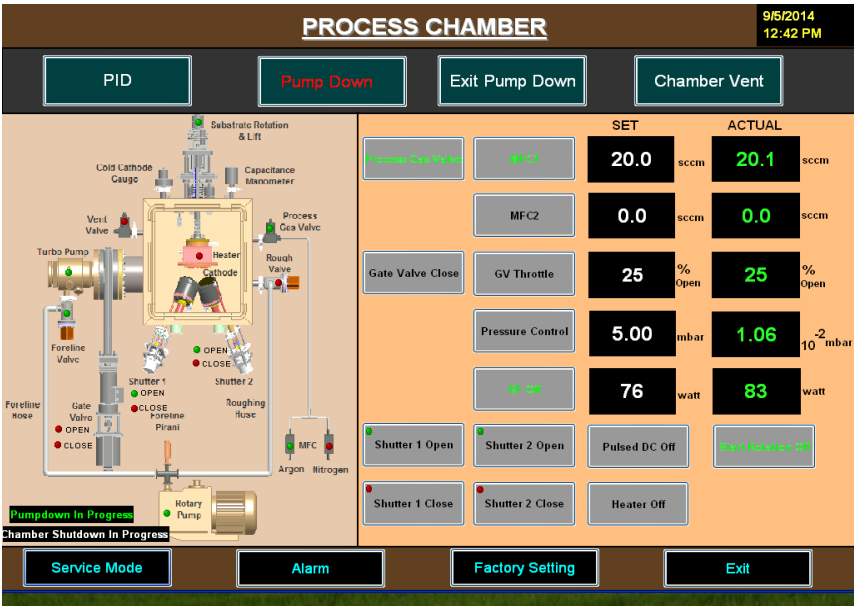


Fig. 3.4: Control panel of RF magnetron sputtering system

The thickness of the deposited films was estimated using a Profilometer. Bruker D8 Discover diffractometer equipped with Cu K_{α} ($\lambda = 1.5405 \text{ \AA}$) was used for XRR measurements (glancing angle was 0.5°). RBS measurements were performed using 2 MeV He^{2+} at a scattering angle of 165° at IUAC, New Delhi. Calibration offset value of 74 keV and energy per channel of 0.9725 keV/ch were determined using a standard calibration sample (Au/glass). SIMNRA software was used for RBS simulations [12]. Transmittance and Reflectance (T&R) measurements were performed in the wavelength range of 190–2000 nm using JASCO V-570 Photo Spectrometer to measure the bandgap of HfO_2 films, consequently, the refractive index was estimated.



Fig. 3.5: e-beam evaporation system at IAUC, New Delhi (inset –Cu crucible and a substrate holder) [12]

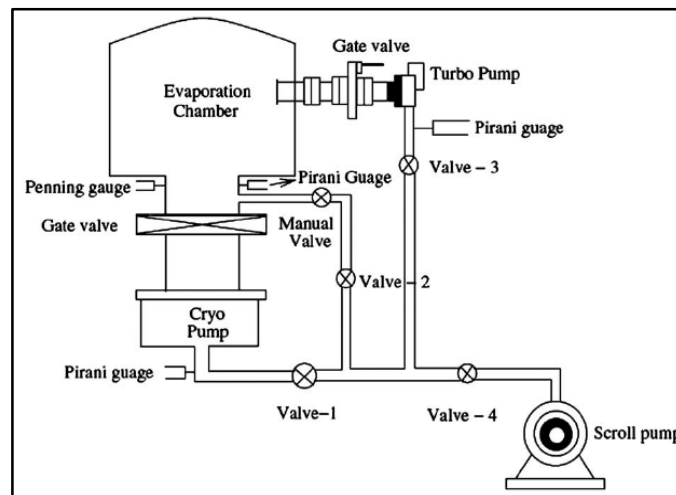


Fig. 3.6: Schematic of e-beam system at IUAC (13)

e-beam evaporation has been performed at IUAC, New Delhi. The e-beam evaporation system (see Fig. 3.5) attains an Ultra-High Vacuum (UHV) of the order of 10^{-9} Torr with

the help of a scroll pump, a turbo molecular pump and a cryo-pump. This system is equipped with a 15 kW electron gun and a four pocket copper crucible. Currents of the order of 100 mA are used to evaporate the target material of choice. A quartz crystal thickness monitor is used to monitor the rate of deposition and hence the thickness of the films. The schematic diagram of the UHV chamber is shown in Fig. 3.6.

A pellet made of 98% pure HfO_2 powder (2% impurity may be attributed to the presence of Zr as Hf and Zr are chemically similar structures) was evaporated. The target to substrate distance has been kept at around 24 cm. The rate of deposition was maintained at $\sim 0.1 \text{ \AA/s}$, the current was kept at 75 mA and the observed pressure during deposition was 8.4×10^{-3} mbar. $\sim 15 \text{ nm}$ HfO_2 thin films were deposited on Si. These films are termed as EB-AD series samples. Some of the samples were annealed in the O_2 atmosphere at 450°C for an hour to obtain a better stoichiometric HfO_2 films which are termed as EB-AN series samples.



Fig. 3.7: Thermal evaporation system available at CFN, UoH

Thermal evaporation technique has been used for depositing Au metal contacts. A photograph of the thermal evaporation system situated at CFN, UoH is shown in Fig. 3.7. This system is equipped with a rotary pump and a turbo molecular pump. This system can provide a vacuum of the order of 4×10^{-6} Torr and during deposition, it is found to be 3×10^{-5} Torr. This system is also equipped with a quartz crystal thickness monitor which enables us to monitor the rate of deposition as well as the thickness of films. A deposition rate of 2 \AA/sec has been maintained while applying a current of 120 A.

As discussed earlier, HfO₂ thin films were grown by different deposition techniques. These films were characterized by various techniques including XRR, FESEM, Profilometer, RBS, UV-Vis-NIR spectroscopy as described in the previous chapter. Finally, Au metal contacts (250 nm to 300 nm) were deposited on HfO₂ films by thermal evaporation technique for fabricating good quality Au/HfO₂/Si MOS capacitors. I-V and C-V measurements were performed on these MOSCAPs to investigate the leakage current and the variation of capacitance as a function of applied bias. These measurements were performed using an Agilent technologies B1500A semiconductor device analyzer. The applied bias voltage range was -5 V to + 5 V.

3.3 Growth kinetics – Nature of the traps associated during film growth

Growth mechanism and kinetics that are associated during the deposition are very important to elucidate the properties of thin films. Structural properties of the films may vary with the growth kinetics. During the growth of these films, defects/impurities are unavoidable. The density of these defects/impurities can seriously alter the electrical characteristics of MOS devices. Various kinds of defects such as mobile charges, interface and oxide trapped charges can deteriorate the operation of MOS devices which is evident from I-V and C-V measurements. Each of these defects has a certain impact on the device operation and performance. The nature and origin of these defects have to be understood. Further, the radiation response of these technologically important devices has been discussed in the following chapters. One of the main reasons for employing different growth techniques in this thesis work has been to investigate the influence of growth technique on the nature of defects and their evolution during irradiation studies. Gamma and/or ion irradiation induced annealing / creation of defects and inter-diffusion constituent elements have been studied in detail.

3.4 Results and discussion

3.4.1 HfO₂ thin films deposited by RF magnetron sputtering

HfO₂ thin films were synthesized by RF magnetron sputtering technique. These films were characterized by various techniques to investigate their structural and electrical properties. After optimizing all the conditions, HfO₂ films of ~15 nm thickness were deposited on Si and quartz substrates for further studies.

A. Structural and optical characterization of HfO₂ thin films

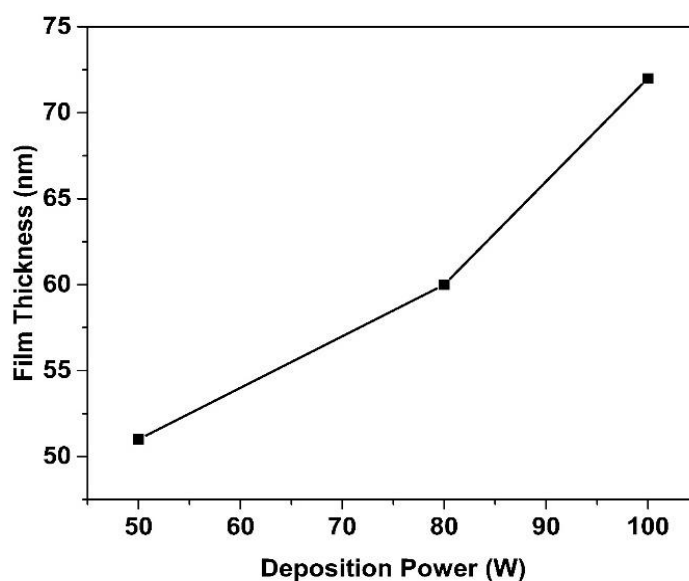


Fig. 3.8: HfO₂ films deposited at different RF powers (from Profilometer)

HfO₂ thin films were deposited on the quartz and Si substrates in each run. Several runs were performed at different deposition conditions such as RF power, deposition pressure, target to substrate distance and Ar flow. The influence of RF power on the formation of HfO₂ thin films was studied by depositing those films at three different powers (50 W, 80 W and 100 W) while maintaining all the other parameters identical in each run. High RF powers have been preferred to obtain reasonable deposition rates owing to the high density of target material (Density of HfO₂ is around 9.68 g/cm³). Moreover, for 2-inch target, 80 W is about the maximum RF power which can be used for sputtering without damaging the sputter target. 100 W RF power has also been tested in this thesis but high powers damage the targets as well as samples due to high fluence of Ar⁺ ions generated in the Plasma. It is well known that all the insulating sputtering targets are brittle in nature and they undergo a temperature gradient as the cathode is cooled down to room temperature during deposition. After several runs, this temperature gradient may lead to the target breakage. Based on these practical implications, the promising results that are obtained from the 80 W RF power depositions indicate that this process yielded good quality HfO₂ thin films with reasonable growth rates. Hence, 80 W RF power has been considered as an optimum power for further depositions of HfO₂ films in our RF magnetron sputtering system. At a fixed RF power and deposition time (1 hr), target to substrate distance and the Ar flow of 10 sccm and 20 sccm were varied. Since, better growth rates are observed with

10 sccm Ar flow, the depositions were all carried out at this flow rate. Fig. 3.8 shows the film thickness as a function of RF power for HfO₂ films deposited on Si at 10 sccm Ar gas flow and at 12 cm target to substrate distance for 1 hr deposition time. RBS and Profilometer measurements have been employed to estimate the film thickness. Then a set of HfO₂ films were prepared at different “target to substrate distances” and 80 W power while maintaining all other parameters as specified above. The thickness of films was estimated by RBS and Profilometer measurements. The deposition rates have been calculated from Profilometer measurements.

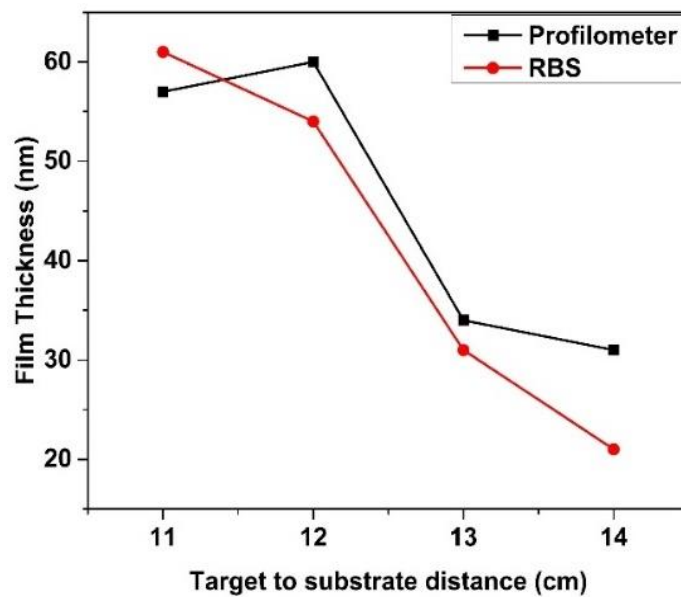


Fig. 3.9: Film thickness variation obtained from Profilometer and RBS as a function of target to substrate distance

Fig. 3.9 shows the film thickness obtained from RBS and Profilometer measurements at different target to substrate distances (11 cm to 14 cm). As the target to substrate distance increases, HfO₂ film thickness decreases as expected. Good quality HfO₂ thin films have been attained at 12 cm “target to substrate distance”. So 12 cm target to substrate distance has been considered as the optimum distance for further depositions. Hence the RF power, target to substrate distance, Ar flow were kept constant at 80 W, 12 cm and 10 sccm respectively for further depositions performed as a part of this thesis work.

Fig. 3.10 displays the RBS spectra of these films. Areal density has been observed from 196×10^{15} to 409×10^{15} atoms/cm². These areal density values have been converted to thickness in nm (see table 3.1) by considering the actual density of HfO₂ as 9.68 g/cm³.

The atomic concentrations of Hf has been found to be 33% and Oxygen is 67%. So, stoichiometric HfO₂ has been formed on Si substrates. These results are tabulated in table 3.1.

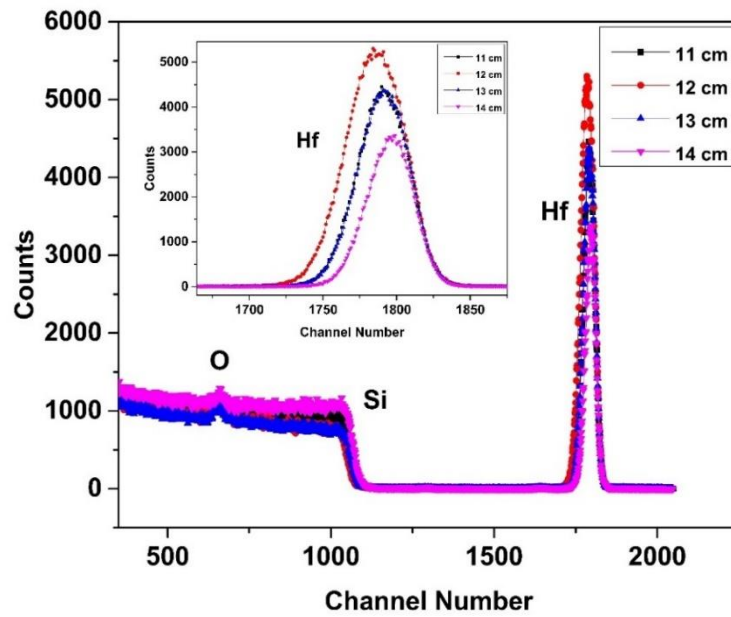


Fig. 3.10 RBS spectra of HfO₂ films deposited at various target to substrate distances

Table 3.1: Thickness, growth rate obtained from RBS and Profilometer measurements

Target to Substrate distance (cm)	Profilometer measurements (nm)	RBS measurements (nm)	Growth rate (nm/min)
11 cm	57	61	0.9
12 cm	60	54	1.0
13 cm	34	31	0.5
14 cm	31	31	0.5

UV–vis spectroscopy measurements were performed on both the Si (reflection mode) and quartz (transmission mode) substrates. Spectral dependence of absorption coefficient (α) in the region of fundamental absorption edge is generally studied by the well-known Tauc's relation (see eq. 3.1), which can be used to find out energy band gap of a material [13].

$$\alpha h\nu = B (h\nu - E_g)^r \quad (3.1)$$

where $h\nu$ is the energy of the incident photons and E_g is the value of the optical band gap corresponding to transitions indicated by the value r which is characteristic of the type of the optical transition process. In the literature, it is widely stated that HfO_2 is an indirect band gap material with $r=2$. Hence, the optical band gap (E_g) of HfO_2 films has been determined by the absorption coefficient (α) using the Tauc's relation.

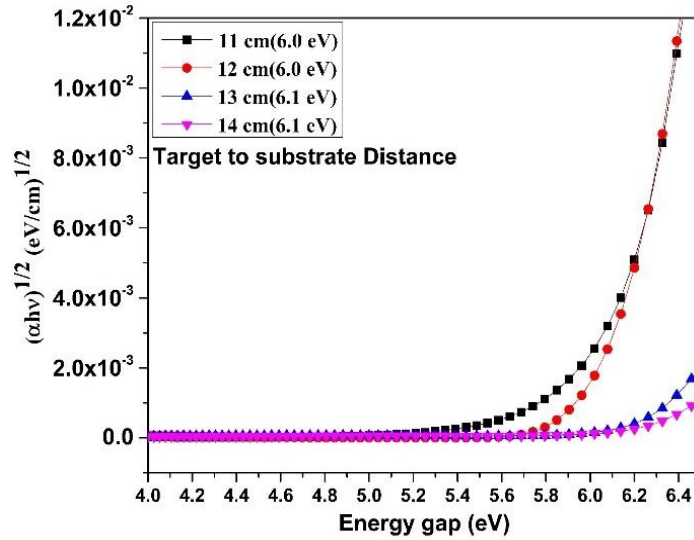


Fig. 3.11: Band gap measurements from transmission spectra at different target to substrate distances

Fig. 3.11 shows the transmission spectra for obtaining the bandgap of the HfO_2 samples as the target to substrate distance was varied between 11 cm to 14 cm. The bandgap of HfO_2 was found to be around ~ 6.0 eV. In the E_g region (high absorption) or above the fundamental absorption edge, the absorption follows a power law as [13]

$$\alpha h\nu = B (h\nu - E_g)^n \quad (3.2)$$

where $h\nu$ is the energy of the incident photon, B is the parameter of the absorption edge width and E_g is the band gap. The exponent n (refractive index) can be determined by the type of the electronic transitions causing the optical absorption.

The refractive index n can be estimated by [13],

$$n = [N + (N^2 - s^2)^{1/2}]^{1/2} \quad (3.3)$$

where
$$N = 2s \frac{T_M - T_m}{T_M T_m} + \frac{s^2 + 1}{2}$$

Generally, n can take values $\frac{1}{2}$ and 2 for direct-allowed and indirect-allowed transitions, respectively. The band gap of thin films can be estimated by extrapolating the linear parts of the curves plotted from the formula where $\alpha(h\nu) = 0$.

T_M and T_m are the extremes of the interference fringes in the transmission spectra. Based on this formula, the refractive index of HfO_2 thin films has been estimated. The estimated refractive index is around ~ 1.6 to 2.0 (see Fig. 3.12).

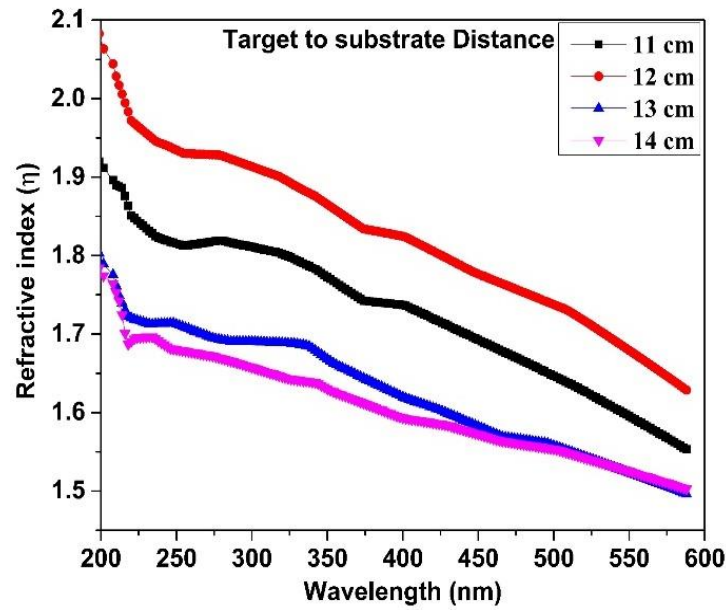


Fig. 3.12: Refractive index measured at various target to substrate distances

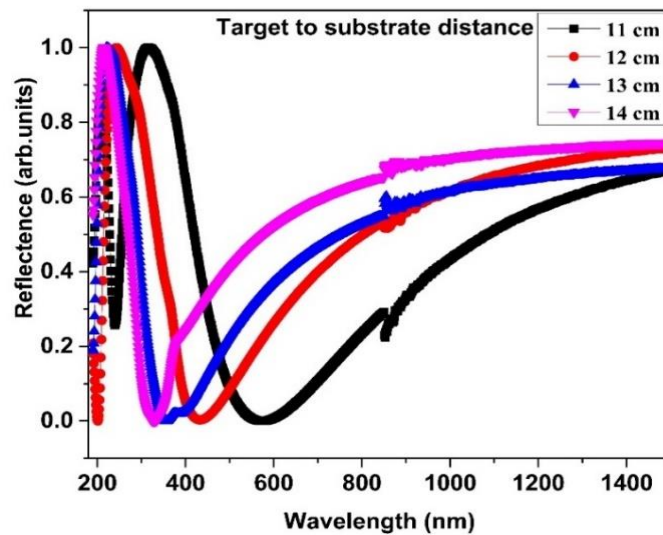


Fig. 3.13: Reflectance spectra of HfO_2/Si samples prepared at various target to substrate distances

Fig. 3.13 and Fig 3.14 show the Reflectance and absorbance spectra. Reflection and absorption measurements were performed on Si and quartz substrates respectively. A precise estimation of optical absorption constant (α) enabled the determination of the optical band gap of these films.

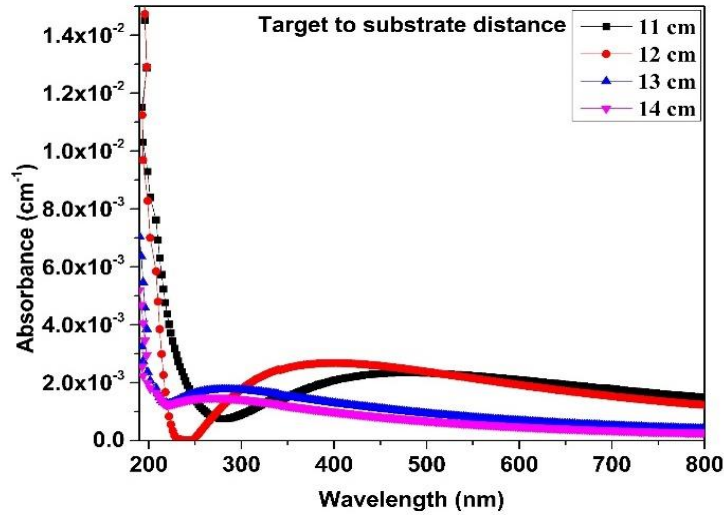


Fig. 3.14: Absorbance spectra of HfO₂/quartz prepared at various target to substrate distances

B. Samples of interest (Structural, optical and electrical characterization of HfO₂ thin films)

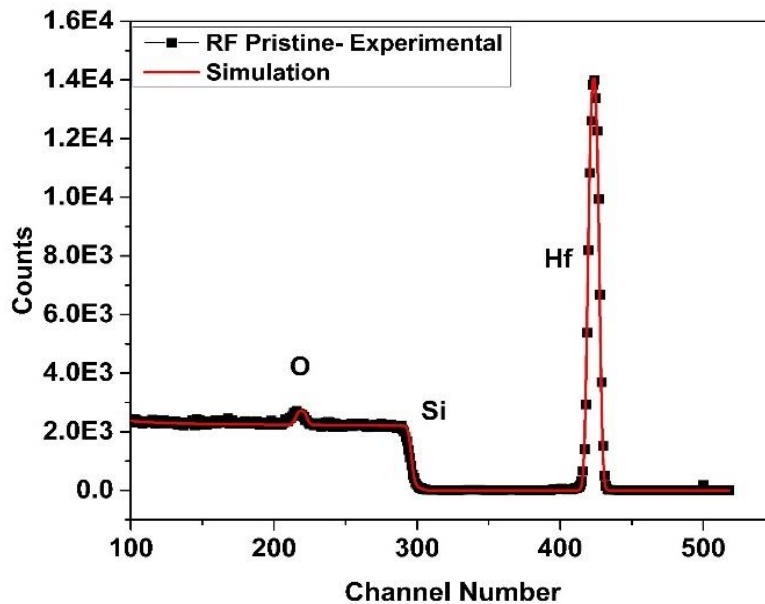


Fig. 3.15: RBS spectrum for pristine samples deposited by RF magnetron sputtering system

After optimizing all these conditions, good quality RF series HfO₂ thin films (~15 nm) were deposited at 80 W RF power, 12 cm target to substrate distance and the 10 sccm Ar flow for 15 minutes. Structural, optical and electrical measurements were performed on these

samples. However, many sets of ~ 15 nm HfO_2 thin films were grown under these identical conditions for further studies such as gamma and SHI irradiation studies presented in this thesis. Hence it is important to study these films in more detail for elucidating their structural, optical and electrical properties. This particular set of samples have therefore been studied extensively by employing various characterization techniques. The detailed analysis of these samples is presented in this section.

Fig. 3.15 shows the RBS spectrum of a ~ 15 nm HfO_2 film deposited on Si. RBS simulations were performed using SIMNRA software. The intense peak in RBS spectrum at highest channel numbers corresponds to Hf. The RBS peaks / surface edge related to other elements are indicated in Fig. 3.15. The RBS simulations confirmed the formation of stoichiometric HfO_2 films with 33% of Hf and 67% of O. The areal density of these films is found to be around 120×10^{15} atoms/cm². The physical thickness of this film is estimated to be around ~ 15 nm by considering the standard density of HfO_2 films (i.e. 9.68 g/cm³).

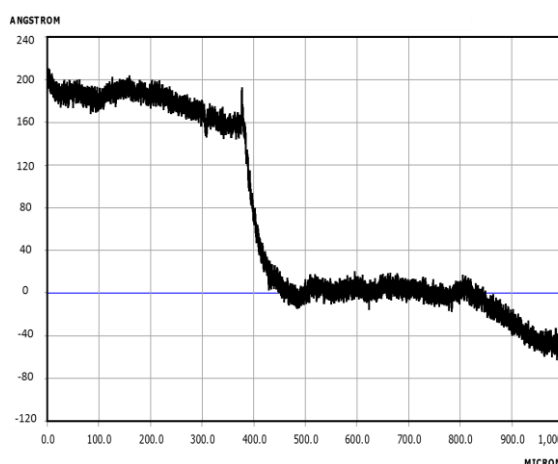


Fig. 3.16: Profilometer measurements of HfO_2 thin films deposited on Si

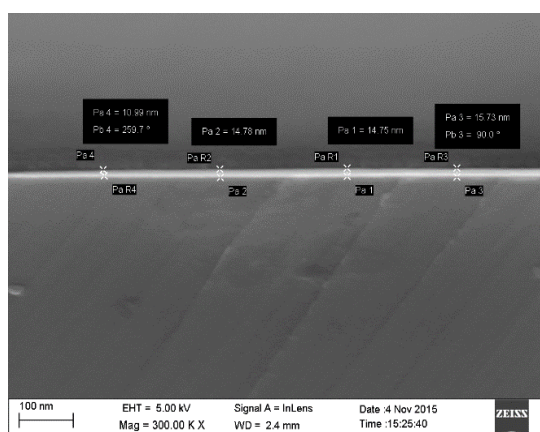


Fig. 3.17: Cross-sectional FESEM of HfO_2 thin film deposited on Si

Further, the Profilometer measurements shown in Fig. 3.16 suggests that the thickness of this film is around ~20 nm. The thickness of the films was also estimated by cross-sectional FESEM. Fig. 3.17 displays the cross-sectional FESEM picture of ~15 nm HfO₂ thin film deposited on Si. The thickness of the sample estimated by Profilometer, cross-sectional FESEM and RBS measurements are in good agreement with each other (considering the possible variations in film density).

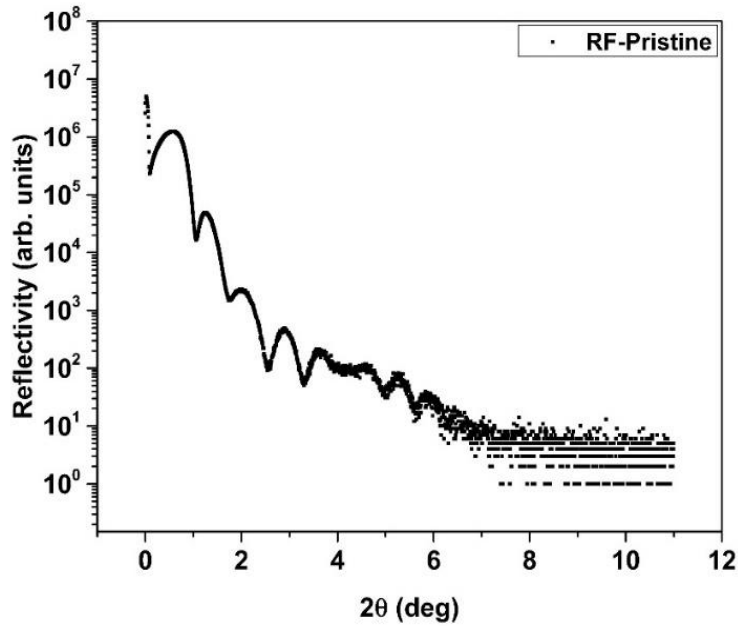


Fig. 3.18: XRR pattern of pristine samples deposited by RF magnetron sputtering

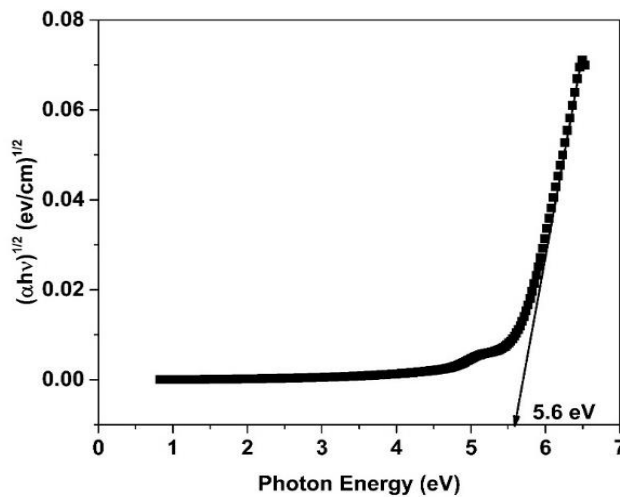


Fig. 3.19: Band gap obtained from transmission spectra

Further, The XRR measurements were performed to estimate the film thickness. XRR pattern is shown in Fig. 3.18. According to Bragg's law (i.e $2d \sin\theta = n\lambda$) the period of the

obtained fringes is proportional to the thickness of the film. The fall in the intensity is proportional to the roughness of the film and the amplitude of the fringes observed in the XRR pattern is proportional to the difference in density of the top (HfO₂ thin film) and bottom (Si substrate) layers. So, the thickness of the HfO₂ thin film has been estimated and it is found around 10 nm. Fig. 3.19 shows the transmission spectra which is used to estimate the band gap of ~15 nm HfO₂ thin films. The bandgap of these HfO₂ films was found to be 5.6 eV. The refractive index was found to be 1.6 (see Fig. 3.20).

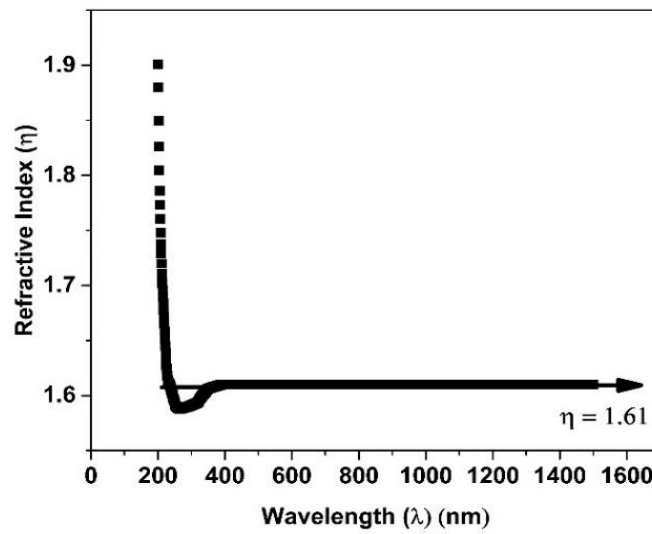


Fig. 3.20: Refractive index obtained from Transmission measurements

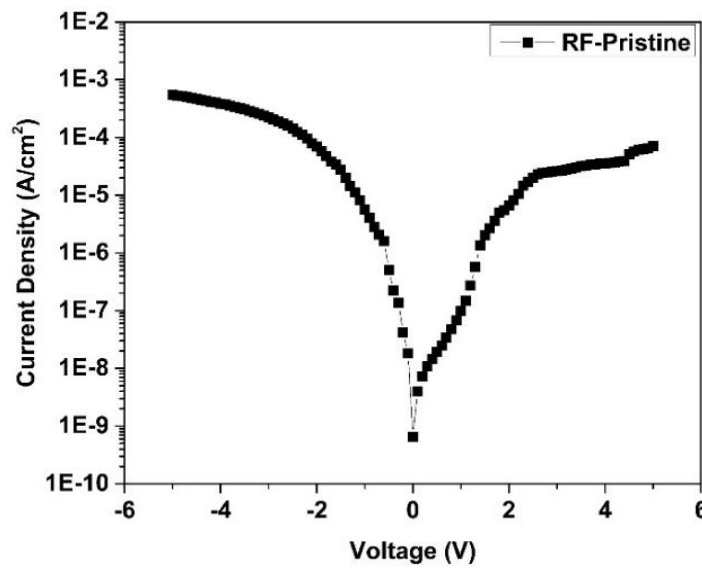


Fig. 3.21: I-V characteristics of pristine samples deposited by RF magnetron sputtering

I-V characteristics of a pristine Au/HfO₂/Si MOS capacitor is shown in Fig. 3.21. Leakage current is measured as a function of applied voltage. Current density is estimated by dividing this measured current by the area of metal (Au) dot. The magnitude of the leakage current density ($|J|$) is plotted as a function of incident voltage, although the current is negative for negative biasing voltages. The absolute value is usually considered so that these variations in leakage current can be displayed on a log scale. These plots are found to be consistent with the relevant literature in this area [14]. The leakage current density of $.5 \times 10^{-4}$ A/cm² has been observed at -5 V (see Fig. 3.21).

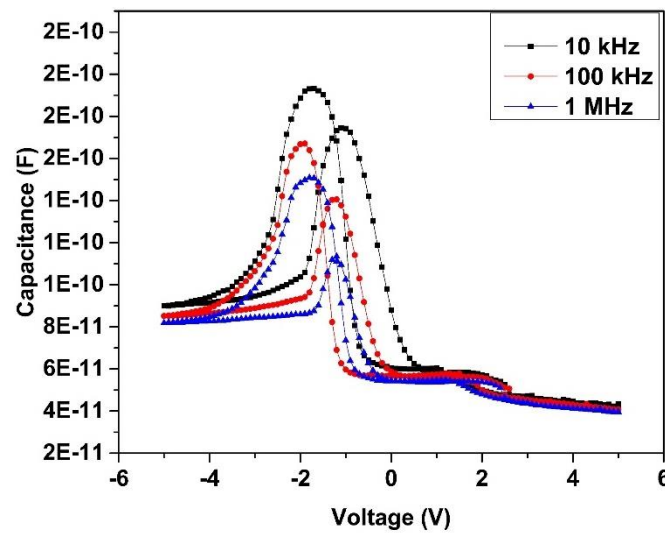


Fig. 3.22: C-V characteristics of pristine samples deposited by RF magnetron sputtering

C-V measurements were performed under different biasing conditions like: i) Accumulation, ii) depletion and iii) inversion, by sweeping the DC biasing voltage from -5 V to +5 V. The capacitance is measured by superimposing a small AC signal in series with the DC biasing voltage. The measured variations in AC current are used to determine the impedance and hence the capacitance of the system. These measurements are repeated for different frequencies of applied AC signal. The equivalent circuit of the MOS capacitor can be considered as a conductance in parallel with a capacitor. Here the conductance represents the leakage current through the capacitor, whereas the capacitance represents the dielectric constant of the gate dielectric. Hence, it is important to note that the device capacitance dominates the leakage current at higher frequencies. Therefore, all C-V measurements were performed at higher (≥ 10 kHz) frequencies in this work. Further, the

capacitance increases if leakage current decreases. Hence, a correlation can be established between I-V and C-V measurements.

The capacitance measurements were performed at three different frequencies, 10 kHz, 100 kHz and 1 MHz. Fig. 3.22 shows the C-V characteristics of the samples at these frequencies. The capacitance values are $\sim 1.9 \times 10^{-10}$ F, 1.7×10^{-10} F and 1.5×10^{-10} F at 10 kHz, 100 kHz and 1 MHz respectively at -2 V in the accumulation region. The anomalous hump observed in the accumulation region can be attributed to the defects that are present in the near surface region of HfO₂ films. Other features observed in these curves will be discussed in later chapters.

The results of the characterization measurements presented in this section suggest that these are reasonably good samples for radiation response studies planned in this thesis work. These well characterized samples have been employed for further investigations in following chapters.

3.4.2 HfO₂ thin films deposited by e-beam evaporation

A. As-deposited samples prepared by e-beam evaporation

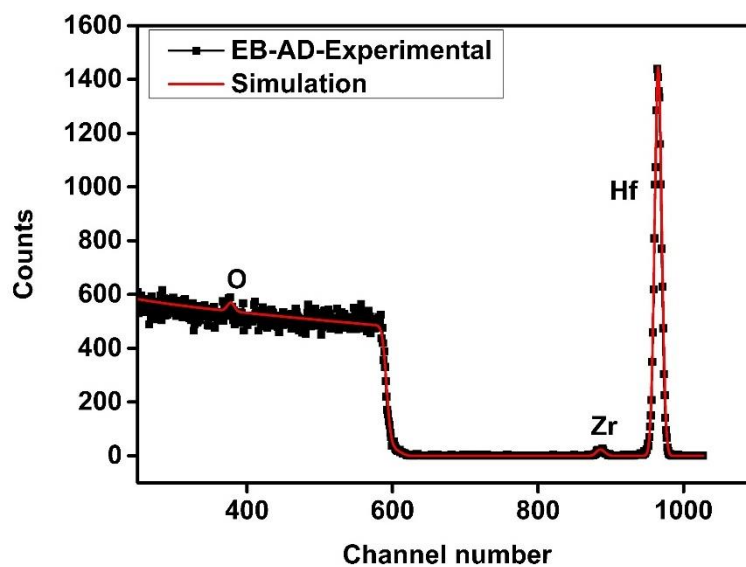


Fig. 3.23: RBS spectrum of pristine samples deposited by e-beam evaporation method

Fig. 3.23 shows the RBS spectrum of the as-grown HfO₂ thin film deposited on Si. It shows the experimental data along with the simulated fit obtained using SIMNRA. 31% Hf and 67% O along with the presence of Zr as an impurity (2%) have been estimated in these as-

grown thin films. The presence of Zr is likely due to the possible contamination of HfO₂ powder used for e-beam evaporation as it is known to be very difficult to chemically separate Zr from Hf. The presence of Zr in HfO₂ samples is not desirable, but it will not influence any chemical/electronic properties of the thin films.

This RBS data clearly indicates the formation of nearly stoichiometric HfO₂ films with an impurity of Zr (2%). Further, the areal density of these films is determined to be 85×10^{15} atoms/cm². The physical thickness of this film is estimated to be around ~30 nm by assuming the natural density of HfO₂ (density of HfO₂ = 9.68 g/cm³). Hence, this study suggests that either the film thickness (~ 30 nm) is more than the nominal thickness (~ 10 nm) or the density of the film is less than that of the natural value (density of HfO₂ = 9.68 g/cm³). XRR pattern of the pristine sample is shown in Fig. 3.24.

The 2θ values at different angles $\theta_1 = 1.4$ and $\theta_2 = 1.85$ (in radians) from Fig. 3.24 have been used to estimate the thickness. It is approximately ~ 11 nm which is very close to nominal value.

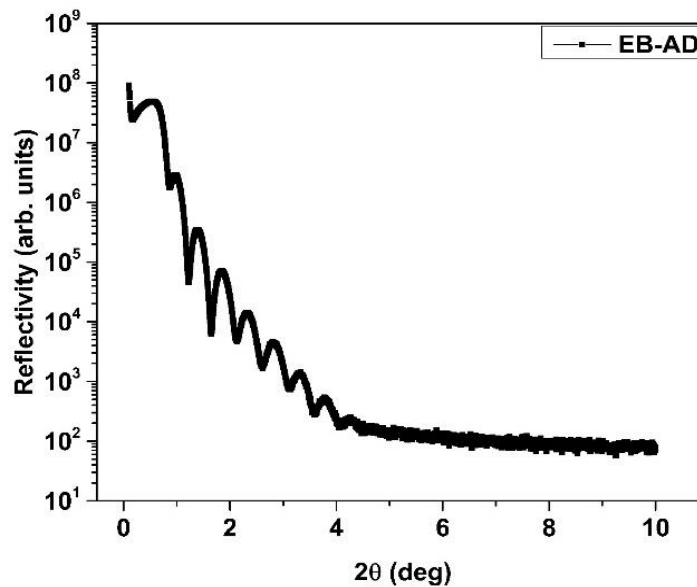


Fig. 3.24: XRR pattern of pristine samples deposited by e-beam evaporation

Hence, XRR together with RBS suggests that the film density is less than that of the nominal value of HfO₂. However, some of this oxygen may belong to the native oxide (SiO₂) or possibly to SiO₂ clusters here and there. Normally *Hf*-rich oxides are expected to be formed when HfO₂ is deposited using a pellet made of HfO₂ powder in the vacuum. Hence, these samples were annealed in O₂ atmosphere to improve the stoichiometry of

these HfO_2 films. I-V and C-V characteristics of these samples are shown in Fig. 3.25 and Fig. 3.26 respectively.

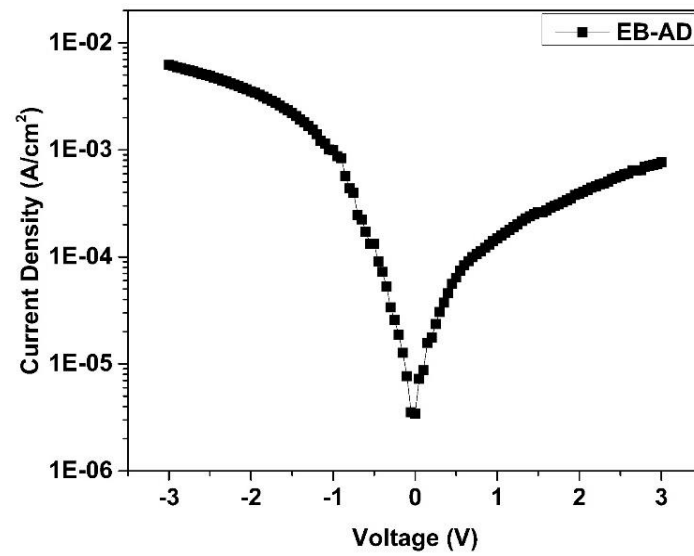


Fig. 3.25: I-V characteristics of pristine samples deposited by e-beam evaporation method

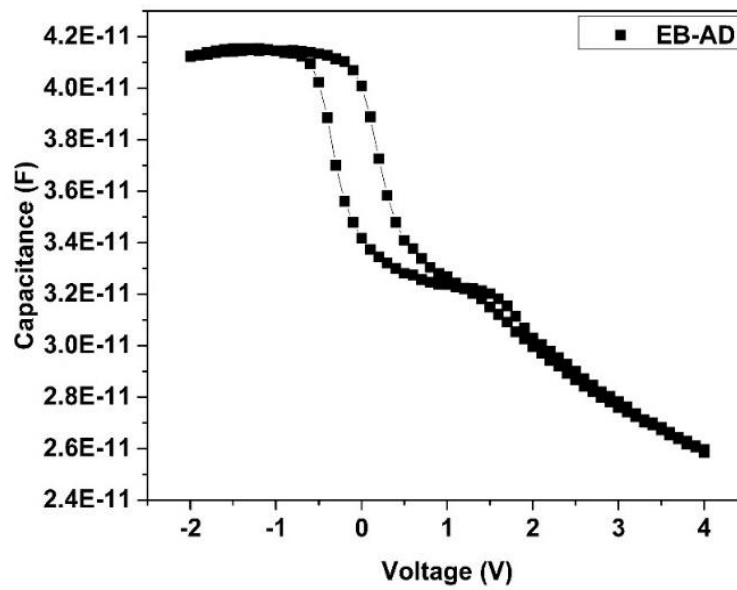


Fig. 3.26: C-V characteristics of pristine samples deposited by e-beam evaporation method

B. Effects of thermal annealing:

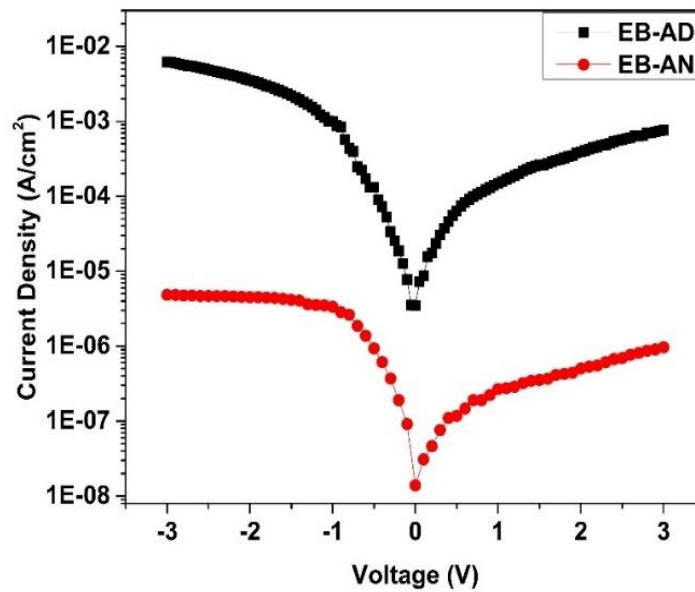


Fig. 3.27: I-V characteristics of annealed samples deposited by e-beam evaporation method

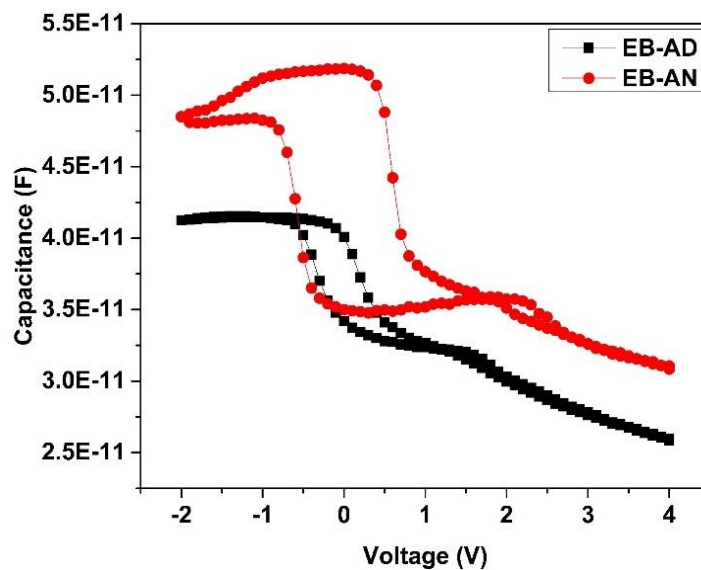


Fig. 3.28: C-V characteristics of annealed samples deposited by e-beam evaporation method

I-V and C-V characteristics of annealed samples are shown in Fig. 3.27 and Fig. 3.28 respectively. From the I-V characteristics of as-deposited and annealed samples, it is evident that in annealed samples the gate leakage current density has been significantly reduced by about 3 orders. The maximum leakage current density is found to be in the range of $\sim 10^{-2}$ A/cm² for as-grown samples and $\sim 10^{-5}$ A/cm² for annealed samples. The observed improvement in the leakage current after annealing in O₂ atmosphere may be attributed to the improvement in the stoichiometry of HfO₂ films. The accumulation capacitance of as-

deposited samples at 1 MHz frequency has been found to be 4.1×10^{-11} F whereas it is 4.8×10^{-11} F for annealed samples. Specific details of the I-V and C-V measurements are discussed in the following chapters.

3.4.3 HfO₂ ultra-thin films deposited by Atomic Layer Deposition (ALD)

Table 3.2: Sample specifications

S.No.	Sample series	Sample structure	Growth technique	Characterization techniques
1.	R	HfO ₂ (~15 nm) / Si	RF magnetron sputtering	RBS, XRR, EDS, Profilometer, I-V and C-V
2.	E	HfO ₂ (~15 nm) / Si	E-beam	RBS, XRR, EDS, Profilometer, I-V and C-V
3.	H1	HfO ₂ (3.0 nm) / SiO ₂ (0.7 nm) / Si	ALD	HRBS, XRR and I-V
4.	H2	HfO ₂ (2.5 nm) / SiO ₂ (1 nm) / Si	ALD	HRBS and XRR
5.	H3	HfO ₂ (2.7 nm) / SiO ₂ (0.6 nm) / Si	ALD	HRBS, XRR, and in-situ I-V and C-V

ALD grown HfO₂ samples were obtained from SEMATECH, USA. The typical sample structure is “HfO₂ (2 nm to 3 nm)/ SiO₂ (0.6 nm to 1 nm)/ Si”. SHI irradiation was performed on these samples using 80 MeV Ni, 120 MeV Au and 120 MeV Ag ions. Specific details of the pristine and irradiated samples are discussed in the respective chapters.

All the sample specifications grown by RF magnetron, e-beam evaporation and ALD methods are tabulated in the table 3.2. These samples were used in the following chapters for further investigations.

3.5 Conclusions

HfO₂ thin films were deposited on Si and quartz substrates by a newly installed RF magnetron sputtering system. Synthesis of these samples have been carried out at different deposition conditions by varying RF power, target to substrate distance, Ar flow and

deposition time. Thickness variation with target to substrate distance (11 cm to 14 cm) has been estimated by both RBS and Profilometer measurements. Depositing conditions have been optimized at 80 W RF power, 12 cm target to substrate distance, Ar flow of 10 sccm for 1 hr deposition. These films were characterized by UV-Vis spectroscopy to elucidate the band gap and refractive index. Transmission, absorption and reflection measurements were also performed. After optimizing all the deposition conditions, ~ 15 nm good quality HfO₂ thin films were obtained by limiting the deposition time to 15 minutes. From the RBS measurements, the formation of stoichiometric HfO₂ thin films was confirmed. The thickness of these films was cross-checked by different techniques including RBS, FESEM, Profilometer and XRR. Optical characterization of these films yields a band gap of 5.6 eV and a refractive index of 1.6. I-V and C-V measurements were also performed on these samples to verify their suitability for performing radiation response studies. Moreover, ~10 nm HfO₂ thin films were also grown by e-beam evaporation technique. These films were characterized by RBS and XRR measurements to confirm the film thickness and stoichiometry. Some of these samples were annealed in the O₂ atmosphere at 450 °C for one hour and the electrical characteristics suggest that the annealed samples show a decrease in the leakage current and an increase in the capacitance as a function of applied voltage. The specific details of these results are discussed in the respective chapters. Finally, Au/HfO₂/Si MOS capacitors were fabricated by both the RF magnetron sputtering and e-beam evaporation techniques for further studies.

One of the main reasons for employing different growth techniques in this thesis work has been to investigate the influence of growth technique on the nature of defects and their evolution during irradiation studies. The results of the characterization measurements presented in this chapter suggest that these samples are reasonably good candidates for radiation response studies planned in this thesis work. These well characterized samples have been employed for further investigations in following chapters. Gamma and/or ion irradiation induced annealing / creation of defects and inter-diffusion of constituent elements have been studied in detail. These studies presented in this thesis provide useful information for understanding the radiation response of HfO₂ based MOS devices in view of their potential applications in terrestrial space and other radiation environments.

3.5 References

1. B. Davari, R.H. Dennard and G.G. Shahidi, *Proc. IEEE*, **83** (1995) 595.
2. R.H. Dennard, F.H. Gaensslen, H.N. Yu, V.L. Rideout, E. Bassous and A.R. LeBlanc, *IEEE J. Sol. State Circuits*, **9** (1974) 256.
3. G. Sai Halaz, *Proc. IEEE*, **83** (1995) 20.
4. K. Roy, S. Mukhopadhyay and H. Mahmoodi-Meimand, *Proc. IEEE*, **91** (2003) 305.
5. Krishna Seshan, Handbook of thin-film deposition processes and techniques (Principles, Methods, Equipment and Applications) Second Edition, William Andrew Publishing Norwich, New York, U.S.A 2002.
6. D.M. Mattox, Handbook of Physical Vapor Deposition (PVD) Processing, second ed., William Andrew, Norwich, 2010.
7. C.T. Sah, *Proc. IEEE*, **76** (1988) 1280.
8. International Technology Roadmap for Semiconductors, semiconductor industry association. Available at <http://www.public.itrs.net>[online].
9. J.E. Mahan, Physical Vapor Deposition of Thin Films, Wiley-Interscience, New York, 2000.
10. S.K. Dixit, Ph.D. thesis, Vanderbilt University, Nashville, TN, USA, 2008 and refs. therein.
11. W. Kern and D. A. Puotinen, *RCA Rev.* **31** (1970) 187.
12. M. Mayer, SIMNRA: Simulation of RBS, ERD and NRA spectra. <http://www.rzg.mpg.de/~mam/>
13. R. Swanepoel, *J. Phys. E: Instrum.*, **16** (1983) 1214.
14. F. C. Chiu, S. A. Lin, J. Y. Lee., *Microele. Reliability*, **45** (2005) 961.

Gamma irradiation studies of HfO₂ based MOSCAPs

This chapter presents the gamma irradiation effects on the electrical properties of HfO₂ based MOSCAPs. HfO₂ thin films were deposited on Si by both RF and e-beam evaporation techniques. Gamma irradiation was performed on these samples at different doses starting from 1 kGy to 10 kGy. The influence of gamma irradiation and pre-existing defects on the evolution of oxide and interface traps have been studied.

4.1 Introduction

HfO₂ has already been incorporated in commercial integrated circuit technology and has emerged as a consistent material with superior qualities over all the other high-k gate oxides because of its stability, durability and reliability [1]. The performance of MOS devices in space applications under various cosmic ray environments is an interesting study [2]. The radiation effects on SiO₂ based MOS devices have been extensively studied over the years [3-5]. Similar level of understanding is essential for HfO₂ based devices. Especially in space applications, the functionality of these modern generation MOS devices is a challenging task [6]. Gamma radiation is one of the major cosmic radiations in space and the effects of this radiation on the HfO₂/Si devices are of current interest [7]. Such studies elucidate the radiation hardness, tolerance and persistence of HfO₂ based MOS devices.

The effects of Gamma irradiation on the I-V and C-V characteristics of HfO₂/Si system is of current interest. It is well-known that Gamma irradiation can cause ionization and produce Electron Hole Pairs (EHPs) in the gate oxide. These mobile charges get trapped by the inherent defects of the oxide and interface traps and can affect the electrical properties (I-V and C-V) of MOS devices [8]. Hence the evolution of gamma irradiation-induced damage depends on the traps that already existed before irradiation. The trap-rich characteristic resides in high-k materials arising from dangling bonds, bulk oxide defects and structural defects which result in the transient effects of the leakage current [9]. The present work is carried out at relatively low doses starting from 1 kGy to 10 kGy [10]. Further, the influence of pre-existing defects on the evolution of gamma irradiation induced defects has also been studied. In order to study these effects, the samples have been prepared by three different methods: 1) e-beam evaporation, 2) e-beam evaporation followed by thermal annealing and 3) RF sputtering. This systematic study yields some useful information for elucidating the effects of gamma irradiation on HfO₂ based MOS devices at low doses.

4.2 Experimental details

HfO₂ thin films were synthesized by electron beam evaporation and RF magnetron sputtering techniques as discussed in chapter 3. Both the techniques are well-established deposition techniques for depositing HfO₂ films. 10 nm HfO₂ films were deposited on

p-type boron doped Si (100) [1-10 Ω -cm resistivity]. The standard RCA process was followed for removing the native oxide on Si.

4.2.1 e-beam evaporation

Primarily, the e-beam chamber was evacuated to 1.3×10^{-8} mbar, using an UHV system available at IUAC, New Delhi. A pellet made of 98% pure HfO_2 powder (2% impurity may be attributed to the presence of Zr as Hf and Zr are of chemically similar structure) was evaporated using an e-beam obtained from a 15 kW electron gun. The deposition rate was maintained at $\sim 0.1 \text{ \AA/s}$, current was kept at 75 mA and the observed pressure during deposition was 8.4×10^{-3} mbar. Some of the samples were annealed in O_2 atmosphere at 450°C for an hour to obtain a better stoichiometric HfO_2 films (EB-AD series samples are as-deposited samples whereas EB-AN samples are annealed samples).

4.2.2 RF magnetron sputtering

HfO_2 thin films were deposited on silicon by RF magnetron sputtering technique. The HfO_2 target is of 2 inch diameter with 99.99% purity. $\sim 15 \text{ nm}$ HfO_2 thin films were deposited after a thorough investigation and optimization of all the deposition conditions. The RF power was maintained at an optimum value of 80 W, the target to substrate distance was fixed at 12 cm and the deposition time was half an hour. The Ar gas of 99.99% purity was used and the flow rate was kept at 10 sccm. Initially, the chamber was pumped down to a base pressure of 1×10^{-6} mbar and during deposition it was maintained at 4×10^{-3} mbar. These samples are termed as *RF series samples*.

Au metal contacts were deposited by using an in-house thermal evaporation technique on both the set of samples deposited by RF and EB series samples. Au metal contacts of 300 nm thickness and 1 mm in diameter were deposited on the top of the HfO_2 surface using a suitable mask. Ag paste along with the help of Al foil was used as a backside contact with respect to Si. These samples were then subjected to gamma irradiation by using a ^{60}Co gamma (1.25 MeV γ) source (1200 Gamma chamber available at IUAC, New Delhi). Gamma irradiation was performed on all the samples with a constant dose rate of 4.64 kGy/h. The samples were irradiated at various doses ranging between 1-10 kGy. I-V (leakage current) and C-V measurements were performed using an in-house Agilent technologies B1500A semiconductor device analyzer. Electrical measurements were performed to study the effects of Gamma irradiation on all the samples. The applied bias

voltage range was -5 V to + 5 V and C-V measurements were performed at 1 MHz frequency. From I-V measurements leakage current was estimated and from C-V measurements the variation of accumulation capacitance upon irradiation doses has been studied. The reproducibility of electrical measurements was established by repeating such measurements on a number of metal dots (4 to 5 devices / sample) that are deposited on the samples.

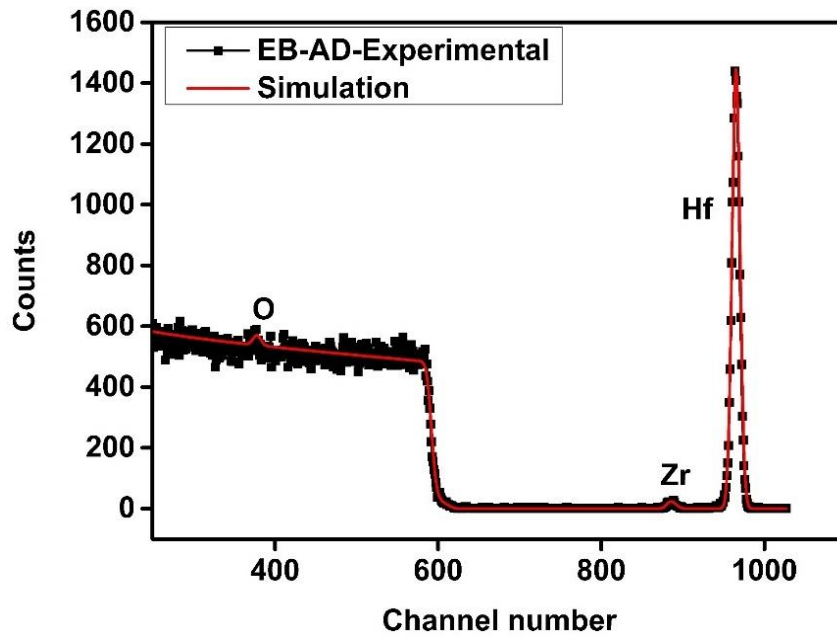


Fig. 4.1: RBS spectrum of pristine samples deposited by e-beam evaporation method

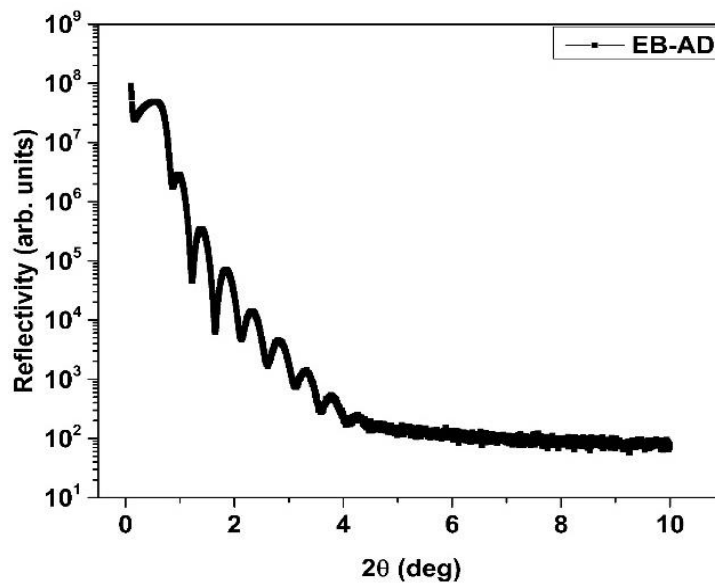


Fig. 4.2: XRR pattern of pristine samples deposited by e-beam evaporation

The structural characterization of the samples was performed by using Rutherford Backscattering Spectrometry (RBS) (see Fig. 4.1) and XRR measurements (Fig. 4.2). The thickness and stoichiometry of these films have been estimated by RBS. RBS measurements were performed using 2 MeV He ions at a scattering angle of 165°. A calibration offset value of 74 keV and an energy per channel of 0.9725 keV/ch were determined using a standard calibration sample (Au/glass). These measurements were carried out at IUAC, New Delhi. Simulations were performed using SIMNRA software.

4.3 Results and Discussion

4.3.1 HfO₂ thin films deposited by e-beam evaporation

A. Effects of thermal annealing

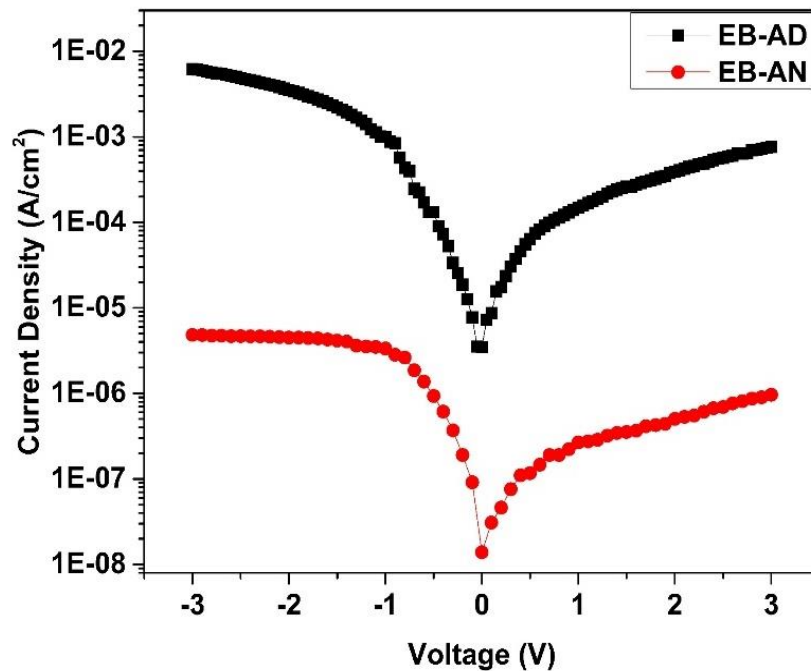


Fig. 4.3: I-V characteristics of annealed samples deposited by e-beam evaporation method

I-V and C-V characteristics of as-deposited samples are shown in Fig. 4.3 and 4.4 respectively and those of annealed samples are shown in Fig. 4.5 and 4.6 respectively. From the I-V characteristics of as-deposited and annealed samples, it is evident that in annealed samples the gate leakage current density has been significantly reduced by about 3 orders. The maximum leakage current density is found to be in the range of $\sim 10^{-2}$ A/cm² for as-

grown samples and $\sim 10^{-5}$ A/cm² for annealed samples. The observed improvement in the leakage current after annealing in O₂ atmosphere may be attributed to the improvement in the stoichiometry of HfO₂ films. The accumulation capacitance of as-deposited samples is found to be 4.1×10^{-11} F, whereas it is 4.8×10^{-11} F for annealed samples. From the C-V characteristics, positive oxide trapped charges and interface trapped charges have been observed.

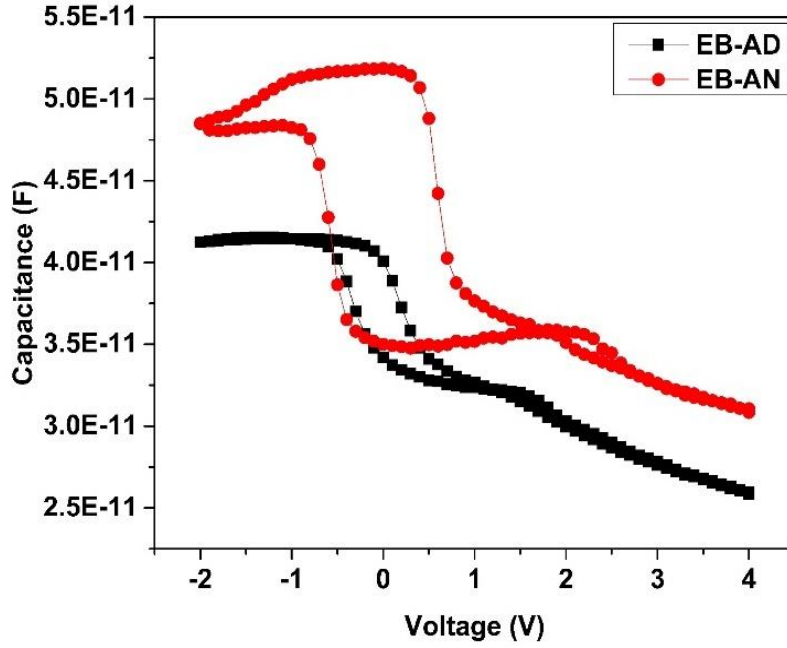


Fig. 4.4: C-V characteristics of annealed samples deposited by e-beam evaporation method

The influence of the positive oxide trapped charges in the oxide is to initiate a flatband shift in the C-V plot and the slope of the curve has been altered by the interface trapped charges [13]. The accumulation capacitance and the width of the hysteresis loop are found to increase in annealed samples as compared to those of the as-deposited samples. Such an increase in capacitance of the annealed samples is acceptable as there is a reduction in leakage current. Moreover, the pre-existing oxide and interface traps have increased the charge trapping during gamma irradiation.

B. Effects of Gamma irradiation

I-V and C-V characteristics of as-deposited and annealed samples are shown in Fig. 4.5 to 4.8. Gamma irradiation was carried out at different doses: 1 kGy, 2 kGy, 4 kGy, 6 kGy, 8 kGy and 10 kGy at a constant dose rate of ~ 4.64 kGy/h. A systematic increase in the leakage current is observed as the irradiation dose increases. This similar trend of increase

in the leakage current upon increase in the irradiation dose has also been observed in the annealed samples. The maximum leakage current density increases with irradiation dose. The leakage current density at -3V for as-deposited samples changes from $6.2 \times 10^{-3} \text{ A/cm}^2$ to $4.0 \times 10^{-2} \text{ A/cm}^2$ and for annealed samples it changes from is $4.8 \times 10^{-6} \text{ A/cm}^2$ to

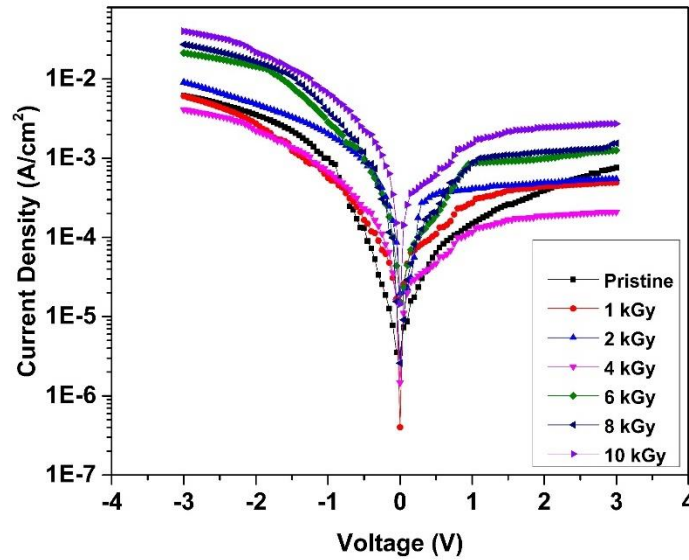


Fig. 4.5: Leakage current density vs. Voltage for EB-AD pristine and irradiated samples.

$1.7 \times 10^{-5} \text{ A/cm}^2$ (see Fig. 4.6). (The annealing step has been performed prior to gamma irradiation). This significant increase can be attributed to the increase in the density of oxide and interface trapped charges. This is further confirmed by the C-V measurements.

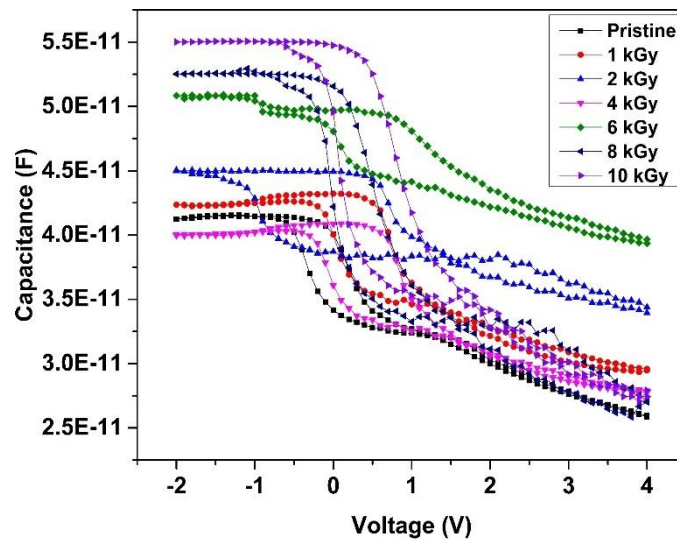


Fig. 4.6: Capacitance vs. Voltage for EB-AD pristine and irradiated samples

The accumulation capacitance with irradiation dose changes from 4.1×10^{-11} F to 5.5×10^{-11} F for as-deposited samples whereas for annealed samples it changes from 4.8×10^{-11} F to 6.0×10^{-11} F at -2 V. There is a systematic increase in the accumulation capacitance with increase in the irradiation dose.

From these measurements, the irradiation induced charges due to creation of defects in the oxide layer have been observed in both the as-deposited and annealed samples. Further, the flat band shift is more prominent in the case of annealed samples.

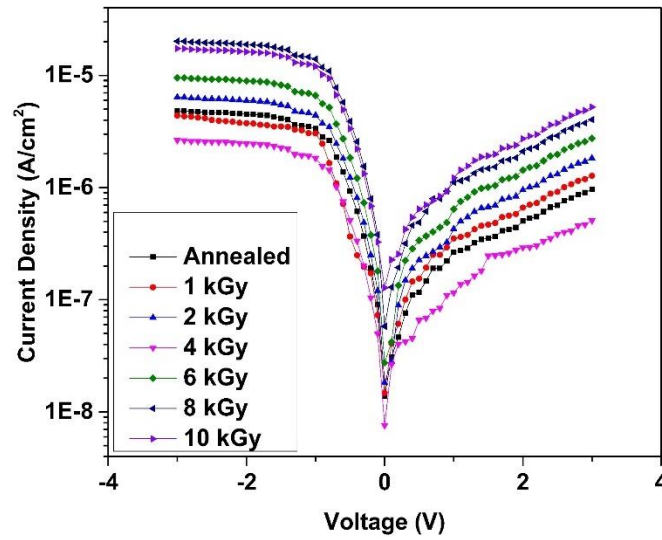


Fig. 4.7: Current vs. Voltage characteristics of EB-AN pristine and irradiated samples

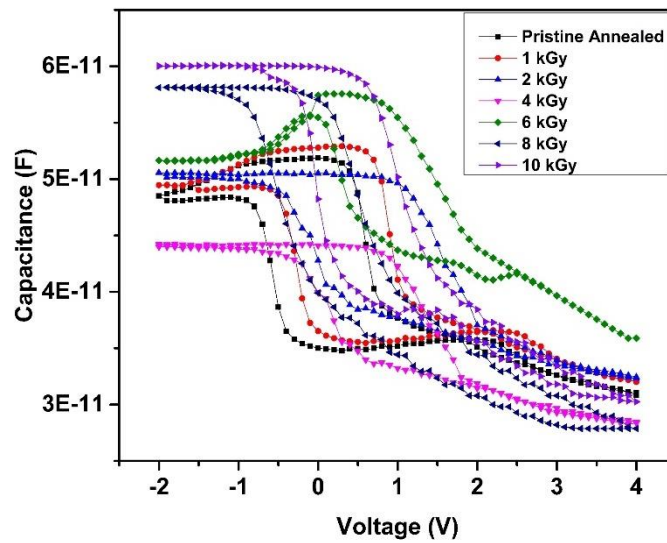


Fig. 4.8: Capacitance vs. Voltage for EB-AN pristine and irradiated samples

The oxide trapped charges also increase with an increase in the irradiation dose resulting in the shifts of C-V plots. This is due to the presence of high density of oxide charges in the pristine samples itself. This shift in C-V plots (see Fig. 4.8) increases and shifts towards the positive side of the voltage. This effect suggests that there is trapping of more number of negative charges. Moreover, the slope of these curves is also changing as the irradiation dose changes from 1 kGy to 10 kGy, indicating the increase in the interface traps. Annealing has increased the density of the trapped charges and this increment has been further stimulated by the gamma irradiation which induced more number of EHPs. Since the generation of the defects is predominantly due to the recombination process, the hysteresis loop width has been found to increase with an increase in the irradiation dose. This trend is more significant in the irradiation of annealed samples as compared to as-deposited samples.

4.3.2 HfO₂/Si samples deposited by RF magnetron sputtering

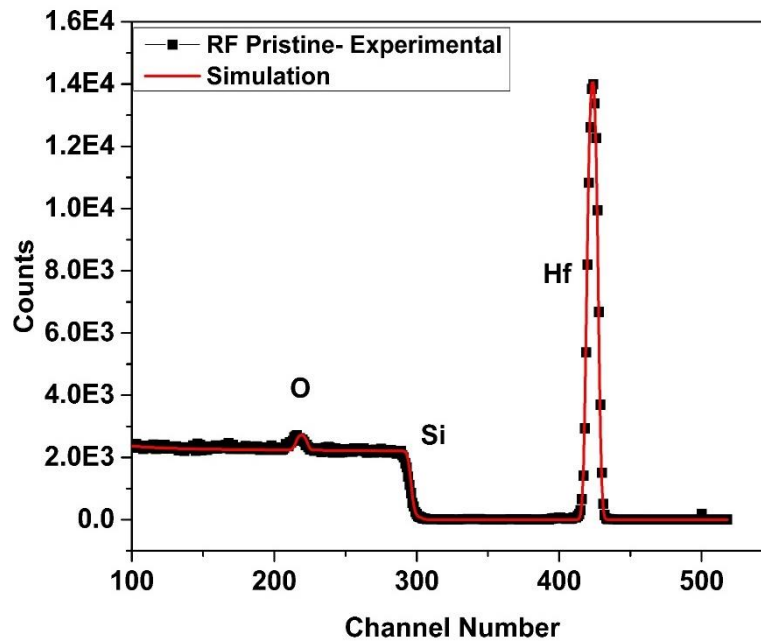


Fig. 4.9: RBS Spectrum of RF pristine sample

Fig. 4.9 shows the RBS spectrum of 10 nm HfO₂ films deposited on Si. RBS simulations were performed using SIMNRA software. The spectrum shows that the sample is nearly stoichiometric HfO₂ with 33% of Hf and 67% of O. The areal density of these films is found to be around 120×10^{15} atoms/cm². The physical thickness of this film is estimated to be

around ~ 15 nm by considering the standard density of HfO_2 films (HfO_2 density is 9.68 g/cm^3). Further the thickness has been estimated by XRR measurements and is found to be ~ 10 nm. Fig. 4.10 shows the XRR pattern. Both the results suggest that there is a ~ 15 nm HfO_2 film that was grown on Si. Annealing was not performed in the case of samples deposited by RF magnetron sputtering as films are found to be nearly stoichiometric.

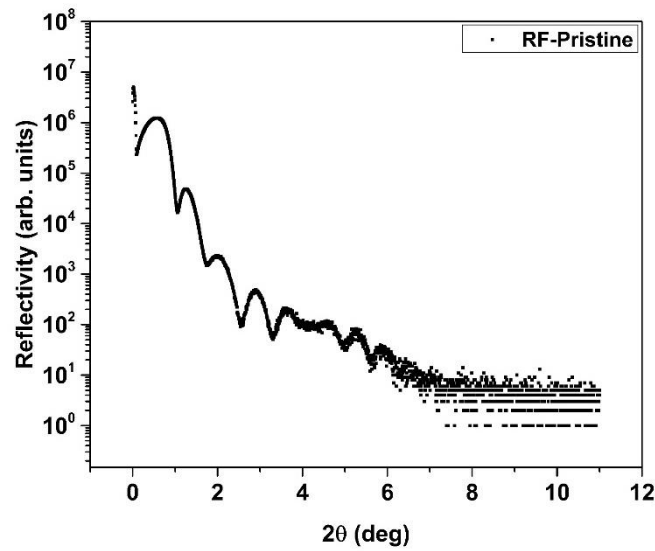


Fig. 4.10: XRR pattern of RF pristine sample

I-V characteristics of pristine and irradiated samples are shown in Fig. 4.11. As the gamma irradiation dose increases, a systematic increase in both the leakage current and capacitance is observed. This is in a good agreement with the EB series samples.

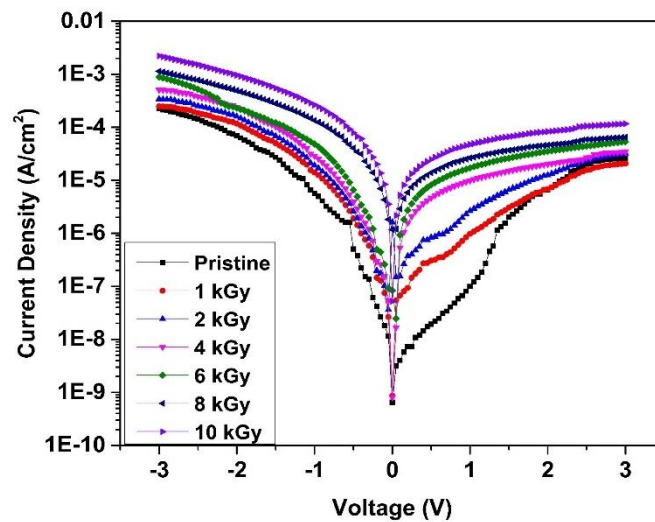


Fig. 4.11: Leakage current density vs. Voltage of gamma irradiation on RF series samples

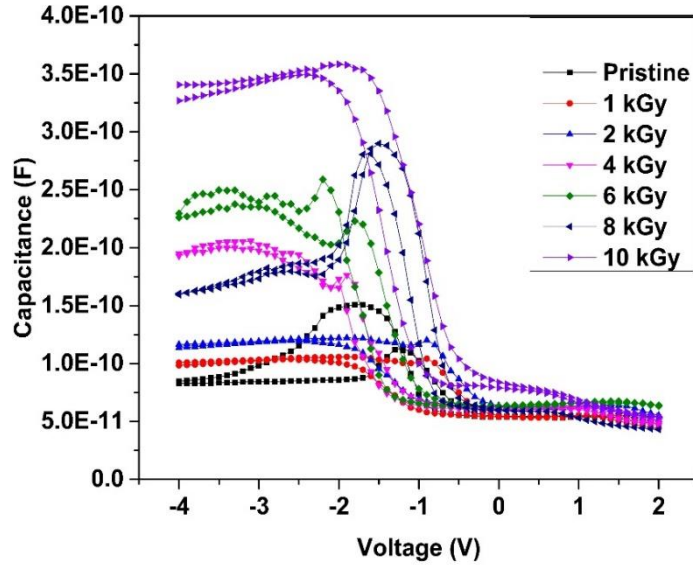


Fig 4.12: Capacitance vs. Voltage of gamma irradiated RF series samples

The leakage current density with irradiation dose changes from $2.2 \times 10^{-4} \text{ A/cm}^2$ to $2.2 \times 10^{-3} \text{ A/cm}^2$ at -3 V . From the C-V measurements, we noticed that the accumulation capacitance at -4 V changes from $8.5 \times 10^{-11} \text{ F}$ to $3.4 \times 10^{-10} \text{ F}$, as a function of irradiation dose. The accumulation capacitance as a function of the irradiation dose is shown in Fig. 4.12. In contrast to the EB series samples, RF series samples exhibit positive traps and interface trap densities. These trap densities have been increased upon gamma irradiation. Fig. 4.13 depicts the leakage current density as a function of irradiation dose at $\pm 1 \text{ V}$ for all the samples.

Similarly, the accumulation capacitance as a function of irradiation dose at -2 V is shown in Fig. 4.14. The data presented in Fig. 4.13 indicate the fact that the EB-AN series and RF series samples are of better quality because the leakage current in these samples is a few orders lower than that of EB-AD series samples. This is in agreement with the structural analysis, as RBS measurements also suggest that the stoichiometry of these EB-AN series samples and RF series samples is better than that of EB-AD series samples. The increase in leakage current with increase in gamma dose is higher in EB-AD series samples when compared to that of EB-AN series samples. Particularly, it is important to note that the variation of leakage current with gamma dose is very weak in the case of RF series samples. When it comes to high frequency C-V Characteristics, EB-AN and RF series samples exhibit proper depletion features whereas the C-V characteristics of EB series samples are either driven to deep depletion or to accumulation regions.

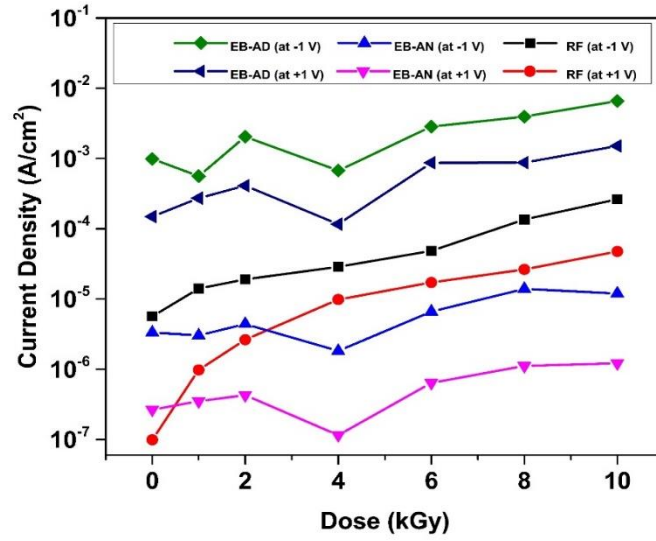


Fig 4.13: Leakage current density vs. Irradiation
Dose at ± 1 V

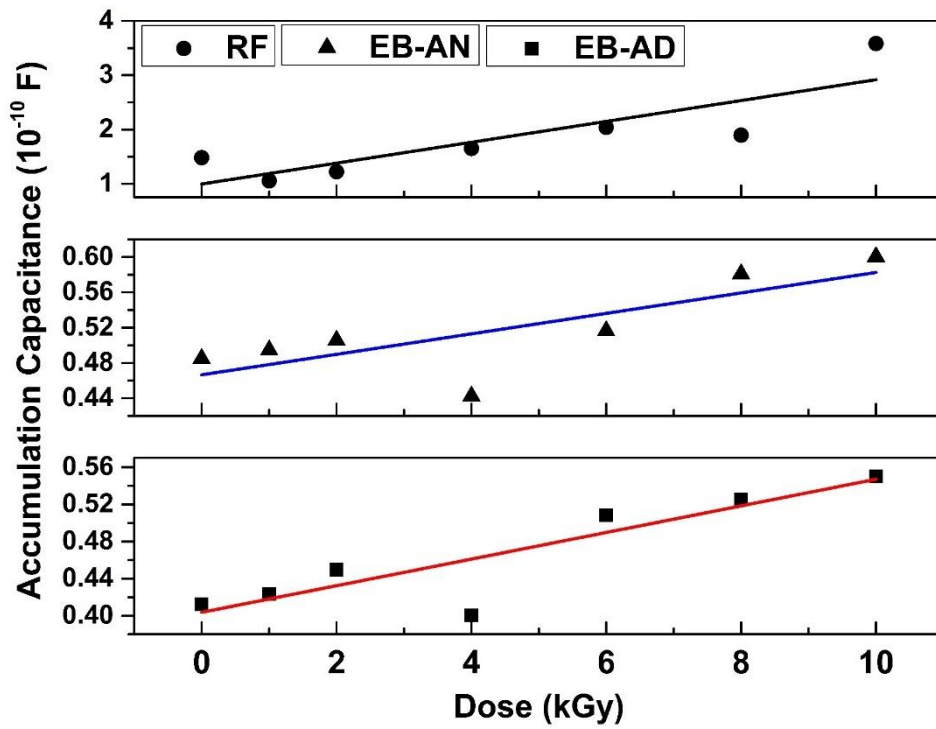


Fig. 4.14: Accumulation Capacitance vs. Irradiation Dose at -2 V
(Straight lines represent the linear fits)

The oxide / accumulation capacitance of as-grown RF series samples is higher than that of as-grown EB-AD and EB-AN series samples, may be due to the expected changes in film-thickness, film-stoichiometry and the nature and density of pre-existing oxide traps. The oxide capacitance of RF series samples can be higher if films were thinner than that of EB

series samples. However, this would lead to higher leakage currents in RF series samples. Lower leakage currents, together with high capacitance, suggest that the changes in thickness and stoichiometry among samples are not that significant. The existence of trapped charges can obviously increase the capacitance of oxide layers. Hence, the presence of pre-existing oxide traps predominantly contribute to the accumulation capacitance of RF series samples. Moreover, C-V measurements clearly suggest the existence of positive oxide traps in as-grown RF series samples and negative oxide traps in as grown EB series samples.

As shown in Fig. 4.14, the oxide capacitance increases almost linearly in all samples, with an increase in irradiation dose. The slope of this linear dependence suggests that the rate of increase in oxide capacitance of RF series samples is much higher than that of the EB series samples. This indicates that the initial structure and pre-existing defects of the oxide layers can influence the consequent evolution of gamma irradiation-induced defects in these structures. Pre-existing traps can efficiently trap the EHPs generated during gamma irradiation before they recombine. The recombination probability of EHPs would be more in the absence of any charges and / or external biasing voltage during irradiation. However, the presence of accumulated defects (over time) and biasing conditions are inevitable when electronic devices are operated in radiation environment like space and nuclear electronics. Hence it is important to understand these damage evolution mechanisms in detail.

4.4 Conclusions

HfO₂ films deposited on Si were synthesized by both RF magnetron and e-beam evaporation techniques. Structural and electrical characterizations were performed on both sets of these samples. EB series samples show the presence of negatively trapped charges, whereas RF series samples show positively trapped charges. However, both the sets of samples have shown similar behavior with gamma irradiation. An increase in the leakage current and capacitance have been observed with the increase in the irradiation doses. Flatband shift and increase in the width of the hysteresis in the C-V characteristics clearly indicate the increase of oxide trapped charge densities and changes in the slopes of these curves show the increase of interface traps. The role of these defects on electrical properties has been studied. Hence, it is important to consider these effects whenever HfO₂ based MOS devices are used in a radiation environment, like space and nuclear electronics.

4.5 References

1. N. Manikanthababu, T. K. Chan, A. P. Pathak, G. Devaraju, N. Srinivasa Rao, P. Yang, M. B. H. Breese, T. Osipowicz and S. V. S. Nageswara Rao, *Nucl. Inst. and Meth. in Phys. Res. B*, **332** (2014) 389.
2. R. K. Nahar, Vikram Singh and Aparna Sharma, *J. Mat. Sci.: Mat. In Ele.*, **18** (2007) 615.
3. T. Yunogami and T. Mizutani, *J. Appl. Phys.*, **73** (1993) 8184.
4. M. C. Busch, A. Slaoui, P. Siffert, E. Dooryhee and M. Toulemonde, *J. Appl. Phys.*, **71** (1992) 2596.
5. T. P. Ma, Y. Nishioka, E. F. da Silva, “The Physics and Chemistry of SiO₂ and the Si-SiO₂ Interface”, (ed. by) C. R. Helms, B. E. Deal, Plenum, New York, (1988).
6. Vikram Singh, N. Shashank, Dinesh Kumar and R. K. Nahar, *Rad. Eff. Def. Solids.*, **3** (2012) 204.
7. F. Belgin Ergin, Rasit Turan, Sergiu T. Shishiyanu and Ercan Yilmaz, *Nucl. Inst. and Meth. in Phys. Res. B*, **268** (2010) 1482.
8. A. Y. Kang, P. M. Lenahan, and J. F. Conley Jr., *IEEE Trans. On Nuclear Science*, **49** (2002) 2636.
9. N. Manikanthababu, N. Arun, M. Dhanunjaya, V. Saikiran, S. V. S. Nageswara Rao and A. P. Pathak, *Rad. Eff. Def. Solids.*, **170** (2015) 207.
10. N. Manikanthababu, N. Arun, M. Dhanunjaya, S. V. S. Nageswara Rao and A. P. Pathak, *Rad. Eff. Def. Solids.*, (2016) (*In Press*).

Chapter 5

SHI irradiation effects on the structural and electrical properties of HfO₂ based MOS devices

This chapter presents SHI induced intermixing effects on the structural properties and consequent effects on the electrical properties of HfO₂ based MOS devices.

5.1. Introduction

SiO₂ has already been replaced by HfO₂ in new generation MOSFETs [1]. However optimization of the synthesis of these materials is still under study [2-7]. Deposition of these high-k materials on Si wafers can result in high concentration of interface defects due to their thermodynamic instability on Si surface [8]. Introduction of thin interlayer of Silicon oxide / nitrides between Si and HfO₂ is expected to improve the interface quality, device reliability and performance [9-10]. Hence it is extremely important to investigate the quality, composition and thickness of this oxide and its inter-layers for fabricating reliable CMOS devices. It has also been reported that Hf silicates like HfSiO are attractive because of their enhanced thermal stability compared to HfO₂ [11]. Hence, it is important to study the composition, thickness and intermixing effects to optimize the fabrication of HfO₂ based MOS devices.

Swift Heavy Ion (SHI) irradiation plays a major role in synthesis, modifications and characterization of materials [12]. Interface engineering schemes using SHI irradiation have been extensively studied over the past few years to elucidate the intermixing / diffusion issues [13]. Such studies are also useful for understanding the diffusion process of various elements across different interfaces. It is well-known that ion beam mixing has an important role in the formation of silicides in various systems like Fe/Si, Co/Si, Mo/Si, Mn/Si, Ti/Si, Zr/Si etc. [14]. To the best of our knowledge, there are no reports on SHI induced mixing of Hf/Si or HfO₂/Si interfaces although some reports exist on ion beam studies of Hf-based high-k dielectric materials [15-16]. Hafnium silicates belong to a new class of alternate high-k dielectric materials with tunable electrical and thermal properties [6-7, 17-18]. Hence it is important to optimize the synthesis processes and to study ion beam mixing of this technologically important interface. Particularly, it is of great interest to understand defect creation and mixing at the interface due to ion irradiation and its impacts on the material properties and the device performance when HfO₂ based devices are used in terrestrial / space applications. Here we present a study on ion beam characterization and modification HfO₂/SiO₂/Si and HfO₂/Si samples.

To the best of our knowledge, there are no previous studies on SHI induced diffusion of Hf in Si and SiO₂ layers. Our present study demonstrates unambiguously, the SHI induced diffusion of the constituent elements across HfO₂/SiO₂ and HfO₂/Si interfaces and consequent effects on their electrical properties by employing various well-established

structural and electrical characterization techniques. Hence, the experimental data presented in this chapter forms the basis for studying SHI induced structural and electrical modifications in technologically important HfO₂ based MOS devices.

5.2. Experimental

ALD grown HfO₂ samples were obtained from SEMATECH, USA. Room temperature SHI irradiation was performed in a high vacuum chamber ($< 10^{-6}$ mbar) at a constant beam current of one particle nano Ampere (~ 1 pA). The beam (of 1 mm in diameter) is uniformly scanned over 1 cm x 1 cm area on samples using magnetic scanners to achieve uniform irradiation profiles. SHI irradiation was performed to ensure uniform electronic energy deposition throughout the dielectric stack. The details of irradiation and sample ids are given in table 5.1.

Table 5.1: Sample structure and irradiation details

Sample	Ion & Energy	Irradiation Fluence (ions/cm ²)
H2A	----	Pristine
H2C	Ni, 80 MeV	5×10^{12}
H2D	Ni, 80 MeV	5×10^{13}
H1A	----	Pristine
H1B	Au, 120 MeV	1×10^{13}
H1C	Au, 120 MeV	5×10^{13}
H1D	Au, 120 MeV	1×10^{14}
RNi -A	Ni, 80 MeV	Pristine
RNi -B	Ni, 80 MeV	1×10^{11}
RNi -C	Ni, 80 MeV	1×10^{12}
RNi -D	Ni, 80 MeV	1×10^{13}
RNi -E	Ni, 80 MeV	5×10^{13}

HRBS / Channeling measurements were performed on all samples at National University of Singapore (NUS). For these HRBS measurements we used 500 keV He⁺ incident beam with scattering angle of $\theta = 65^\circ$ and energy resolution of 1.3 keV. Incident angle (α) and exit angle (β) were kept at 55° and 60° respectively. Beam was channeled in the substrate

(along $\langle 111 \rangle$ axis of Si) to minimize background scattering from Silicon and to analyze amorphous layers ($\text{SiO}_2/\text{HfO}_2$) on Si surface. Further details about HRBS-measurement system can be found elsewhere [19-20]. HRBS spectra were analyzed using SIMNRA simulation software.

Samples were further investigated by high resolution X-ray specular reflectometry at grazing incidence angle in the X-ray demonstration and development (XDD) beam line at Singapore Synchrotron Light Source (SSLS). The pure reflectivity was obtained by subtracting the diffuse scattering from the raw data. The simulations were performed using M805 and LEPTOS 1.07 release 2004 (Bruker) simulation software. XRR measurements were also performed using Bruker D8 Advance diffractometer with an incidence angle of 0.4° , using an in-house $\text{Cu-K}\alpha$ (1.5406 \AA) source. I-V measurements were performed to study the effects of SHI irradiation. The applied bias voltage range was -5 V to $+5 \text{ V}$. The RTA on the samples was performed using Anneal Sys AS-One 150 system. I-V measurements were performed to study the RTA annealing effects on the Leakage current as a function of irradiation fluence.

5.3. Results and Discussion:

5.3.1 Ultra-thin HfO_2 films deposited by ALD

A. Effects of 80 MeV Ni ion irradiation

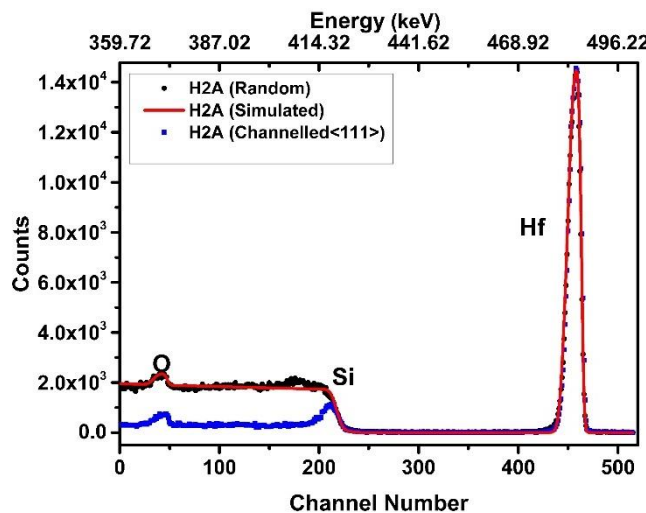


Fig. 5.1: Random and channelled HRBS spectra of pristine sample (H2A). Solid line represents the SIMNRA simulation of random HRBS spectrum

The typical sample structure was “HfO₂ (2.5 nm) / SiO₂ (1 nm) / Si (substrate)”. These samples have been named as H2 series samples. Although there are H1 series samples, we have started our experiments with H2 series samples. This sample was cut into several pieces for irradiation studies. Random and channeled HRBS spectra of pristine sample (H2A) are shown in Fig. 5.1. The probe beam is channeled in the substrate along Si <111> direction to minimize background scattering from silicon. Prominent surface peaks corresponding to Si and O from amorphous layers on surface are observed due to a reduction of about 85% in the back scattering yield of Si ($\chi_{\min} = \sim 15\%$) in <111> aligned spectrum. The elemental composition of the surface layer is estimated using the relative intensities of these Hf, Si and O peaks ($Y_{\text{Hf}}/\sigma_{\text{Hf}} : Y_{\text{Si}}/\sigma_{\text{Si}} : Y_{\text{O}}/\sigma_{\text{O}}$) in channeled spectra.

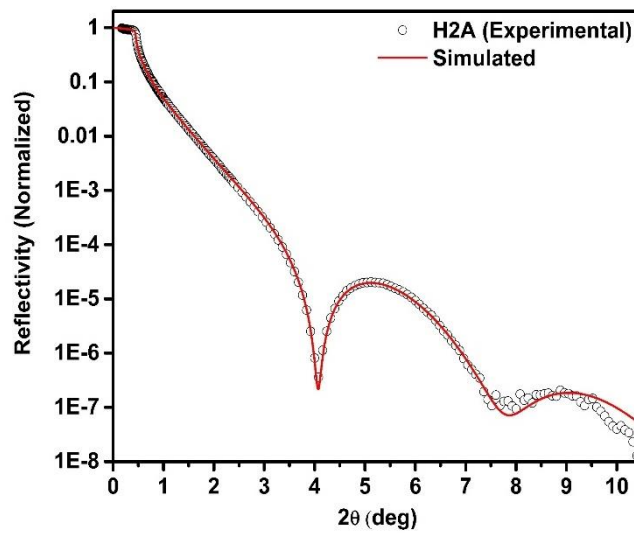


Fig. 5.2: HR-XRR Spectra of pristine sample (H2A). Solid line represents the LEPTOS simulation of HR-XRR data

The counts estimated for 3 mono layers (ML) of Si ($\sim 2.04 \times 10^{15} \text{ cm}^{-2}$) were subtracted from the total yield of Si to eliminate / minimize the contribution of Si-surface peak because the contribution of reconstructed Si-peak is expected to be from these 3 ML [21-22]. This analysis of pristine sample suggests the formation of a mixed Hf_{0.18}Si_{0.33}O_{0.45} layer instead of pure SiO₂ and HfO₂ layers as intended. Random HRBS spectrum was analyzed using SIMNRA simulation software. The SIMNRA fit shown in Fig. 5.1 (solid line) further confirms the formation of a mixed Hf_{0.18}Si_{0.32}O_{0.5} (0.6 nm) interlayer between Si-substrate and HfO₂ (1.8 nm) layer. Pure SiO₂ and HfO₂ layers are considered for analyzing the HR-XRR data shown in Fig. 5.2, where the interface roughness is attributed to mixing effects. Further, XRR analysis also provides an estimate of surface roughness.

HRBS, Channeling and XRR results of pristine sample, summarized in table 5.2, are comparable to each other and to nominal values within experimental limits. These measurements convincingly suggest the formation of a mixed HfSiO layer instead of a pure SiO₂ layer on Si-surface. Although it is well-known that SiO₂ is very much stable on Si surface.

Table 5.2: Sample structure obtained from HRBS and HR-XRR

Sample structure obtained from different methods				
Nominal values (As per growth)	HRBS	Channelling (From Surface peaks)	HR-XRR	Roughness estimated by HR-XRR
HfO ₂ (2.5 nm)	HfO ₂ (~ 1.8 nm)	--	HfO ₂ (2.37 ± 0.03 nm)	0.37 ± 0.05 nm (at surface)
SiO ₂ (1 nm)	Hf _{0.18} Si _{0.32} O _{0.5} (~ 0.6 nm)	Hf _{0.18} Si _{0.33} O _{0.49}	SiO ₂ (1.8 ± 0.1 nm)	0.24 ± 0.03 nm (at interface)
Si (bulk)	Si (Bulk)	Si (Bulk)	Si (Bulk)	

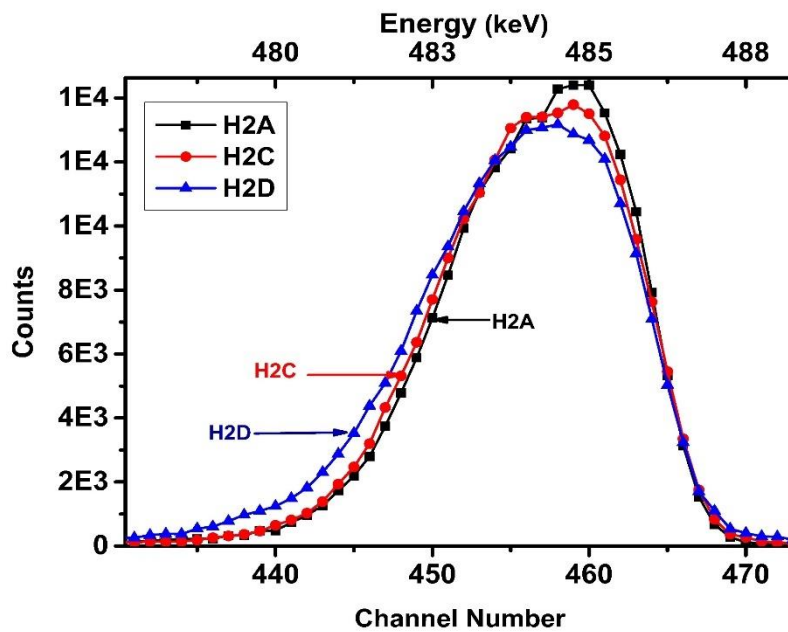


Fig. 5.3: HRBS spectra (zoom on Hf-peak) of irradiated and un-irradiated samples

Hence this mixed layer might have been formed either during or after the deposition of HfO_2 layer. Inter diffusion of Hf into SiO_2 and Si into HfO_2 at $\text{SiO}_2/\text{HfO}_2$ interface is likely to be responsible for the observed mixed layer. This information is expected to be useful for understanding of the kinetics of growth during atomic layer deposition.

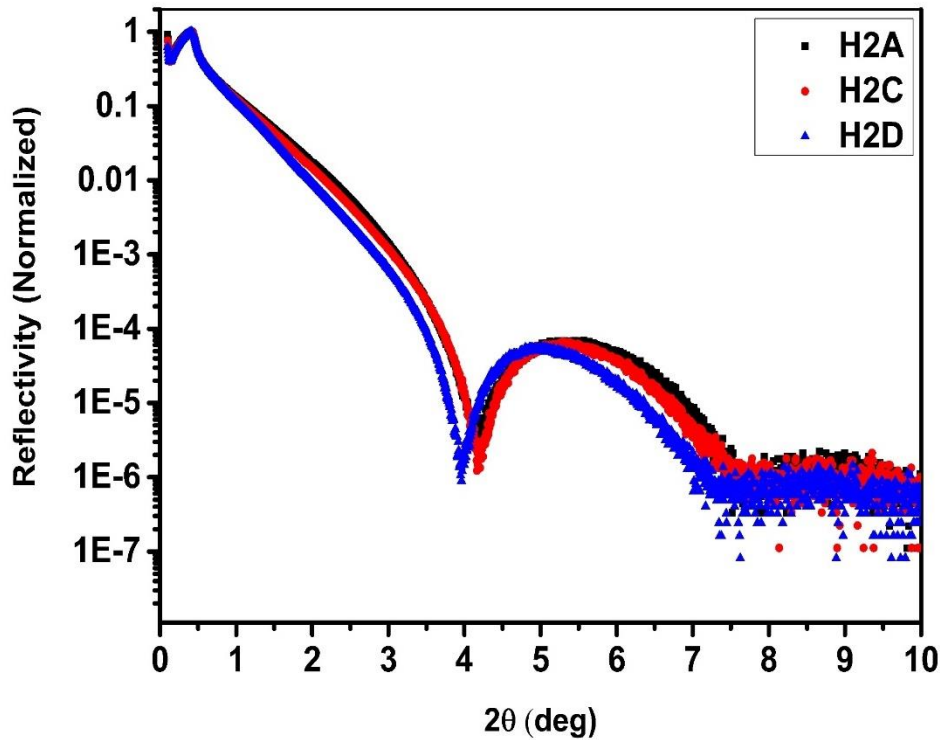


Fig. 5.4: XRR spectra of irradiated and un-irradiated samples

As mentioned earlier, SiO_2 is considered as an interlayer in HfO_2 -based MOS technology [9-10]. Hence it is important to study the stability of $\text{SiO}_2/\text{HfO}_2$ interface over Si/HfO_2 interface. Further it is well known that SiO_2 is more susceptible over Si to swift heavy ion induced track formation. This prompted us to study the effects of SHI on $\text{SiO}_2/\text{HfO}_2$ interface although SHI induced mixing is not reported in Si/HfO_2 and $\text{SiO}_2/\text{HfO}_2$ systems.

80 MeV Ni ion irradiation induced inter-diffusion of Si and Hf across $\text{HfSiO}/\text{HfO}_2$ interface is evident in the HRBS and XRR spectra. Fig. 5.3 shows the HRBS spectra (zoom on Hf-peak) of irradiated and pristine samples. The lower energy edge of this Hf-peak in H2D sample clearly confirms the diffusion of Hf into HfSiO interlayer. Similar effects are also observed in the XRR spectra shown in Fig. 5.4.

Table 5.3 summarizes the results of HRBS/channeling analysis of irradiated and un-irradiated samples.

Table 5.3: HRBS/channeling analysis of irradiated and un-irradiated samples

Sample	$\chi_{\min}\%$	Hf:Si:O
		$Y_{\text{Hf}}/\sigma_{\text{Hf}}: Y_{\text{Si}}/\sigma_{\text{Si}}: Y_{\text{O}}/\sigma_{\text{O}}$ (Estimated from corresponding peaks in channelling spectra.)
H2A	15%	0.182 : 0.328 : 0.451
H2C	12%	0.177 : 0.326 : 0.449
H2D	19%	0.183 : 0.314 : 0.469

As mentioned earlier, a χ_{\min} of about 15% is observed in the near surface channels of Si <111> aligned spectra of pristine (H2A) sample. The χ_{\min} in H2C and H2D is estimated to be 12% and 19% respectively. As mentioned earlier, the elemental composition of the surface layer is estimated using the relative intensities of Hf, Si and O peaks ($Y_{\text{Hf}}/\sigma_{\text{Hf}}: Y_{\text{Si}}/\sigma_{\text{Si}}: Y_{\text{O}}/\sigma_{\text{O}}$) in channeled spectra after subtracting the contribution of Si-surface peak. No significant changes in the relative concentrations of various elements in mixed layers are noticed as a function of fluence. This is reasonable because this analysis assumes a single amorphous layer to start with. However, SIMNRA simulation of random spectrum suggests the existence of a pure HfO₂ (1.8 nm) layer on the surface of interlayer. Table 5.4 summarizes the results of SIMNRA analysis of HRBS spectra obtained from irradiated and un-irradiated samples.

Table 5.4: SIMNRA analysis of HRBS spectra of irradiated and un-irradiated samples

Sample	Layer I Hf:O (Surface)	Layer I Thickness 10^{15} Atoms/cm ²	Layer II Hf:Si:O	Layer II Thickness 10^{15} Atoms/cm ²
H2A	0.333:0.667	13	0.180:0.320:0.500	7
H2C	0.320:0.680	12	0.156:0.396:0.448	8
H2D	0.306:0.694	12	0.145:0.360:0.495	12

A systematic increase in the concentration of Si relative to that of Hf in interlayer is noticed as a function of fluence. Similarly a systematic increase in the thickness of interlayer is also observed. These two observations together with XRR analysis confirm that SHI can induce intermixing across HfSiO/HfO₂ interface. As mentioned earlier, SiO₂ is more susceptible

to SHI induced track formation when compared to Si. Hence more prominent SHI induced intermixing effects are expected in HfSiO/HfO₂, SiO₂/HfO₂ systems when compared to Si/HfO₂ system. However, an interlayer is essential for HfO₂ based MOS devices because HfO₂ itself is not thermally stable on Si surface. Hence, it is important to study the irradiation effects on “interlayer/HfO₂” interface. Present study provides useful information for understanding the effects of SHI irradiation on such “interlayer/HfO₂” interface.

B. Effects of 120 MeV Au ion irradiation:

As shown earlier, 80 MeV Ni ion irradiation has provided some useful information of SHI induced intermixing. To attain more diffusion of Hf across the interface of HfO₂/SiO₂, 120 MeV Au ion irradiation was performed on H1 samples (see Table 2.1). The typical sample structure in H1 series samples is “HfO₂ (3 nm) / SiO₂ (0.6 nm) / Si (substrate)”. HRBS was performed in both, the random and channeled directions on the pristine and irradiated samples.

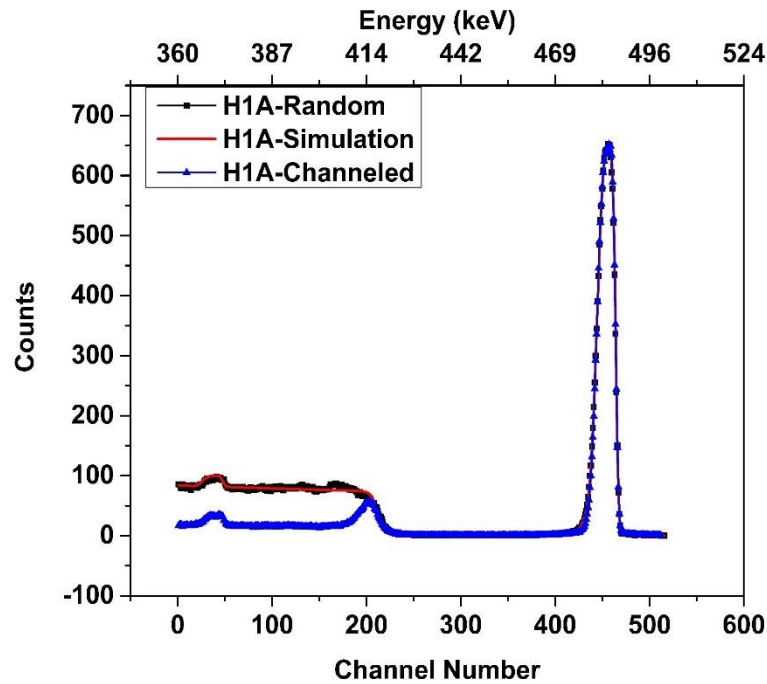


Fig. 5.5: Random, channeled and simulated HRBS spectra of pristine sample (H1A)

Fig. 5.5 shows both the random, channeled and simulated spectra of pristine sample H1A. The composition and the areal densities have been estimated and are given in the table 5.5. Fig. 5.6 shows the zoom of Hf peak of all the samples, which clearly shows the diffusion of Hf across HfO₂/SiO₂ interface. From the HRBS measurements, it is quite evident that the interlayer is a mixed layer of HfSiO and SiO₂ layers instead of a pure SiO₂ layer.

Further, the thickness of HfSiO layer is increased with increase in the fluence. Fig. 5.7 depicts the depth profiles of pristine and irradiated samples. The analogy of depth profiles from the HRBS results confirm the increase in the physical thickness of the interlayer as the irradiation dose increases. The composition of each layer has been converted into depth profile for better understanding of the diffusion of Hf across the interface of HfO₂/HfSiO.

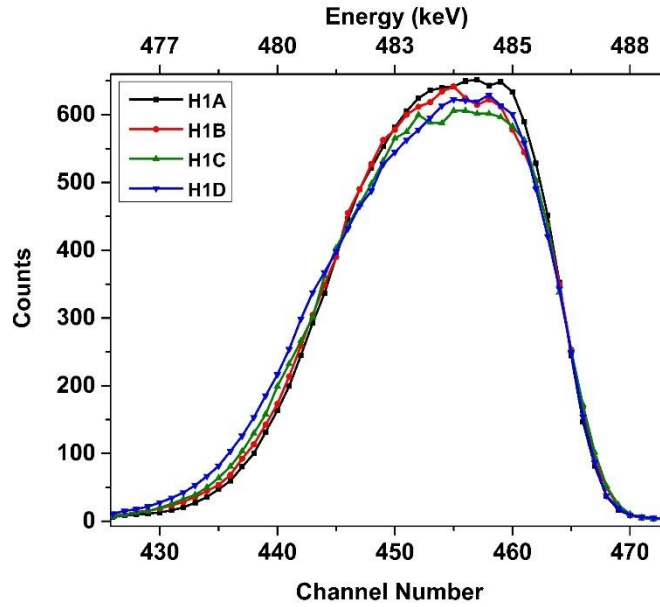


Fig. 5.6: HRBS spectra (zoom on Hf-peak) of pristine and irradiated samples

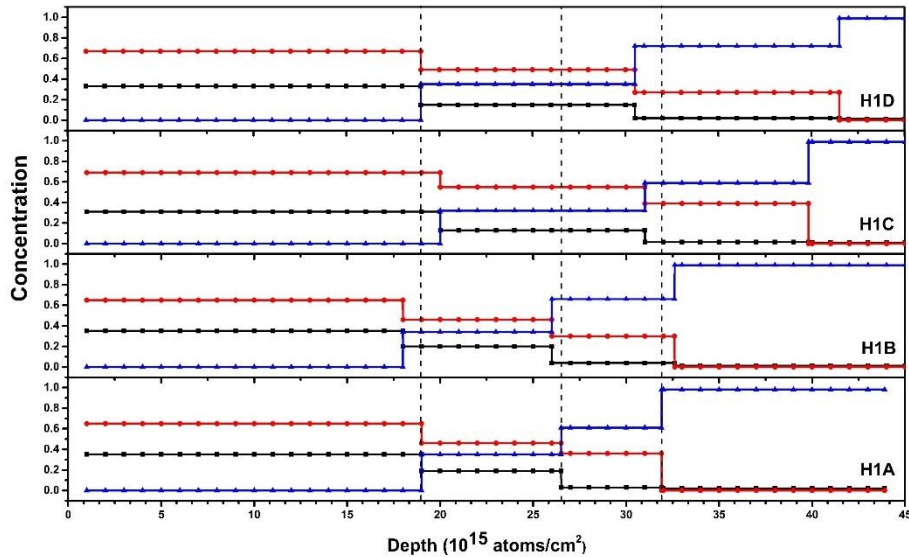


Fig. 5.7: Depth profiles of pristine and irradiated samples

Table 5.5: SIMNRA analysis – Composition of Hf, Si and O

H1A					H1B				
Layer	Thickness ($\times 10^{15} \text{ cm}^{-2}$)	Composition			Layer	Thickness ($\times 10^{15} \text{ cm}^{-2}$)	Composition		
		Hf	O	Si			Hf	O	Si
1	19	0.35	0.65	0	1	19	0.35	0.65	0
2	7.5	0.19	0.46	0.35	2	8.0	0.20	0.46	0.34
3	5.4	0.03	0.36	0.61	3	6.6	0.04	0.30	0.66
4	>12.0	0	0	1.0	4	>13.0	0	0	1.0
Si (Bulk)					Si (Bulk)				

H1C					H1D				
Layer	Thickness ($\times 10^{15} \text{ cm}^{-2}$)	Composition			Layer	Thickness ($\times 10^{15} \text{ cm}^{-2}$)	Composition		
		Hf	O	Si			Hf	O	Si
1	19	0.35	0.65	0	1	19	0.33	0.67	0
2	11.0	0.13	0.55	0.32	2	11.5	0.15	0.50	0.35
3	8.8	0.02	0.39	0.59	3	11.0	0.01	0.27	0.72
4	>16.0	0	0	1.0	4	>20.0	0	0	1.0
Si (Bulk)					Si (Bulk)				

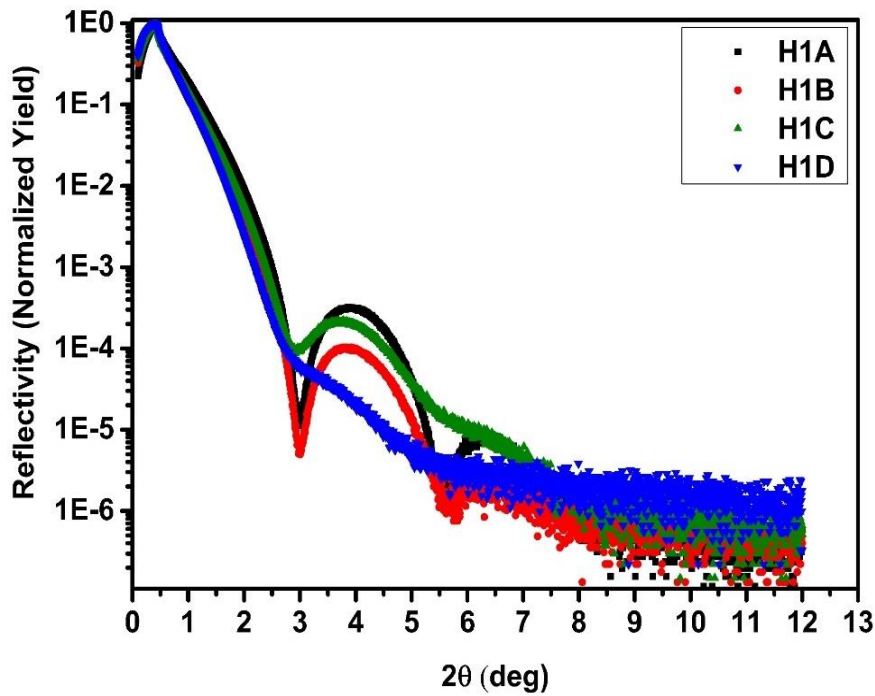
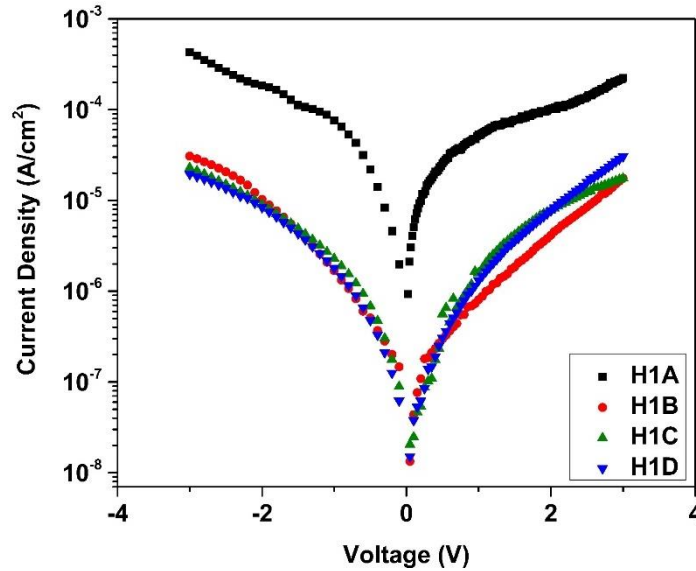


Fig. 5.8: XRR pattern of pristine and irradiated samples

These results are further confirmed by the XRR measurements. Fig. 5.8 shows the XRR pattern of all the samples. XRR measurements yielded the thickness, surface/interface roughness and density of the layers.

Table 5.6: XRR analysis of H1 samples

H1A	Thickness (nm)	Roughness (nm)			H1B	Thickness (nm)	Roughness (nm)	
HfO ₂	2.97	0.42			HfO ₂	2.88	0.46	
HfSiO	0.36	0.26			HfSiO	0.44	0.30	
Si					Si			
H1C	Thickness (nm)	Roughness (nm)			H1D	Thickness (nm)	Roughness (nm)	
HfO ₂	2.75	0.62			HfO ₂	2.67	0.73	
HfSiO	0.52	0.49			HfSiO	0.72	0.64	
Si					Si			

**Fig. 5.9:** I-V characteristics of pristine and irradiated samples

From these measurements, it is observed that both the roughness and the thickness of the interlayer increases as the fluence increases. The increase in the roughness is quite understandable because of the interaction of a very high energy 120 MeV Au ion beam with the sample. In addition to the increase in the roughness, the results of XRR measurements clearly indicate the intermixing and increase in the physical thickness of the interlayer HfSiO. Layer thickness and surface/interface roughness are given in the table 5.6 by considering the nominal densities of HfO₂ and HfSiO. From both the HRBS and XRR measurements, it is clear that the SHI irradiation can induce interface mixing at the HfO₂/SiO₂ interface. Further, the electrical response (I-V characteristics) of this MOS device has been studied.

Significant effects of 120 MeV Au ion irradiation have been observed on the pristine and irradiated samples from the I-V characteristics. There is an order of magnitude difference in the leakage current density of pristine and irradiated samples. Based on the HRBS and XRR analysis, the ion irradiation prompts the formation of a thicker HfSiO interlayer which is likely to be responsible for the observed reduction in leakage current of irradiated samples, as shown in Fig. 5.9.

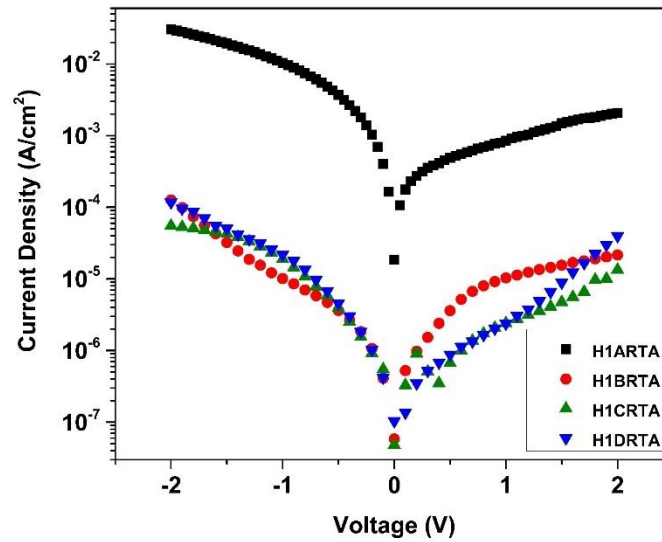


Fig. 5.10: I-V characteristics of pristine and irradiated samples after RTA

All the samples were subjected to RTA to study the annealing kinetics. The optimum temperature and time were fixed after a thorough literature survey [23-24]. RTA was performed on all the samples in N₂ atmosphere for 60 seconds. Fig. 5.10 shows the I-V characteristics after performing RTA. I-V characteristics evinced that the leakage current increases by one order, for all the samples. It is due to an increase in the density of the defects during RTA processing.

5.3.2 HfO₂ thin films deposited by RF magnetron sputtering – Effects of 80 MeV Ni ion irradiation

So far, all the studies were carried out on ALD grown samples in which there is an interfacial layer SiO₂ in between HfO₂ and Si. This interfacial layer improves the quality of HfO₂/Si interface. Now, the interest is to study the HfO₂/Si system without any such interfacial layer. It is well-known that the HfO₂/Si interface is not that much stable interface as compared to SiO₂/Si interface. The density of defects in the pristine samples itself shows

some impact on the structural and electrical properties of this interface. Moreover, SHI induced tuning of the HfO_2/Si interface is an important study in this thesis. SHI induced intermixing effects which increase the interlayer thickness may predominantly reduce the leakage currents. Moreover, the defect density during the growth and the defects that are created during irradiation may also alter the electrical properties of the materials. Hence, HfO_2/Si MOS capacitors have been fabricated by RF magnetron sputtering technique and these samples have been irradiated by 80 MeV Ni ion irradiation at various fluences. The HfO_2/Si thin films were irradiated by 80 MeV Ni ion for studying the effects on the structural and electrical properties. XRR measurements have been performed on these samples to elucidate the thickness and interface roughness (see Fig. 5.11).

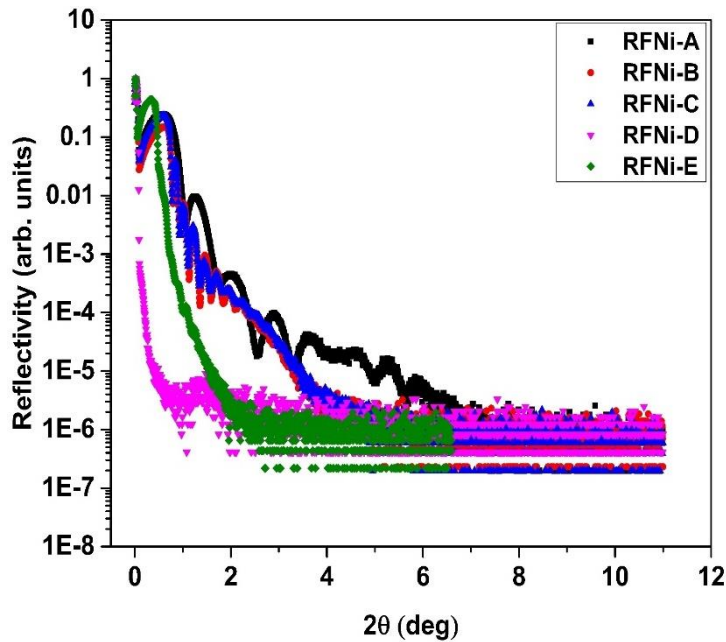


Fig. 5.11: XRR measurements of 80 MeV Ni irradiation at different fluences (ions/cm²)

From XRR measurements, we see an increase in the surface and interface roughness with increase in the irradiation fluence. This qualitative information from XRR measurements is further strengthened by I-V measurements. Au/ HfO_2/Si MOS capacitors were fabricated and the I-V measurements were performed on these devices. These I-V characteristics are shown in Fig. 5.12. Leakage current density as a function of irradiation fluence at ± 1 V is shown in the Fig. 5.13. The leakage current density has been found to decrease with increase in the irradiation fluence. These values show a variation from 8.2×10^{-5} A/cm² to 1.4×10^{-7} at -2 V with the irradiation fluence. A systematic decrease in the leakage current with applied voltage has been observed. This reduction in the leakage current has been

attributed to the SHI induced intermixing effects, nature of the pre-existing defects and the defects that were created by 80 MeV Ni ion irradiation. SHI induced intermixing effects which results in a thicker interlayer of HfSiO may also be a possible reason for this decrease in the leakage current density. So, from the I-V measurements, a decrease in the leakage current density has been observed with increase in the irradiation fluence.

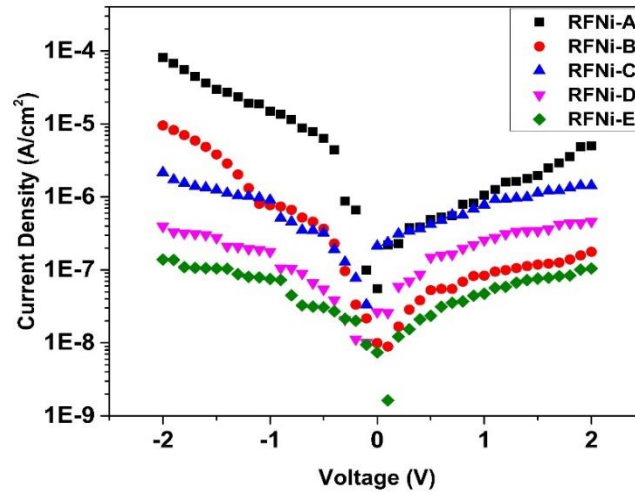


Fig. 5.12: Leakage current density vs. applied bias voltage of 80 MeV Ni irradiation at various fluences

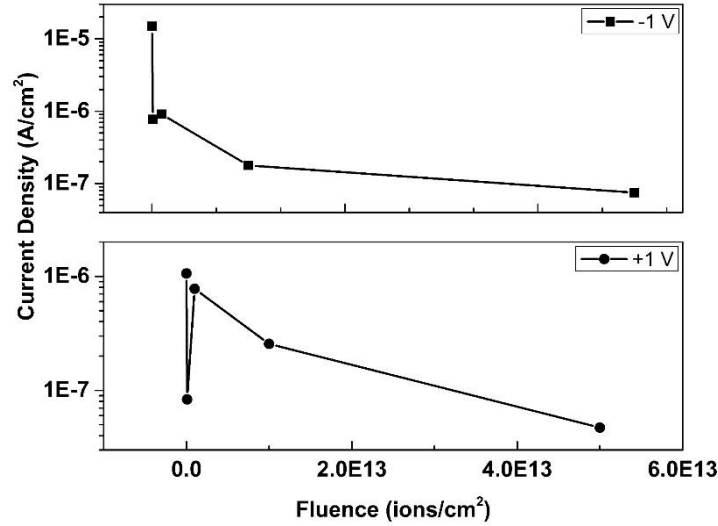


Fig. 5.13: Leakage current density vs. voltage at ± 1 of 80 MeV Ni ion irradiation at different fluences

5.4. Conclusions

HRBS, Channeling, XRR and I-V measurements were performed on ALD grown HfO₂/SiO₂/Si based H1 and H2 series samples. These measurements suggest that the interlayer is a mixed HfSiO layer instead of a pure SiO₂ layer, as intended. In H2 (HfO₂

(2.5 nm)/SiO₂ (1 nm)/Si) series samples, the effects of 80 MeV Ni ion irradiation on this interface have been studied. The thickness of this interlayer is also found to increase with increase in fluence. These observations together with XRR analysis confirm that SHI can induce inter-diffusion of Hf and Si across HfSiO/HfO₂ interface. Further, 120 MeV Au ion irradiation was performed on H1 (HfO₂ (3 nm)/SiO₂ (0.7 nm)/Si) series samples to study the influence of SHI irradiation on the structural and electrical properties. The thickness of the interlayer (HfSiO) has been found to increase with increase in the irradiation fluence which is evident from HRBS and XRR measurements. In addition to HRBS and XRR analysis, I-V measurements were performed. The leakage current is found to decrease by one order upon irradiation which can be attributed to the increase in the physical thickness of the interlayer. The samples are further subjected to RTA at 600 °C in N₂ atmosphere for 60 seconds for studying the annealing kinetics.

Moreover, HfO₂ thin films deposited on Si substrates by using RF magnetron sputtering technique have been studied. 80 MeV Ni ion irradiation induced effects have been observed on the electrical properties of these films. A systematic decrease in the leakage current density as a function of irradiation fluence has been observed. The effects of defects together with the SHI induced intermixing effects on HfO₂/Si MOS devices have been studied.

SHI induced intermixing effects on the structural and electrical properties of HfO₂ based MOS devices have been studied as an important part of this thesis work. To the best of our knowledge, there are no prior reports about these studies in HfO₂/SiO₂/Si and HfO₂/Si systems. In view of the thermal budget, interface engineering schemes to tune the material properties by SHI irradiation is a suitable study. The spatial selectivity opted for irradiation on any given material is the main asset of SHI irradiation. SHI induced intermixing effects and defects dynamics in the process of irradiation have a certain impact on the structural and electrical properties of these technologically important HfO₂ based devices.

Even though offline electrical measurements (after irradiation) yielded promising results, there may be a small discrepancy in the leakage currents and capacitances due to various aspects such as metal contacts and their adhesion on HfO₂ or Si. In order to resolve these issues, in-situ electrical measurements were performed. These results unambiguously reveal a better understanding of SHI induced intermixing effects and the defect dynamics. These reliable and promising results have been discussed in detail in the following chapter.

5.5 References

1. Chau, R., S. Datta, M. Doczy, J. Kavalieros, and M. Metz, Extended Abstracts of International Workshop on Gate Insulator (IWGI), Tokyo, Japan, 124 (2003).
2. A. S. Foster, F. L. Gejo, A. L. Shluger, and R. M. Nieminen, *Phys. Rev. B*, **65** (2002) 174117.
3. W. J. Zhu, T. P. Ma, S. Zafar, and T. Tamagawa, *IEEE Electron Device Lett.*, **23** (2002) 597.
4. A. Y. Kang, P. M. Lenahan, and J. F. Conley Jr., *IEEE Trans. Nucl. Sci.*, **49** (2002) 2636.
5. K. Xiong, J. Robertson, M. Gibson, and S. J. Clark, *Appl. Phys. Lett.*, **87** (2005) 183506.
6. S.K. Dixit, Ph.D. Thesis, Vanderbilt University, Nashville, TN, USA and refs. therein (2008).
7. G.D. Wilk, R.M. Wallace, J.M. Anthony, *J. Appl. Phys.*, **89** (2001) 5243.
8. L. Pereira, *Mat. Sci. and Engg. B*, **109** (2004) 89.
9. J. K. Schaeffer, S. B. Samavedam, D. C. Gilmer, V. Dhandapani, P. J. Tobin, J. Mogab, B.-Y. Nguyen, B. E. White, Jr., S. Dakshina-Murthy, R. S. Rai, Z.-X. Jiang, R. Martin, M. V. Raymond, M. Zavala, L. B. La, J. A. Smith, R. Garcia, D. Roan, M. Kottke and R. B. Gergory, *J. Vac. Sci. Technol. B*, **21** (2003) 11.
10. I. S. Park, T. Lee, H. Ko and J. Ahn, *J. Korean Phys. Soc.*, **49** (2006) 760.
11. G. D. Wilk and R. M. Wallace, *Appl. Phys. Lett.*, **74** (1999) 2854.
12. D. K. Avasthi and G. K. Mehta, “Swift Heavy Ions for Materials Engineering and Nanostructuring”, Capital Publishing Company, New Delhi (2011).
13. I. C. Kizilyalli, R. Y. S. Huang and P. K. Roy, *IEEE Electron Dev. Lett.*, **19** (1998) 423.
14. D.K. Avasthi, *Def. Sci. Journal*, **59** (2009) 401.
15. Xiangkun Yu , Lin Shao, Q.Y. Chen, L. Trombetta, Chunyu Wang, Bhanu Dharmaiahgari, Xuemei Wang, Hui Chen, K.B. Ma, Jiarui Liu and Wei-Kan Chu, *Nucl. Instr. Meth. Phys. Res. B*, **249** (2006) 414.
16. A. Benyagoub, *Nucl. Instrum. Methods Phys. Res. B*, **245** (2006) 225.
17. H. Gruer, *Thin Solid Films*, **509** (2004) 47.
18. W. Nieveen, *Appl. Surf. Sci.*, **556** (2004) 231.

19. Chan Taw Kuei, Ph.D. Thesis, National University Of Singapore, Singapore, and refs. therein (2009).
20. T Osipowicz, HL Seng, TK Chan and B Ho, **249** (2008) 915.
21. A. Bongiorno, A. Pasquarello, M. S. Hybertsen, and L. C. Feldman, *Phys. Rev. Lett.*, **90** (2003) 186101.
22. A. Bongiorno, A. Pasquarello, M. S. Hybertsen, and L. C. Feldman, *Microelectron. Engg.*, **72** (2004) 197.
23. B. H. Lee, L. Kang, R. Nieh, W.-J. Qi, and J. C. Lee, *Appl. Phys. Lett.*, **76** (2000) 1926.
24. Tingting Tan, Zhengtang Liu, Hongcheng Lu, Wenting Liu and Feng Yan, *Vacuum*, **83** (2009) 1155.

Chapter 6

In-situ studies on the electrical properties of HfO₂ based MOSCAPs under SHI irradiation

This chapter presents in-situ studies on the electrical properties of HfO₂ based MOSCAPs under SHI irradiation. ALD grown samples were studied during 120 MeV Ag ion irradiation whereas the samples grown by RF magnetron sputtering were studied during 120 MeV Au ion irradiation.

6.1 Introduction

Thermodynamic instability and the lower band offsets are the practical limitations which normally restrict the applicability of high-k dielectric materials in device fabrication [1-3]. HfO₂ has evolved in the commercial arena despite the trade-off between the dielectric constant and the band offsets [4,5]. This inevitable compromise is taken care, to some extent, by introducing a thin interfacial layer of SiO₂ between Si and HfO₂ layer in HfO₂ based MOS devices [6,7]. The interface of HfO₂/Si is still under an extensive debate over the years in various aspects of radiation exposure [8,9]. SHI irradiation has been widely used for the material modifications in order to tune their properties [10]. SHI induced mixing / modifications at the interfaces can yield relatively new materials [11]. SHI induced tuning of the material properties could be one of the reliable ways to overcome the high thermal budgets [12]. Moreover, SHI irradiation offers spatial selectivity as it is possible to irradiate specific locations on sample surface through properly designed masks. SHI irradiation effects on the HfO₂ based MOS devices have not been explored to sufficient extent in SiO₂ [13-16]. In the present study, SHI irradiation has been used to tailor the gate dielectric materials to attain desired objectives. As discussed earlier, any energetic ion/particle while passing through a material loses its energy in that medium via electronic (S_e) and nuclear energy (S_n) loss mechanisms. Electronic (S_e) energy loss dominates at high ion energies ($> 1 \text{ MeV}/\mu$) while nuclear energy loss (S_n) dominates at low energies ($< 1 \text{ keV}/\mu$). The nuclear energy loss produces defects such as vacancies, interstitials etc. whereas the electronic energy produces deep defects and trap centers together with inter-diffusion of constituent elements by excitation and ionization of the adjoining atoms of the target material. This has impelled us to study the SHI induced intermixing effects on the structural properties and consequent effects on the electrical properties of the HfO₂ based MOS devices. Reliable in-situ electrical measurements were performed on these devices fabricated by ALD and RF sputtering techniques and these devices have been tested for their reliability and sustenance by in-situ electrical characteristics which directly yielded the device's electrical parameters. All the in-situ measurements at different ion fluences were performed on the same device to avoid any inconsistency in the electrical characteristics due to the variation in preliminary parameters of devices/sample. Moreover, in-situ measurements evade any environment induced modifications of the electrical characteristics in the device.

In this chapter, we have presented a thorough investigation on the electrical response of these devices and the interfaces as a function of irradiation fluences.

6.2 Experimental details

ALD grown ultra-thin device quality $\text{HfO}_2/\text{SiO}_2/\text{Si}$ samples, obtained from SEMATECH, USA, have been used for 120 MeV Ag ion irradiation whereas HfO_2 (15 nm)/Si samples grown by RF magnetron sputtering have been used for 120 MeV Au ion irradiation. The typical sample structure of ALD grown samples is “ HfO_2 (2.7 nm) / SiO_2 (0.6 nm) / Si (substrate)”. These samples were termed as H3 series samples. The nominal structure of RF series samples is “ HfO_2 (~15 nm) / Si (substrate)”. Irradiation details of these samples are given in table 6.1.

Table 6.1: Irradiation details

Sample	Ion & Energy	Irradiation Fluence (ions/cm ²)
H3A	----	Pristine
H3B*	Ag, 120 MeV	1×10^{14}
RA	----	Pristine
RB*	Au, 120 MeV	1×10^{14}

**Note: However, in-situ I-V and C-V measurements were performed for various intermediate fluences.*

For RF magnetron sputtering, the p-Si (100) wafer of resistivity $\sim 1\text{-}10 \text{ } \Omega\text{-cm}$ (with $N_A \sim 10^{15} \text{ cm}^{-3}$) has been used for fabricating MOS capacitors. Si wafer was cleaned and etched using the standard RCA cleaning procedure. Finally, the wafer was dried using pressurized nitrogen gas. On top of the HfO_2 sample surface Au metal contacts (Diameter: 2 mm and Thickness: 300 nm) were deposited by thermal evaporation technique. H3 and RF series samples were mounted on a specially designed ladder for SHI irradiation to measure I-V and C-V characteristics. On an average there were four devices connected on each sample for in-situ measurements. SHI irradiation was performed at room temperature at IUAC, New Delhi. Low beam currents have been preferred for reducing the damage of the device. 0.5 pA was maintained throughout the experiments and the ion fluence has been varied from 1×10^{10} to 1×10^{14} ions/cm². Conferring to MIL-STD 750 method, after

every ion fluence the electrical measurements were performed within 15 minutes of time to elude the time dependent annealing of defects/damage caused by the energetic ion beam. The current–voltage characteristics were carried out using a B1500 semiconductor device analyzer. HRBS measurements were performed to elucidate the SHI induced intermixing effects on both the set of samples (Pristine and highest dose samples only at NUS, Singapore).

6.3 Results and Discussions

6.3.1 Effects of 120 MeV Ag ion irradiation on ALD grown H3 series samples

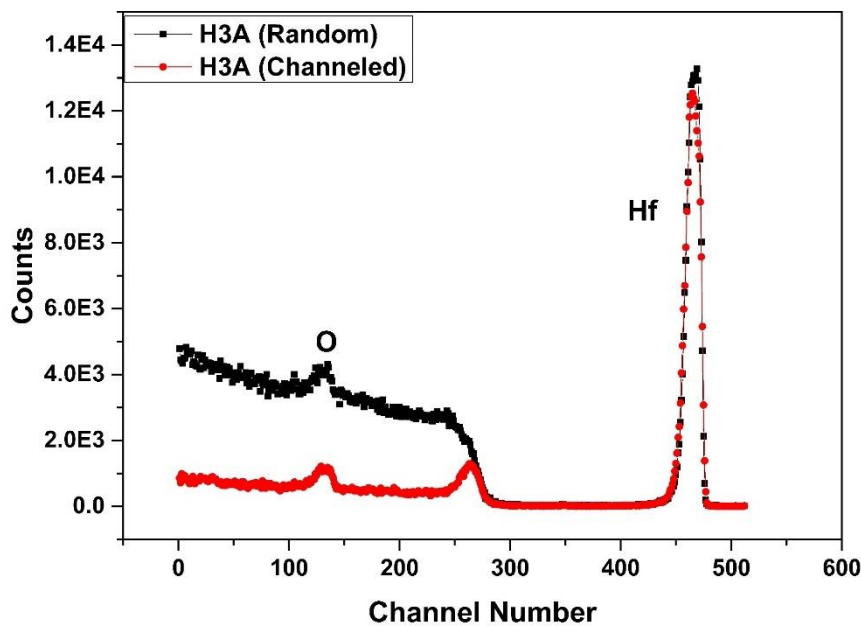


Fig. 6.1: Random and channeled HRBS spectra of H3A pristine sample

HRBS measurements were performed on H3A and H3B samples. Random and channeled HRBS spectra of pristine sample (H3A) is shown in Fig. 6.1. Beam is channeled in the substrate along Si $\langle 111 \rangle$ direction to minimize the background scattering from silicon. Fig. 6.2 shows the Random HRBS spectra of H3A and H3B Samples. The yield of Hf seems to be less everywhere in the irradiated sample as compared to that of pristine sample. The width of this peak is also slightly higher in irradiated sample. This indicates possible increase in the thickness and decrease in the density of the irradiated samples. As demonstrated in previous chapter, SHI irradiation causes a slight but clear intermixing in similar samples.

In-situ I-V and C-V measurements were performed during the 120 MeV Ag ion irradiation in H3 series sample as a function of fluence (from 1×10^{11} to 1×10^{14} ions/cm²). The in

situ I–V characteristics of H3 sample at various fluences are shown in Fig. 6.3. SHI induced annealing effects have been observed in the lower fluences upto 1×10^{12} ions/cm².

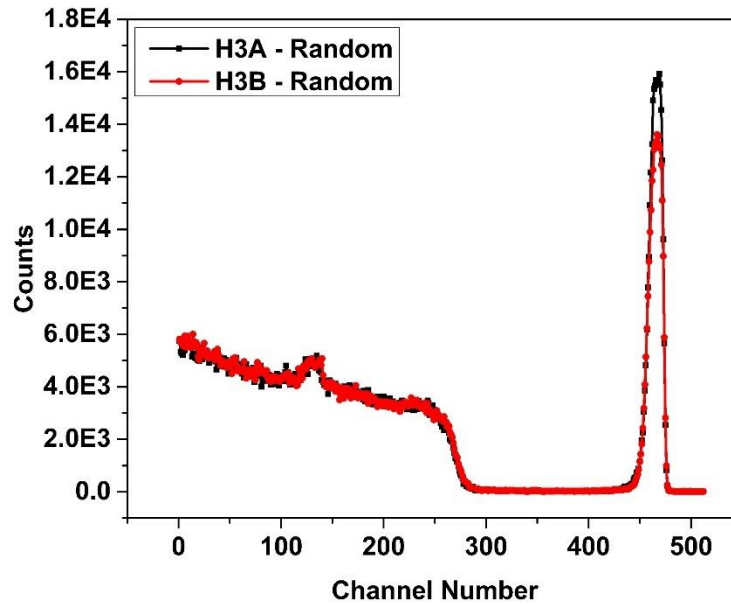


Fig. 6.2: Random HRBS spectra of H3 pristine and irradiated sample

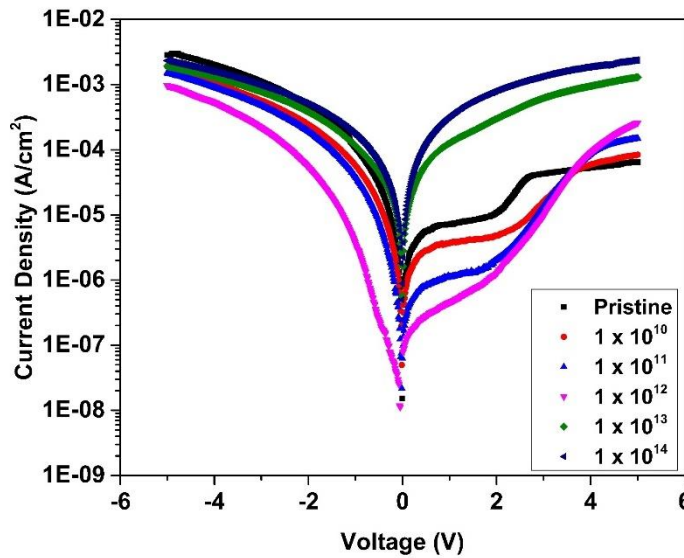


Fig. 6.3: In-situ I-V characteristics of sample
(fluence: ions/cm²)

Fig. 6.4 depicts the leakage current density as a function of irradiation fluence at ± 1 V. The reduction of leakage current with fluence is evident in this regime. This reduction in leakage current density can be attributed to the improvement of the device as the defects get annealed during SHI irradiation. However, after 1×10^{12} ions/cm² fluence, the leakage current has been observed to increase up to the fluence of 1×10^{14} ions/cm². The sustenance and device tolerance have been evicted from these higher fluences. At the higher fluences,

the degradation of the device performance has been observed in terms of its increase in the leakage current. On the other hand, in the negative bias region, the leakage currents are found to be less because the device is in depletion region. However, the increase in the leakage current with the increase in irradiation fluence has also been observed even in this region. It is also important that the depletion region is not observed at higher dose indicating that the device is driven to inversion region. This is possible because the presence of defects can influence carrier recombination processes.

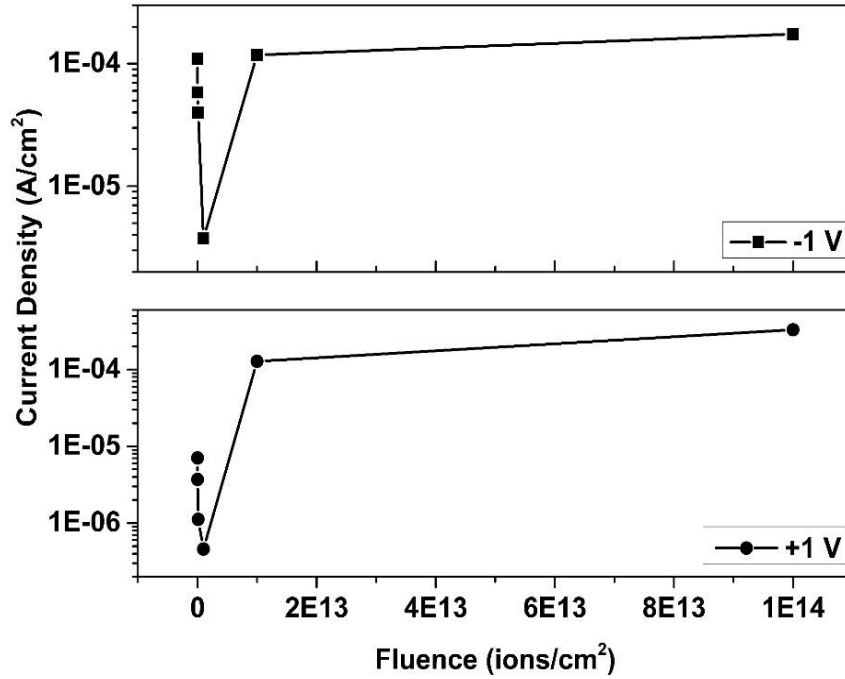


Fig. 6.4: I-V characteristics at ± 1 V of H3 sample

Defects annealing at lower fluences and creation of defects at higher fluences is the signature of SHI irradiation. These defects cause defect-assisted tunneling of electrons across the interface. Thus current transport across oxide interface is caused by tunneling. The dynamic equilibrium of two competing processes such as defects creation and annealing by ion beam occur in the interaction of SHI with a given material. The defect creation is primarily due to the displacement of atoms during elastic collisions (S_n) of ions with atoms whereas annealing of defects takes place due to inelastic collisions (S_e) instigating the excitation and ionization of atoms and their consequent relaxation. However, after a critical dose, both the processes can lead to the formation of defects and inter-diffusion of elements. These processes are responsible for the observed increase in leakage current at higher doses.

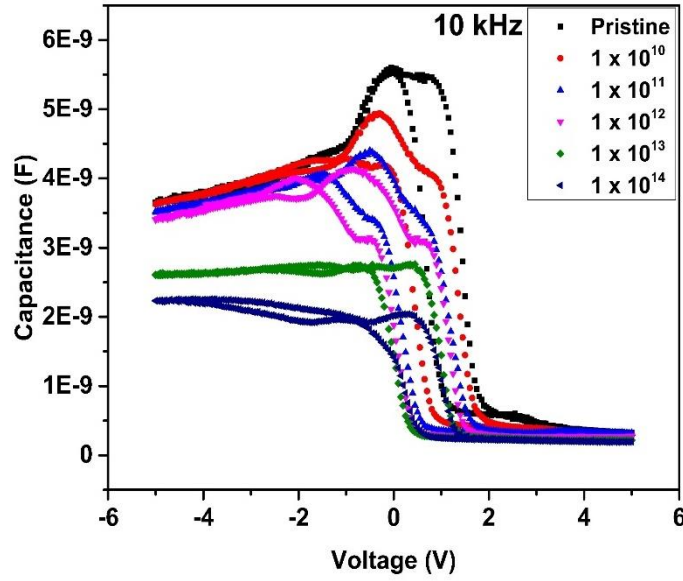


Fig. 6.5: In-situ C-V characteristics of H3 series sample at 10 kHz frequency

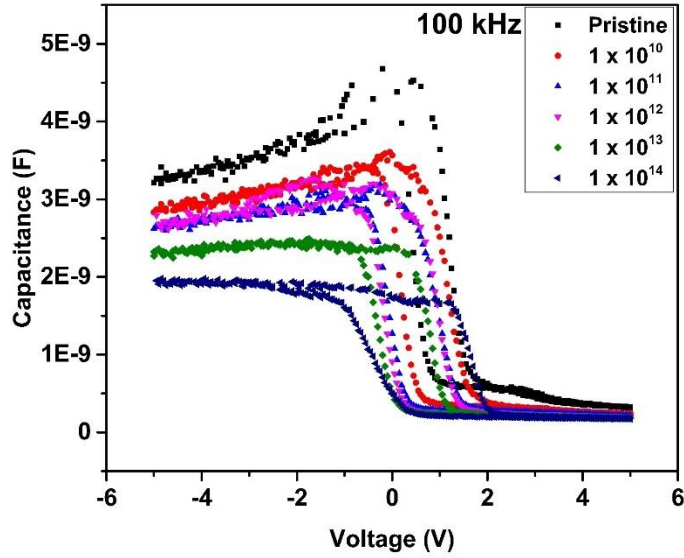


Fig. 6.6: In-situ C-V characteristics of H3 series sample at 100 kHz frequency

Fig. 6.5 to 6.7 depict the C-V characteristics of H3 samples. These in-situ C-V measurements were performed at 10 kHz, 100 kHz and 1 MHz respectively. Fig. 6.8 depicts the accumulation capacitance as function of irradiation fluence at -3 V. A systematic decrease in the accumulation capacitance with increase in the irradiation fluence has been observed. This can be attributed to the possible increase in physical thickness and changes in the composition of the interlayer (HfSiO) layer which can affect its dielectric constant.

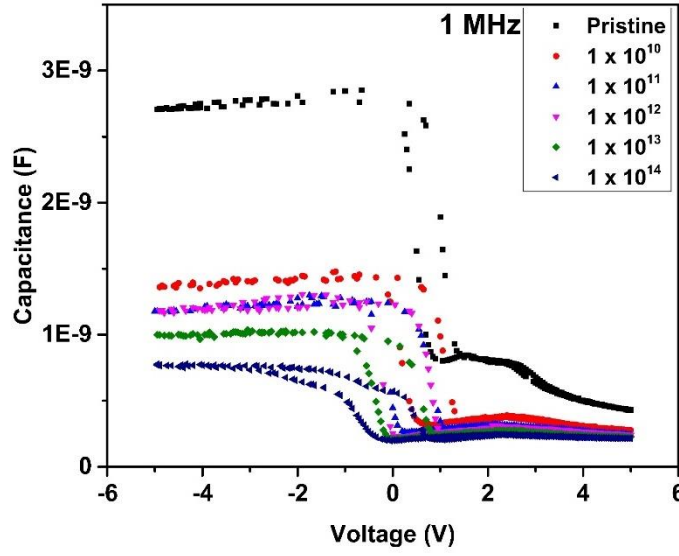


Fig. 6.7: In-situ C-V characteristics of H3 series sample at 1 MHz frequency

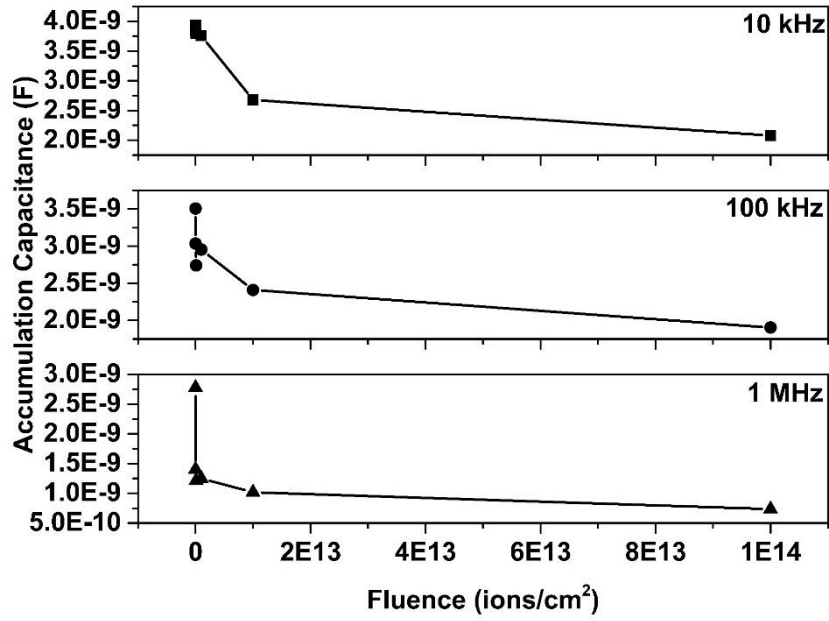


Fig. 6.8: Accumulation capacitance of H3 series samples at -3 V as functions of fluence (ions/cm^2) at different frequencies

Flat band capacitance (C_{FB}), Mid-gap voltage shift (ΔV_{MG}), Flat band voltage shift (ΔV_{FB}), Density of oxide trapped charges (D_{ot}) and Density of interface charges (D_{it}) have been calculated using the high-frequency C-V curves measured at 1 MHz. These values were obtained from the C-V curves as per the standard procedures adopted in literature [17]. The flat band capacitance as a function of irradiation fluence is shown Fig. 6.9. There is a decrease in the C_{FB} corresponding to the observed decrease in the accumulation (oxide) capacitance (see Fig. 6.9). Moreover, the flatband shift has also increased as a function of

irradiation fluence. This increase in the ΔV_{FB} confirms the increase in the defects density in the oxide layer. There is an increase in the mid-gap voltage as function of irradiation fluence. The mid-gap voltage shift as a function of fluence is shown in Fig. 6.10.

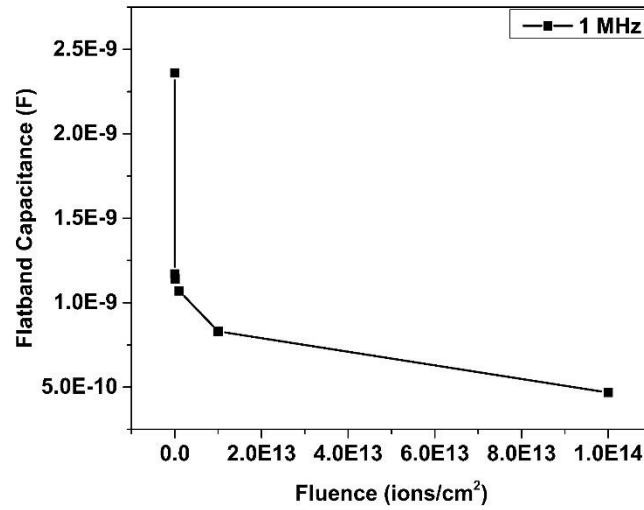


Fig. 6.9: C_{FB} as function of irradiation fluence at 1 MHz frequency in H3 sample

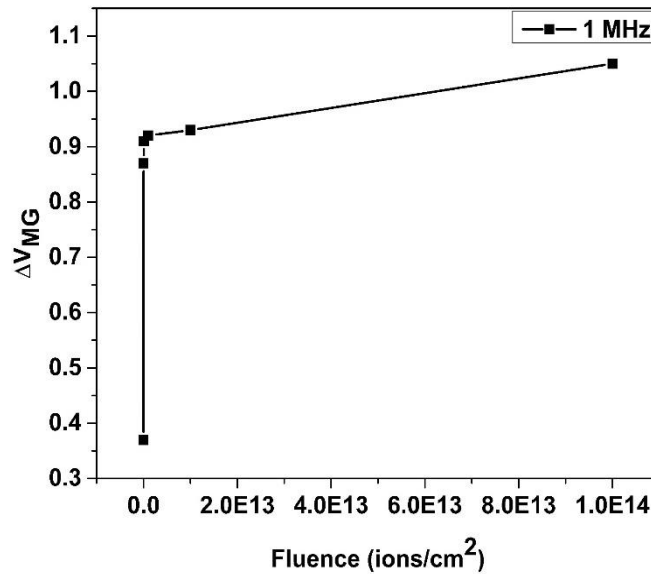


Fig. 6.10: ΔV_{MG} as function of irradiation fluence at 1 MHz frequency in H3 sample

Further, the density of these oxide traps associated with the mid-gap voltage shift has been estimated which is shown in Fig. 6.11. The oxide trap density (D_{ot}) increases up to 1×10^{12} ions/cm² fluence, thereafter there is a decrease in the oxide trap density (see Fig. 6.12). It is well-known that the slope of C-V curves can be altered by the interface traps. The density of interface traps (D_{it}) is directly proportional to the change in the flat band and

mid-gap voltages. A behavior similar to the D_{ot} changes has been observed in the density of interface (D_{it}) charges as shown in Fig. 6.13.

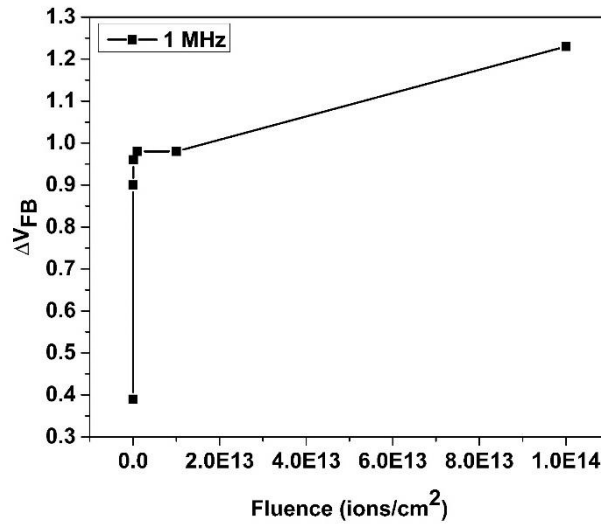


Fig. 6.11: ΔV_{FB} as function of irradiation fluence at 1 MHz frequency in H3 sample

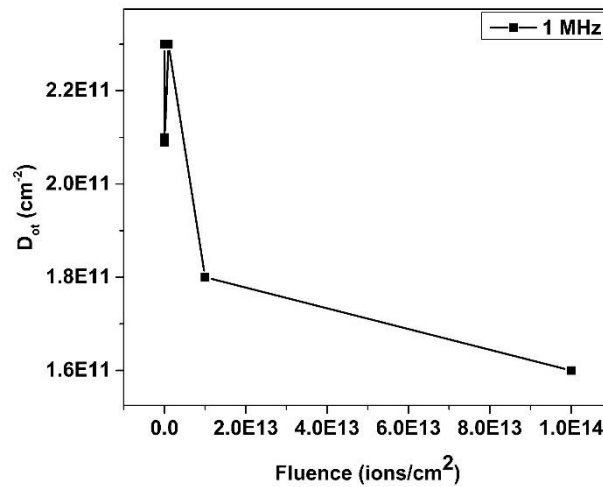


Fig. 6.12: D_{ot} as function of irradiation fluence at 1 MHz frequency in H3 sample

The density of interface traps and oxide traps are well within the acceptable ranges in these device quality ALD grown samples. It is shown that the SHI irradiation can further reduce the defects by annealing effects at lower doses. However, excessive fluences deteriorated these films although the density of defects are not significant even at higher fluences. This can be understood to some extent by the fact that physical thickness is very small and the initial quality of films is very good in this series of samples. Hence, these devices may be considered as radiation hardened for practical applications.

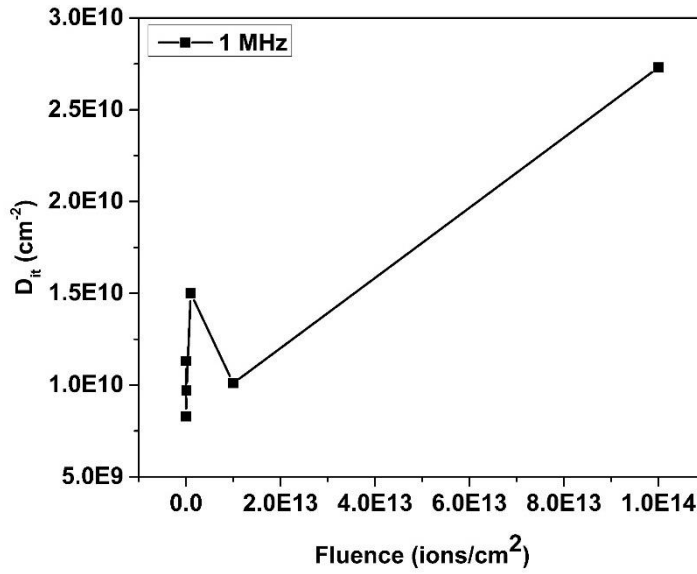


Fig. 6.13: D_{it} as function of irradiation fluences at 1 MHz frequency in H3 sample

6.3.2 Effects of 120 MeV Au ion irradiation on RF series samples

SHI induced inter-diffusion effects are evident but not significant in ultra-thin ALD grown samples. SHI induced diffusion at the interface produced a thick HfSiO layer. Even though these promising results from HRBS measurements have been observed, the diffusion of Hf across the interface is very small as the thickness of the layers itself is very small. So, in order to confirm this established result, we have studied RF series samples for SHI induced mixing studies. These samples are significantly thicker (~ 15 nm) compared to ALD samples. Moreover, these films were directly deposited on Si without any inter-layer. The thickness and composition of these samples were estimated by RBS as discussed in the chapter 3. HRBS spectra of these samples have revealed the significant effects of SHI induced intermixing across this interface. Fig. 6.14 shows the HRBS spectra of pristine and irradiated samples. Clear indication of Hf diffusion is evident from these measurements. The data also indicates possible swelling of HfO₂ films during irradiation as the yield of Hf is lower everywhere. Sputtering effects normally lead to the reduction film thickness and inter-diffusion would stretch the lower edge of the Hf peak. Sputtering effect is not evident although the possible intermixing effects are clear from both the lower edge of Hf peak and higher edge of bulk Si. Hence the reduction in Hf yield can be explained by increase in the thickness of HfO₂ films with reduced concentrations of Hf everywhere. Possible incorporation of oxygen during irradiation can lead to this situation.

Hence our HRBS data suggests that SHI irradiation can result in both, the intermixing and swelling effects in these samples. In-situ I-V and C-V measurements were performed during the 120 MeV Au ion irradiation as a function of fluence (1×10^{11} to 1×10^{14} ions/cm²).

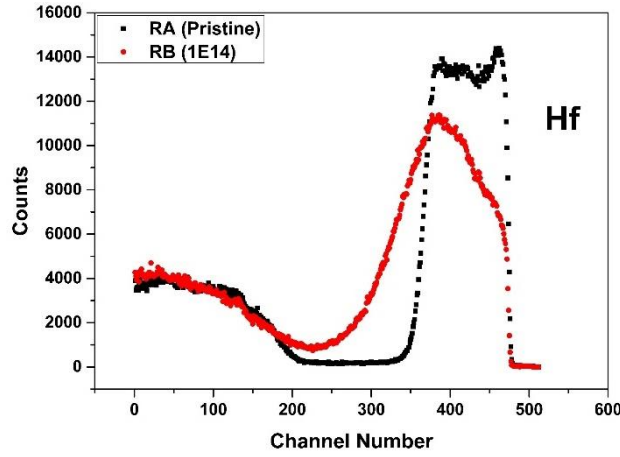


Fig. 6.14: HRBS spectrum of RF series pristine and irradiated samples

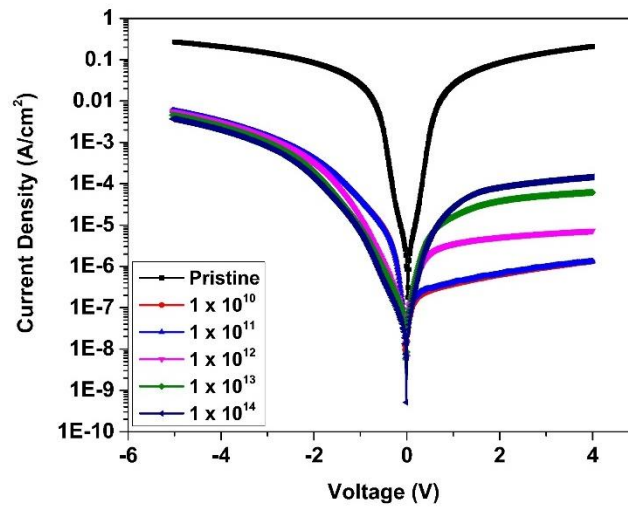


Fig. 6.15: In-situ I-V characteristics of H3 sample (Fluence: ions/cm²)

The in situ I–V characteristics of RF series samples at various fluences of 120 MeV Au ion beam are shown in Fig. 6.15. The leakage currents are considerably high in these samples, particularly in pristine sample. The leakage current reduces by about two orders upon irradiation. Fig. 6.16 depicts the leakage current density as a function of irradiation fluence at ± 1 V. The variation of leakage current with fluence is not that significant in accumulation region. However, a significant increase of leakage current is observed in depletion region with increase in fluence. These results are distinctly different from those of ALD grown

ultra-thin samples. At the higher fluences, the degradation of the device performance has been observed in terms of its increase in the leakage current.

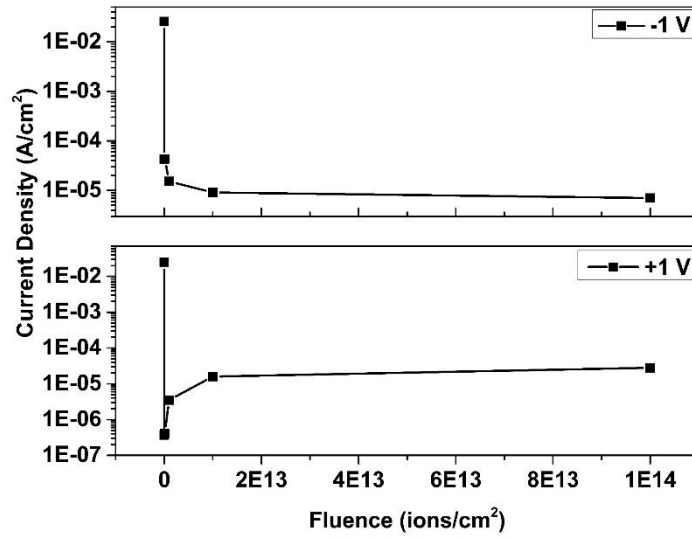


Fig. 6.16: I-V characteristics at ± 1 V of RF sample

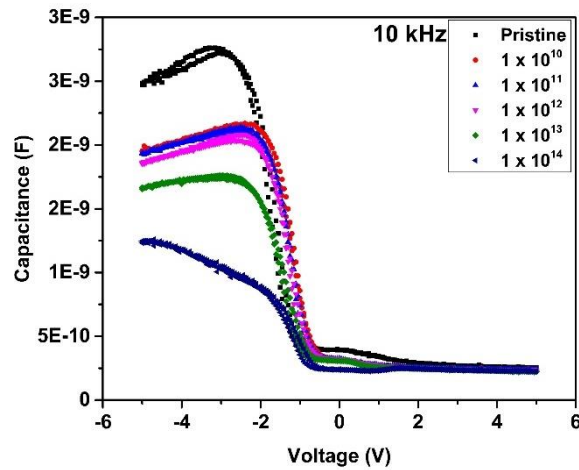


Fig. 6.17: In-situ C-V characteristics of RF series sample at 10 kHz frequency

Fig. 6.17 to 6.19 depict the C-V characteristics of RF series samples. These in-situ C-V measurements were performed at 10 kHz, 100 kHz and 1 MHz. Fig. 6.20 depicts the accumulation capacitance as a function of irradiation fluence at -4 V.

There is a systematic decrease in the accumulation capacitance with increase in the irradiation fluence. This behavior is similar to that seen earlier for H3 series samples. An increase in the thickness of the HfSiO layer could lead to the observed decrease in the dielectric constant. Quantitative estimates of D_{it} and D_{ot} have not been performed because the changes in C-V characteristics are not that significant.

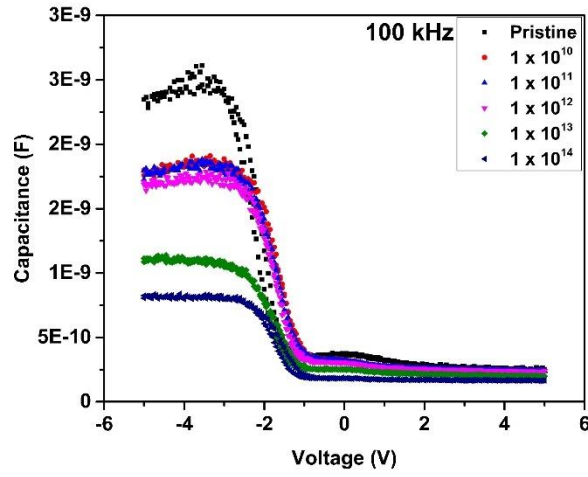


Fig. 6.18: In-situ C-V characteristics of RF series sample at 100 kHz frequency

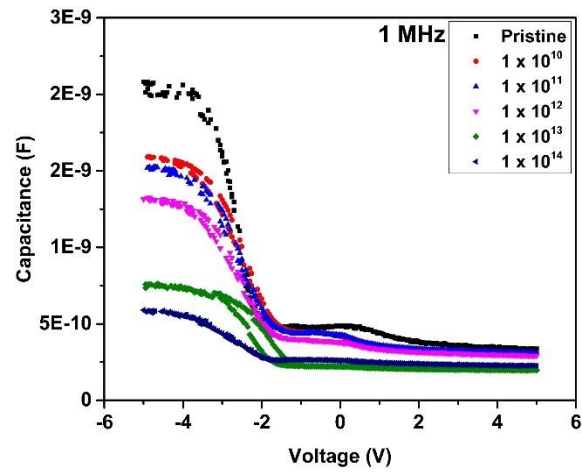


Fig. 6.19: In-situ C-V characteristics of RF series sample at 1 MHz frequency

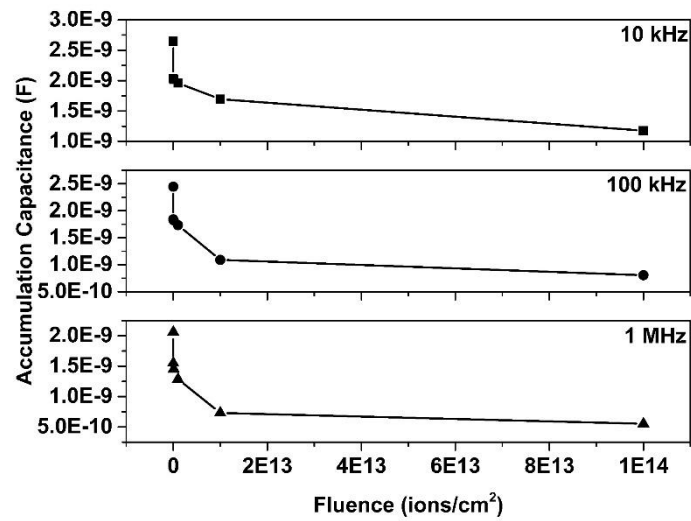


Fig. 6.20: Accumulation capacitance for RF samples at -4 V as functions of fluence (ions/cm^2) at different frequencies

6.4 Conclusions

Consistent in-situ electrical measurements were performed on the H3 and RF series MOSCAPs. 120 MeV Ag ion irradiation elucidated SHI induced intermixing effects, annealing and creation of defects. Leakage current density has been found to decrease at lower fluences, and increase at higher fluences. These changes can be attributed not only to the increase in the physical thickness of the dielectric layer but also to the possible annealing/creation of defects during irradiation. The Flat band shift and mid-gap shift at 1 MHz frequency have been found to increase as function of irradiation fluence. The density of oxide traps has been found to decrease whereas the density of interface traps has been found to increase with the irradiation fluence. However, the densities of oxide and interface traps were found well within the accepted range even after irradiation. Similar results have been observed from the RF series samples which further strengthened the SHI induced intermixing effects.

6.5 References:

1. Y.H. Kim and J.C. Lee, *Microelectronics & Reliab.*, **44** (2004) 183.
2. H. Kim, P.C. McIntyre and K.C. Saraswat, *Appl. Phys. Lett.*, **82** (2003) 106.
3. L.V. Goncharova, M. Dalponte, T. Feng, T. Gustafsson, E. Garfunkel, P.S. Lysaght and G. Bersuker, *Phys. Rev. B*, **83** (2011) 115329.
4. P. D. Kirsh, C. S. Kang, J. Lozano and J. C. Lee, *J. Appl. Phys.*, **91** (2002) 4353.
5. Byoung Hun Lee, Laegu Kang, Renee Nieh and Jack C. Lee, *Appl. Phys. Lett.*, **76** (2000) 1926.
6. J.K. Schaeffer, S.B. Samavedam, D.C. Gilmer, V. Dhandapani, P.J. Tobin, J. Mogab, B.-Y. Nguyen, B.E. White Jr., S. Dakshina-Murthy, R.S. Rai, Z.-X. Jiang, R. Martin, M.V. Raymond, M. Zavala, L.B. La, J.A. Smith, R. Garcia, D. Roan, M. Kottke, R.B. Gergory, *J. Vac. Sci. Technol. B*, **21** (2003) 11.
7. I.S. Park, T. Lee, H. Ko and J. Ahn, *J. Korean Phys. Soc.*, **49** (2006) 760.
8. A. Benyagoub, *Nucl. Instr. Meth. Phys. Res. B*, **245** (2006) 225.
9. N. Manikanthababu, N. Arun, M. Dhanunjaya, V. Saikiran, S. V. S. Nageswara Rao and A. P. Pathak, *Rad. Eff. Def. Solids.*, **170** (2015) 207.
10. D.K. Avasthi, *Defence Sci. J.*, **59** (2009) 401.
11. S.K. Srivastava, S.A. Khan, P. Sudheer Babu and D.K. Avasth, *Nucl. Instr. Meth. Phys. Res. B*, **332** (2014) 377.
12. H Amekura, S Mohapatra, U B Singh, S A Khan, P K Kulriya, N Ishikawa, N Okubo and D K Avasthi, *Nanotechnology*, **25** (2014) 435301.
13. I.C. Kizilyalli, R.Y.S. Huang and P.K. Roy, *IEEE. Ele. Dev. Lett.*, **19** (1998) 423.
14. A.S. Foster, F.L. Gejo, A.L. Shluger, R.M. Nieminen, *Phys. Rev. B*, **65** 174117 (2002).
15. A.Y. Kang, P.M. Lenahan and J.F. Conley Jr., *IEEE Trans. Nucl. Sci.*, **49** (2002) 2636.
16. K. Xiong, J. Robertson, M. Gibson and S.J. Clark, *Appl. Phys. Lett.*, **87** (2005) 183506.
17. P. S. Winokur, J. R. Schwank, P. J. McWhorter, P. V. Dressendorfer, and D. C. Turpin, *IEEE. Trans. on Nucl. Sci.*, **31** (1984) 1453.

Chapter 7

Summary and Future scope

This chapter summarizes the prominent features of the present thesis work and projects the promising future scope in this field.

7.1 Summary of the results

In this thesis, we have studied the synthesis, characterization, radiation response and reliability of HfO₂ based MOS devices. HfO₂ samples prepared by ALD, RF magnetron sputtering (RF) and e-beam evaporation (EB) methods have been studied in this work. One of the main reasons for employing different growth techniques in this thesis work has been to investigate the influence of growth technique on the nature of defects and their evolution during irradiation studies. In brief, we have presented our studies on 1) the optimization of synthesis of HfO₂ thin films by a newly established RF magnetron sputtering system under different deposition conditions on different substrates. These samples have been characterized by several well established techniques, 2) the effects of gamma irradiation on the electrical properties of HfO₂/Si MOSCAPs fabricated by both the RF magnetron sputtering and e-beam evaporation techniques and 3) SHI induced diffusion of Hf across HfO₂/SiO₂/Si and HfO₂/Si interfaces and the consequent effects on their electrical properties.

Good quality HfO₂ thin films were deposited on Si and quartz substrates after the optimization of the synthesis parameters. Au/HfO₂/Si MOSCAPs have been fabricated by e-beam evaporation and RF magnetron sputtering techniques to study the gamma irradiation effects on their electrical properties. Structural and electrical characterizations were performed on both sets of these samples. EB series samples have shown the presence of negatively trapped charges, whereas RF series samples have shown positively trapped charges. Both the sets of samples have shown similar behavior with gamma irradiation. Both the leakage current and accumulation capacitance have been found to increase with increase in the irradiation dose. Flatband shift and increase in the width of the hysteresis in the C-V characteristics clearly indicate the increase of oxide trapped charge densities and changes in the slopes of these curves show the increase of interface traps. These studies provide useful information for understanding the gamma irradiation response of HfO₂ based MOSCAPs in view of their applications in radiation environments.

On the other hand, SHI induced intermixing effects on the structural properties and consequent effects on the electrical properties of HfO₂ based MOS devices have been studied. ALD grown (H1, H2 and H3 series) HfO₂/SiO₂/Si and HfO₂/Si samples deposited by RF magnetron sputtering technique (RF series) have been used for this study. In H2 (HfO₂ (2.5 nm)/SiO₂ (1 nm)/Si) series samples, the effects of 80 MeV Ni ion irradiation on this interface have been studied. The thickness of this interlayer is also found to increase with increase in fluence.

Corresponding changes in the composition of these interlayers have also been estimated. These observations together with XRR analysis confirm that SHI can induce inter-diffusion of Hf and Si across HfSiO/HfO₂ interface. The studies on H1 series also yielded similar results, wherein the thickness of the interlayer (HfSiO) has been found to increase with increase in the irradiation fluence as evidenced by HRBS and XRR measurements. In addition to HRBS and XRR analysis, I-V measurements have also been performed. The leakage current is found to decrease by one order upon irradiation which can be attributed to the increase in the physical thickness of the interlayer.

The samples are further processed to RTA at 600° C in N₂ atmosphere for 60 seconds for studying the annealing kinetics. The increase in the density of the defects during RTA processing might be responsible for the observed increase in leakage currents during the device operation. Further, 80 MeV Ni ion irradiation induced effects have been studied on the electrical properties of HfO₂/Si samples. A systematic decrease in the leakage current density as a function of irradiation fluence has been observed. The effects of the defects together with the SHI induced intermixing effects on HfO₂/Si MOS devices have been studied.

Promising and reliable in-situ electrical measurements were performed on the H3 series samples using 120 MeV Ag ion irradiation and RF series samples by 120 MeV Au ion irradiation. These results unambiguously reveal the influence of SHI induced intermixing effects and the defect dynamics on the electrical properties of these devices. A systematic decrease in the leakage current and capacitance are evident from electrical properties. These in-situ measurements were further strengthened by HRBS measurements. Defects annealing/creation and SHI induced mixing have been observed. Hence, SHI can be used as an important technique in material modification with spatial selectivity to tune the structural and electrical properties.

The observed reduction in the leakage current and accumulation capacitance with increase in fluence under SHI irradiation are in contrast with the observed increase in these parameters with increase in dose in similar samples under gamma irradiation. Here it is important to note that the ion irradiation can induce structural modifications, like inter-diffusion of constituent elements, in addition to beam induced creation and annealing of defects. This implies that the effects of structural modification caused by ions dominates the effects caused by simple point defects. Hence, these results are distinctly different from those of gamma irradiation effects. Both the ion and gamma irradiation together give the complete picture of possible

modifications of the electrical properties of HfO_2 based MOS devices when used in radiation environments. SHI irradiation is generally used to simulate the effects caused by the possible light-ion irradiation in space over longer periods in shorter intervals in laboratory. Our study suggests that the intermixing effects are to be accounted in such studies as these effects are not significant in light ion irradiation. Moreover, ion irradiation results are also useful for tuning the stoichiometry of HfSiO_x films with spatial selectivity. This explains the reasons for performing both ion and gamma irradiation studies in this thesis work. Another important aspect of this thesis has been to study the influence of the initial state of oxide on the formation and evolution of defects during irradiation. In essence, these studies provide some useful information for understanding the influence of swift heavy ion and gamma irradiation on the structural and electrical properties of HfO_2 based high-k dielectric materials.

7. 2 Future scope

Annealing studies on the samples deposited by RF magnetron sputtering have to be performed during and after growth. These studies can yield some useful information on the structural, electrical and optical properties of HfO_2 based thin films. Ternary oxides of HfO_2 such as HfSiO and HfSiON are the future objectives to be tested as gate oxide materials. SHI induced effects on the structural, optical and electrical properties are also important to test their radiation hardness and reliability for practical applications.

Semiconducting nanocrystals (NCs) that are embedded in gate dielectrics (Like SiO_2 or HfO_2) have important applications in electronic, photonic and photovoltaic industries. Recently, nonvolatile memory devices using nanoparticles as a charge storage element or floating gates have attracted much attention. There are numerous reports on ion induced modification of various kinds of NPs embedded in SiO_2 . Ion beam shaping has been employed to realize nanostructures of high aspect ratios by suitably choosing irradiation parameters. To the best of our knowledge, so far there are no reports on ion beam modification of NP's and concerning size dependent ion beam shaping of NCs in HfO_2 matrix. Therefore, one of the future objectives is to investigate the irradiation induced effects in semiconductor nanoparticles of different sizes embedded in HfO_2 based high-k materials. Further, it is important to investigate the possible role of these materials in realizing electronic devices like Floating gate memories and Resistive Random Access Memories. The objective should be to improve the basic properties of these non-volatile memories and to study their sensitivity to radiation environments for practical applications.

List of publications

1. Ion beam studies of Hafnium based alternate high-k dielectric films deposited on silicon, [N. Manikanthababu](#), T. K. Chan, A. P. Pathak, G. Devaraju, N. Srinivasa Rao, P. Yang, M. B. H. Breese, T. Osipowicz, S. V. S. Nageswara Rao, *Nucl. Inst. and Meth. in Phys. Res. B*, **332** (2014) 389.
2. Synthesis, characterization and radiation damage studies of high-k dielectric (HfO₂) films for MOS device applications, [N. Manikanthababu](#), N. Arun, M. Dhanunjaya, V. Saikiran, S. V. S. Nageswara Rao and A. P. Pathak, *Rad. Eff. Def. Solids.*, **170** (2015) 207.
3. Gamma irradiation induced effects on the electrical properties of HfO₂ based MOS devices, [N. Manikanthababu](#), N. Arun, M. Dhanunjaya, S. V. S. Nageswara Rao and A. P. Pathak, *Rad. Eff. Def. Solids.*, (2015) (*in press*).
4. SHI induced effects on the electrical and optical properties of HfO₂ thin films deposited by RF sputtering, [N. Manikanthababu](#), M. Dhanunjaya, S. V. S. Nageswara Rao and A. P. Pathak, *Nucl. Inst. and Meth. in Phys. Res. B*, (2015) (*accepted*).
5. Ion induced intermixing and consequent effects on the leakage currents in HfO₂/SiO₂/Si systems, [N. Manikanthababu](#), T. K. Chan, V. Saikiran, S. K. Srivastava, A. P. Pathak, M. B. H. Breese, T. Osipowicz and S.V.S. Nageswara Rao, (2015) (*to be submitted*).
6. Reduced leakage currents in ion irradiated HfO₂/SiO₂/Si systems, [N. Manikanthababu](#) et al., (*to be submitted*).
7. Analysis of high electronic excitation induced defect dynamics in HfO₂ based MOS devices by in-situ electrical measurements, [N. Manikanthababu](#) et al., (*to be submitted*).

CONTRIBUTED/ATTENDED CONFERENCES/WORKSHOPS

1. Participated and worked as a volunteer in **25th National Symposium on Cryogenics** from 8th to 10th December 2014 at UoH, Hyderabad.
2. Presented a poster in **SHIMEC 2014**, from 14th to 17th October 2014, New Delhi, India.
3. Presented a poster and given an oral presentation in **CAARI 2014**, from 25th to 30th May 2014, Texas, USA.
4. Participated and worked as a volunteer in **AP Science Congress 2013**, from 14th to 16th November 2013 at UoH, Hyderabad.
5. Participated in **Awareness workshop of UGC-DAE Consortium for Scientific research**, from 28th to 30th Oct 2013 at UoH, Hyderabad.
6. Presented a poster (one of the Authors Prof. A P Pathak has presented on behalf of me) in **ICACS 2012**, from 21st to 25th Oct 2012, Kyoto, Japan.
7. Presented a poster in **SHIMEC 2012**, from 9th to 12th Oct 2012, New Delhi, India.
8. Presented a poster in **Frontiers in Physics 2012**, from 27th to 29th Sep 2012, at UoH, Hyderabad.
9. Participated in **India-Singapore joint symposium -2010**, from 19th to 21st February 2010 at UoH, Hyderabad.

CURRICULAM VITAE

NETHALA MANIKANTHA BABU

Research Scholar,
School of Physics,
University of Hyderabad,
Hyderabad-500046.

Email: maniphysics07@gmail.com
ph09ph19@uohyd.ernet.in

Objective: Quest to work in a real professional atmosphere that enables me to cope up with the emerging latest technology in science and technology which gives me the scope of widening the spectrum of my knowledge.

Current Position: Research scholar (**Ph.D. student**) under the supervision of Dr. S V S Nageswara Rao and Prof. Anand P. Pathak, School of Physics, University of Hyderabad.

ACADEMIC PROFILE

	Degree	Subject	University/Institution	Year	% of marks
1.	Ph.D.,	Physics	University of Hyderabad, Hyd	2010-Till Date	-----
2.	M.Sc.,	Physics	Andhra University, Visakhapatnam	2007	62.8
3.	B.Sc.,	Maths, Physics, Chemistry	Andhra University, Visakhapatnam	2001-2004	60.6
4.	Intermediate	Maths, Physics, Chemistry	Vikas Junior College, Rajahmundry	1999-2001	72.0
5.	SSC	Maths, Science, Social Studies	Govt. High School, Korukonda	1998-1999	76.8

RESEARCH EXPERIENCE

Over Four years of good hands on experience in following in house synthesis and characterization techniques:

1. RF Sputtering
2. X-ray diffraction (XRD)
3. Micro Raman Spectroscopy
4. Atomic force microscopy (AFM)
5. Field emission scanning electron microscopy (FESEM)
6. Transmission electron microscopy (TEM) and

Experience in Ion Beam related experiments such as RBS, Ion Implantation and Ion Irradiation at Indian Ion Beam Laboratories IUAC, New Delhi and IGCAR- Kalpakkam.

Publications:

1. Ion beam studies of Hafnium based alternate high-k dielectric films deposited on silicon, *N. Manikanthababu*, T. K. Chan, A. P. Pathak, G. Devaraju, N. Srinivasa Rao, P. Yang, M. B. H. Breese, T. Osipowicz, S. V. S. Nageswara Rao, *Nucl. Inst. and Meth. in Phys. Res. B*, **332** (2014) 389.
2. Synthesis, characterization and radiation damage studies of high-k dielectric (HfO₂) films for MOS device applications, *N. Manikanthababu*, N. Arun, M. Dhanunjaya, V. Saikiran, S. V. S. Nageswara Rao and A. P. Pathak, *Rad. Eff. Def. Solids.*, **170** (2015) 207.
3. Gamma irradiation induced effects on the electrical properties of HfO₂ based MOS devices, *N. Manikanthababu*, N. Arun, M. Dhanunjaya, S. V. S. Nageswara Rao and A. P. Pathak, *Rad. Eff. Def. Solids.*, (2015) (*in press*).
4. SHI induced effects on the electrical and optical properties of HfO₂ thin films deposited by RF sputtering, *N. Manikanthababu*, M. Dhanunjaya, S. V. S. Nageswara Rao and A. P. Pathak, *Nucl. Inst. and Meth. in Phys. Res. B*, (2015) (*accepted*).
5. Ion induced intermixing and consequent effects on the leakage currents in HfO₂/SiO₂/Si systems, *N. Manikanthababu*, T. K. Chan, V. Saikiran, S. K. Srivastava, A. P. Pathak, M. B. H. Breese, T. Osipowicz and S.V.S. Nageswara Rao, (2015) (*to be submitted*).
6. Reduced leakage currents in ion irradiated HfO₂/SiO₂/Si systems, *N. Manikanthababu* et al., (*to be submitted*).
7. Analysis of high electronic excitation induced defect dynamics in HfO₂ based MOS devices by in-situ electrical measurements, *N. Manikanthababu* et al., (*to be submitted*)

CONTRIBUTED/ATTENDED CONFERENCES/WORKSHOPS:

1. Participated and worked as a volunteer in **25th National Symposium on Cryogenics** from 8th to 10th December 2014 at UoH, Hyderabad.
2. Presented a poster in **SHIMEC 2014**, from 14th to 17th October 2014, New Delhi, India.
3. Presented a poster and given an oral presentation in **CAARI 2014**, from 25th to 30th May 2014, Texas, USA.
4. Participated and worked as a volunteer in **AP Science Congress 2013**, from 14th to 16th November 2013 at UoH, Hyderabad.

5. Participated in **Awareness workshop of UGC-DAE Consortium for Scientific research**, from 28th to 30th Oct 2013 at UoH, Hyderabad.
6. Presented a poster (one of the Authors Prof. A P Pathak has presented on behalf of me) in ICACS 2012, from 21st to 25th Oct 2012, Kyoto, Japan.
7. Presented a poster in **SHIMEC 2012**, from 9th to 12th Oct 2012, New Delhi, India.
8. Presented a poster in **Frontiers in Physics 2012**, from 27th to 29th Sep 2012, at UoH, Hyderabad.
9. Participated in **India-Singapore joint symposium -2010**, from 19th to 21st February 2010 at UoH, Hyderabad.

AWARDS RECEIVED:

- Qualified CSIR- UGC Junior Research Fellowship in December 2012.
- Qualified GATE 2012.

PERSONAL PROFILE:

Name : **N. MANIKANTHABABU**

Father's Name : **N. CHITTIAH**

Date of Birth : **03-08-1984**

Languages Known: **English, Hindi and Telugu.**

Addresses:

Present Address:

N. MANIKANTHABABU
Research Scholar,
School of Physics,
University of Hyderabad,
Hyderabad. 500046
A.P. India.

Permanent Address:

N. MANIKANTHABABU,
S/o N. CHITTIAH,
D.No. 1-59, Seetharamanagar,
Korukonda, E.G.Dt,
533289
A.P. India.

References:

- 1) Dr. S V S Nageswara Rao,
Associate Professor,
School Of Physics,
University Of Hyderabad,
Hyderabad-46.
Tel: (040) 2313 4329
svnsp@uohyd.ernet.in
nageshphysics@gmail.com

- 2) Prof. A P Pathak,
School Of Physics,
University Of Hyderabad,
Hyderabad-46.
Tel: (040) 2313 4316
appsp@uohyd.ernet.in
anandp5@yahoo.com

Synthesis, characterization and radiation response of HfO₂ based high-k dielectric materials

ORIGINALITY REPORT

21 %

SIMILARITY INDEX

11 %

INTERNET SOURCES

19 %

PUBLICATIONS

%

STUDENT PAPERS
